DICER1 mutations: clinical applications, novel associations, and functional evaluations

Anne-Laure Chong

Department of Human Genetics

Faculty of Medicine

McGill University, Montreal

November 2021

A thesis submitted to McGill University in partial fulfilment of the requirements

of the degree of Master of Science

ABSTRACT

DICER1 syndrome is a pleiotropic tumour predisposition syndrome defined by the presence of heterozygous germline loss-of-function variants in the *DICER1* gene, occurring in persons with a restricted set of generally well characterised tumour phenotypes. Over the years, various studies have expanded these DICER1-associated phenotypes, which now includes over 20 tumours or tumour-like conditions, which include pleuropulmonary blastoma, Sertoli-Leydig cell tumour, cervical embryonal rhabdomyosarcoma, and multinodular goiter. The various tumours of DICER1 syndrome are rare and display morphologic overlaps with several other neoplasms, giving rise to diagnostic challenges. *DICER1*-associated tumours exhibit a distinctive mutation profile with nearly all tumours harbouring a germline *DICER1* loss-of function variant and somatic so-called "hotspot" variants residing within exons encoding the RNase IIIb domain of DICER1. These hotspot variants affect the metal-ion binding residues that are necessary for processing microRNA precursor stem-loops into mature single-stranded microRNAs by the DICER1 enzyme. The DICER1 RNase IIIa and IIIb domains dimerize through hydrophobic interactions and are stabilized by two "ball and socket" junctions, which bring together the negatively charged side chains needed to activate the DICER1 enzyme. Previous *in vitro* cleavage experiments of a RNase IIIa "socket" residue (p. S1344L) has been shown to behave more like a RNase IIIb variant than a RNase IIIa variant. In this work, we demonstrate the importance of characterizing DICER1 variants in three different contexts: 1) clinical determination, 2) exploration of novel associations and 3) investigation of DICER1 function.

The first part consisted in studying a series of possible DICER1-associated lesions of diagnostic uncertainty. DICER1 sequencing validated the diagnosis of five cases and led to re-diagnosis of

three, thereby providing critical information regarding clinical management, especially for suspected DICER1 syndrome patients. The second part involved the assessment of a series of tumours existing outside of the DICER1 syndrome spectrum which harboured biallelic *DICER1* variants, followed by the investigation of *DICER1*-associated non-small cell lung cancers. Analysis of the *DICER1*-associated lung cancer cases revealed co-occurrence of *DICER1* and *CTNNB1* variants, suggesting an interesting relationship between these two genes as co-occurrence has been previously seen in other *DICER1*-associated lung tumours. The third part aimed to evaluate the effect of various variants affecting "ball and socket" residues on DICER1 cleavage activity by *in vitro* cleavage experiments. DICER1 cleavage activity of the "ball and socket" mutants showed four different cleavage patterns: **wild-type** cleavage, **delayed or reduced** cleavage, **no cleavage activity**, and **trans-acting cleavage**, proposing that DICER1 RNase III interdomain interactions are needed to maintain synchronization of precursor miRNA processing. miRNA expression profiling of at least one mutant belonging to each of the cleavage pattern group validated cleavage findings and also provided insights into pathogenicity of certain mutants.

Findings for this thesis supported the hypothesis that the discovery of *DICER1* variants not only serves a crucial role in proper assessment of possible *DICER1*-associated tumours with diagnostic uncertainty, but also serves to identify new associations of *DICER1* with neoplasms existing outside the classical DICER1 syndrome spectrum. Moreover, not only is the identification of *DICER1* variants important for both clinical and investigative purposes, but the evaluation of various *DICER1* variants can help in getting a better understanding of DICER1 RNase III interactions in miRNA biogenesis.

RÉSUMÉ

Le syndrome *DICER1* est un syndrome de prédisposition tumourale pléiotropique défini par la présence de variants germinaux hétérozygotes de perte de fonction (LOH) dans le gène *DICER1*, survenant chez des personnes généralement présentant un ensemble restreint de phénotypes tumouraux bien caractérisés. Diverses études ont élargi les phénotypes associés à *DICER1*, qui comprennent maintenant plus de 20 tumeurs ou affections semblables à des tumeurs, dont le blastome pleuropulmonaire, la tumeur des cellules de Sertoli-Leydig, le rhabdomyosarcome embryonnaire cervical et le goitre multinodulaire. Les diverses tumeurs du syndrome DICER1 sont rares et présentent des chevauchements morphologiques avec plusieurs autres néoplasmes, causant des difficultés en ce qui concerne le diagnostic. Les tumeurs associées à *DICER1* présentent un profil de mutation particulier, où presque toutes les tumeurs sont porteuses d'un variant germinal LOH de *DICER1* et de variants somatiques dites « hotspot » résidant dans les exons codant pour le domaine RNase IIIb de *DICER1*. Ces variants affectent les résidus de liaison aux ions métalliques qui sont nécessaires pour couper les tiges-boucles des pré-miARNs en microARNs simple brin matures par l'enzyme DICER1. Les domaines RNase IIIa et IIIb de DICER1 se dimérisent par le biais de liaisons hydrophobes et sont stabilisés par deux jonctions « ball and socket », qui rassemblent les résidus nécessaires à l'activation de DICER1. De précédentes analyses *in vitro* de clivage d'un résidu « socket » de la RNase IIIa (p. S1344L) ont montré qu'il agit davantage comme un variant de la RNase IIIb que comme un variant de la RNase IIIa. Dans ce travail, nous démontrons l'importance de la caractérisation des variants de *DICER1* dans trois contextes : 1) la détermination clinique, 2) l'exploration de nouvelles associations et 3) l'étude de la fonction de DICER1.

La première partie comprenait l'étude une série de lésions possiblement associées à *DICER1* et présentant une incertitude diagnostique. Le séquençage de *DICER1* a permis de valider le diagnostic de cinq cas et a conduit au re-diagnostic de trois d'entre eux, fournissant ainsi des informations critiques concernant la prise en charge clinique, notamment pour les patients suspectés de syndrome *DICER1*. La deuxième partie a consisté de l'évaluation d'une série de tumeurs n'appartenant pas au spectre du syndrome *DICER1* mais présentant des variants bialléliques de *DICER1*, puis en l'étude des cancers du poumon « non à petites cellules » (NSCLC) associés à DICER1. L'analyse des cas de NSCLC associés à *DICER1* a révélé la cooccurrence des variants *DICER1* et *CTNNB1*, suggérant une relation intéressante entre ces deux gènes, cette cooccurrence ayant déjà été observée dans d'autres tumeurs pulmonaires associées à *DICER1*. La troisième partie avait pour but d'évaluer l'effet de divers variants affectant les résidus « ball and socket » sur l'activité de clivage de DICER1 par le biais d'analyses *in vitro* de clivage. L'activité de clivage des mutants « ball and socket » de DICER1 a montré quatre différents schémas de clivage : clivage canonique, clivage retardé ou réduit, aucune activité de clivage et clivage trans-actif, proposant que les interactions entre les RNases III de DICER1 sont requises pour maintenir la synchronisation du clivage des pré-miARNs. Le profilage de l'expression des miARNs d'un mutant appartenant à chacun des schémas de clivage a validé les résultats du clivage et a fourni des informations sur la pathogénicité de certains mutants.

Les résultats de cette thèse ont soutenu l'hypothèse selon laquelle la découverte de variants de *DICER1* joue un rôle crucial dans l'évaluation de tumeurs possibles associées à *DICER1* avec une incertitude diagnostique et sert aussi à identifier de nouvelles associations de *DICER1* avec des tumeurs existant en dehors du spectre classique du syndrome de *DICER1*. De plus, l'identification

des variants de *DICER1* n'est pas seulement importante à des fins cliniques et de recherche, mais l'évaluation de divers variants de *DICER1* peut aider à mieux comprendre les interactions des RNases III de DICER1 dans la biogenèse des miARNs.

TABLE OF CONTENTS

LIST OF ABBREVIATIONS

Aa-RNase III	*Aquifex aeolicus* Ribonuclease III
ACTB	Actin beta
aGCT	Adult Granulosa Cell Tumour
AGO	Argonaute
ALK	Anaplastic Lymphoma Kinase
APC	Adenomatous Polyposis Coli
ARID1A	AT-Rich Interaction Domain 1A
B2M	Beta-2-Microglobulin
CADD	Combined Annotation Dependent Depletion
CC1	Cell-Conditioning Solution 1
CDKN2A	Cyclin Dependent Kinase Inhibitor 2A
cDNA	complementary DNA
cERMS	Cervical Embryonal Rhabdomyosarcoma
CHX	Cycloheximide
CN	Cystic Nephroma
CNS	Central Nervous System
COAD	Colon Adenocarcinoma
CPAM	Congenital Pulmonary Airway Malformation
cpm	Counts per minute
cryo-EM	Cryogenic Electron Microscopy
CTNNB1	Catenin Beta 1
DAB	3,3'-Diaminobenzidine
DGCR8	DiGeorge Syndrome Critical Region 8
DMEM	Dulbecco's modified Eagle's medium
DMSO	Dimethylsulfoxide
DNA	Deoxyribonucleic Acid
dNTP	Deoxyribonucleotide Triphosphate
dsRBD	Double-stranded RNA-binding Domain
dsRNA	Double-stranded RNA
DTT	Dithiothreitol
DUF283	Domain of Unknown Function 283
EAC	Endometrioid Adenocarcinoma
Ec-Rnase III	Escherichia coli RNase III
EDTA	Ethylenediaminetetraacetic Acid
EGFR	Epidermal Growth Factor Receptor
ERMS	Embryonal Rhabdomyosarcoma
ETMR	Embryonal tumours with multilayered rosettes

ExAC	Exome Aggregation Consortium
FATHMM	Functional Analysis through Hidden Markov Models
FBS	Fetal Bovine Serum
FFPE	Formalin-Fixed Paraffin-Embedded
FGFR1	Fibroblast Growth Factor Receptor 1
FLAC	Fetal Lung Adenocarcinoma
FOV	Fields of View
FOXL2	Forkhead Box L2
ftERMS	Fallopian Tube Embryonal Rhabdomyosarcoma
GAPDH	Glyceraldehyde 3-phosphate dehydrogenase
gDNA	Genomic DNA
GLOW	Global development delay, Lung cysts, Overgrowth and Wilms tumour
GNAS	Guanine Nucleotide binding protein, Alpha Stimulating activity polypeptide
gnomAD	Genome Aggregation Consortium
GPV	Germline Pathogenic Variant
H-FLAC	High-grade Fetal Lung Adenocarcinoma
HEK 293	Human Embryonic Kidney Cells
HRP	Horseradish Peroxidase
Hs-DICER1	*Homo sapiens* DICER1
IP	Immunoprecipitation
JGCT	Juvenile Granulosa Cell Tumour
KO	Knock-out
KRAS	Kirsten Rat Sarcoma Virus
L-FLAC	Low-grade Fetal Lung Adenocarcinoma
LB	Luria Broth
LOF	Loss-of-Function
LOH	Loss of Heterozygosity
LUAD	Lung Adenocarcinoma
M-CAP	Mendelian Clinically Applicable Pathogenicity
MB	Medulloblastoma
MD-SLCT	Moderately differentiated Sertoli-Leydig Cell Tumour
MET	Mesenchymal Epithelial Transition Factor
miRISC	microRNA-induced Silencing Complex
miRNA	MicroRNA
MLPA	Multiplex Ligation-Dependent Probe Amplification
mmu	*Mus musculus*
MNG	Multinodular Goiter
mRNA	messenger RNA
MSC	Mesenchymal Stromal Cell

MUGQIC	McGill University and Genome Quebec Innovation Centre
myoD1	Myogenic Differentiation 1
NB	Neuroblastoma
NOS	Not Otherwise Specified
NSCLC	Non-Small Cell Lung Cancer
oERMS	Ovarian Embryonal Rhabdomyosarcoma
OGCT	Ovarian Granulosa Cell Tumour
OSCST	Ovarian Sex Cord-Stromal Cell Tumour
PAZ	Piwi-Argonaute-Zwille
PB	Pulmonary Blastoma
PBS	Phosphate Buffered Saline
PCR	Polymerase Chain Reaction
PD-SLCT	Poorly differentiated Sertoli-Leydig Cell Tumour
PIK3CA	Phosphatidylinositol-4,5-Bisphosphate 3-Kinase Catalytic Subunit Alpha
Polyphen2	Polymorphism Phenotyping 2
PPB	Pleuropulmonary Blastoma
PPV	Predicted Pathogenic Variant
pre-miR-122	pre-miRNA 122
pre-miRNA	Precursor microRNA
pri-miRNA	Primary microRNA
PV	Pathogenic Variant
RMS	Rhabdomyosarcoma
RNA	Ribonucleic Acid
RNase III	Ribonuclease III
RPL19	60S Ribosomal Protein L19
rpm	Revolutions per minute
RT	Room Temperature
RT-qPCR	Quantitative Reverse Transcription PCR
SCST-NOS	Sex Cord-Stromal Cell Tumour, not otherwise specified
SDM	Site-Directed Mutagenesis
SIFT	Sorting Intolerant from Tolerant
SLCT	Sertoli-Leydig Cell Tumour
SOC	Super Optimal broth with Catabolite repression
STK11	Serine/Threonine Kinase 11
TCGA	The Cancer Genome Atlas
TEMED	Tetramethylethylenediamine
TH	Thyroid Hormone
THCA	Thyroid Carcinoma
TMA	Tissue Microarray
TRBP1	TAR RNA-binding protein 1

TRBP-BD	Transactivation RNA-binding protein Binding Domain
U2AF1	U2 Small Nuclear RNA Auxiliary Factor 1
UAS	Uterine Adenosarcoma
UCS	Uterine Carcinosarcoma
Urea-PAGE	Urea-Polyacrylamide Gel Electrophoresis
VUS	Variant of Unknown Significance
WB	Western Blot
WD-SLCT	Well-differentiated Sertoli-Leydig Cell Tumour
WDFA	Well differentiated Fetal Adenocarcinoma of the lung
Wnt	Wingless-related integration site
WT	Wilms Tumour
YST	Yolk Sac Tumour

LIST OF FIGURES

LIST OF TABLES

ACKNOWLEDGEMENTS

I would first like to thank my supervisor, Dr William Foulkes for giving the opportunity to learn as a summer student, undergraduate and graduate student in his lab. I would also like to thank him for his support and guidance throughout my graduate studies. I would also like to thank my co-supervisor, Dr Marc Fabian for his advice and for pushing me to sharpen my thinking. To both, thank you for taking the time to meet weekly and providing encouragement, continuous feedback and suggestions.

Many thanks to our collaborating pathologists and scientists: Drs Glenn McCluggage, Blaise Clarke, Gulisa Turashvili, Colin Stewart, Paul Thorner, Dorothée Bouron-Dal Saglio, Ju-Yoon Yoon, Anja Wagner, Zeynep Toth Uzan, Jonathan Rodgers and Naciba Benlimame as well as our collaborators from CARIS Life Sciences Michelle Ellis and Jeff Swensen and Dr Zoran Gatalica for their time and assistance in gathering and review of the samples described in this thesis. I would also like to extend my appreciation to my committee members, Drs Thomas Duchaine, Livia Garzia and Sidong Huang for providing me with valuable feedback and suggestions on my thesis research.

I would also like to acknowledge Dr Mona Wu, a former PhD student in our laboratory for her work in developing the *in vitro* cleavage assay model used in this thesis and would like to say thanks to my fellow lab members, Nelly, Anne-Sophie, Fiona, Dylan and Nancy as well as former lab members, Barbara, Leanne and Maria for their help and support.

I also wish to acknowledge the funding that I received during my graduate studies. I was supported by RI-MUHC Studentship and Fellowship.

Lastly, I am grateful to my family, especially my parents, for their unconditional love and support.

FORMAT OF THE THESIS

This thesis follows the traditional/monograph style and consists of seven chapters. Chapter 1 consists of a literature review with an introduction to *DICER1* syndrome and the DICER1 protein. It also provides background information needed to explain the rationale, hypotheses, and objectives of this thesis. Chapter 2 outlines the materials and methods. Chapter 3, which consists of three sections, presents original research findings, and contains four works that were published in 2020 and 2021 in *Histopathology*, *American Journal of Surgical Pathology* and *International Journal of Gynecological Pathology*. Chapter 3 also contains a recent study that has yet to be published. Chapter 4 comprises a summary of the results and discusses the findings presented in Chapter 3. Chapter 5 consists of the conclusion and discusses the implications of the work presented in this thesis as well as the future directions. Chapter 6 contains all references used in the writing of this thesis. Chapter 7 contains all appendix items.

CONTRIBUTIONS OF AUTHORS

This thesis was entirely written by myself (Anne-Laure Chong). I have performed and analyzed the experiments unless indicated otherwise.

For the tissue microarray, IHC was performed by Dr Naciba Benlimame and review by Dr Paul Thorner. Dr Paul Thorner also provided the PB images.

The author contributions for each published work in Chapter 3 are listed separately, in chronological order:

Somatic tumour testing establishes that bilateral DICER1-associated ovarian Sertoli-Leydig cell tumours represent independent primary neoplasms, Histopathology 2020(1):

W Glenn McCluggage referred the patients and wrote the manuscript. **Anne-Laure Chong** performed DNA extractions and DICER1 sequencing for case 1 and edited the manuscript. Dr **Leanne de Kock** performed DNA extractions and DICER1 sequencing for cases 2 and 3, assisted in the literature review and edited the manuscript. **William D. Foulkes** oversaw the study and edited the manuscript.

Embryonal Rhabdomyosarcoma of the Ovary and Fallopian Tube: Rare Neoplasms Associated With Germline and Somatic DICER1 Mutations, Am J Surg Pathol 2020(2)*:*

W. Glenn McCluggage wrote the manuscript. **Krisztina Z. Hanley**, **Jose E. Velázquez Vega** and **Terri P. McVeigh** referred cases and provided samples. **Anne-Laure Chong** and **Dr Maria**

Apellaniz-Ruiz and performed DNA extractions and DICER1 sequencing for case 1 and for cases 2 and 3, respectively. **William D. Foulkes** oversaw the study. All authors edited the manuscript.

The Value of DICER1 Mutation Analysis in "Subtle" Diagnostically Challenging Embryonal Rhabdomyosarcomas of the Uterine Cervix, 2021: Int J Gynecol Pathol 2021(3)*:*

Ju-Yoon Yoon wrote the manuscript. **Anne-Laure Chong** and **Maria Apellaniz-Ruiz** performed molecular DICER1 testing for cases 1 and 2, respectively and drafted and revised the manuscript and figures. Drs **Zena Slim** and **Stuart G. Salfinger** referred cases and provided clinical details. Drs **Blaise A. Clarke** and **Colin J.R. Stewart** served as expert pathologists and edited the manuscript. **William D. Foulkes** oversaw the study and edited the manuscript. **W. Glenn McCluggage** served as an expert pathologist oversaw the study and edited the manuscript.

1. CHAPTER 1: Introduction

1.1. *DICER1* gene and protein

The human *DICER1* gene locus is located on chromosome 14q32.13 and consists of 27 exons encoding for a 1,922 amino-acid long DICER1 protein, a multi-domain ribonuclease (RNase) that is critical to the biogenesis of mature miRNAs. DICER1 harbours an N-terminal DExD/H-box helicase domain, a transactivation response RNA-binding protein binding domain (TRBP-BD), a domain of unknown function (DUF283), a Platform domain, a Piwi-Argonaut-Zwille (PAZ) domain, two endonuclease III domains and a C-terminal dsRBD(4) (Figure 1a). Cryo-electron microscope reconstructions of DICER1 show that it is shaped like an 'L' (Figure 1b), with the PAZ and Platform domains situated at the 'head' of the protein, the two endonuclease domains located at the lower half of the 'body' of the protein (5, 6) and the DExD/H-box helicase domain and TRBP-BD situated at the 'base' of the 'L' (Figure 1c). The Platform and PAZ domains contain binding pockets for the 5' phosphate and 3' 2-nt overhang of the dsRNA, respectively(7, 8). The two endonuclease domains known as the RNase IIIa and RNase IIIb domains function as an intramolecular dimer, where the RNase IIIa domain processes the 3p miRNA from the 3' strand of the pre-miRNA and the RNase IIIb domain processes the 5p miRNA from the 5' strand of the pre-miRNA(8).

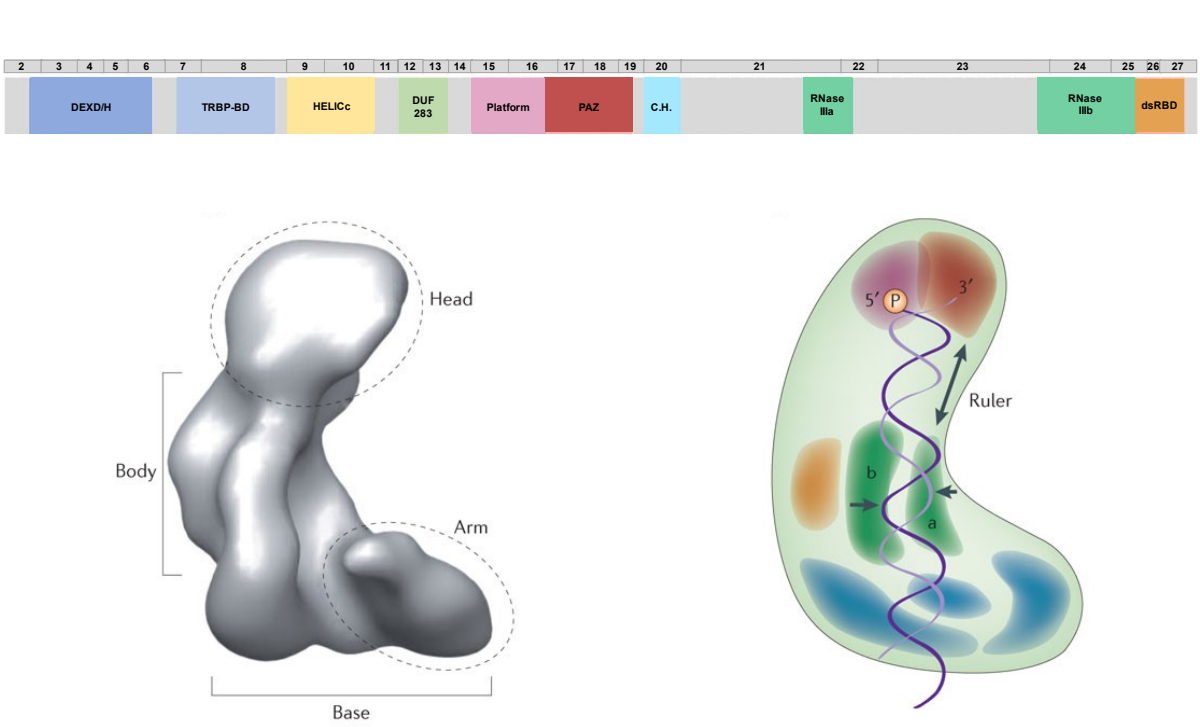

Figure 1: DICER1 protein structure and domains

a Graphical representation of the unfolded DICER1 protein structure. **b** Spatial organization of DICER1 according to cryo-electron based reconstructions by MacRae et al.(5). **c** Domain organization of DICER1. Adapted from Foulkes *et al.*, Nat. Rev. Cancer, 2014.

1.2. microRNA biogenesis and DICER1 molecular functions

MicroRNAs (miRNAs) are a class of single-stranded non-coding RNAs that range from 17-22 nucleotides in length and plays role in regulating the expression of over 30% of human genes (9). The majority of miRNAs-encoding genes are transcribed in the nucleus by RNA polymerase II into primary miRNAs (pri-miRNAs). Pri-miRNAs are subsequently cleaved by the microprocessor complex, which is comprised of DROSHA and DiGeorge syndrome critical region 8 (DGCR8) proteins, into 60-70 nt-long precursor miRNAs (pre-miRNA) stem-loop structures(10). Pre-miRNAs are then exported by Exportin 5 from the nucleus to the cytoplasm, where they are then

further cleaved by DICER1 into a mature miRNA duplex(11-13). Mature miRNA duplex is then loaded into a member of the Argonaute (AGO) which forms miRNA-induced Silencing Complex (miRISC). Within the miRISC, the miRNA duplex will undergo strand selection, with a guide strand being retained and the other passenger strand discarded(14). Strand selection is believed to select the strand with the less stably paired 5' end(15, 16). The guide strand will then bind via perfect base-pairing of the miRNA seed sequence (usually positions 2-8 of the 5' end of the miRNA) and imperfect complementary of the 3' end downstream of the seed sequence to sequences found in the 3' UTR of mRNAs causing mRNA degradation or translational repression(17-20) (Figure 2).

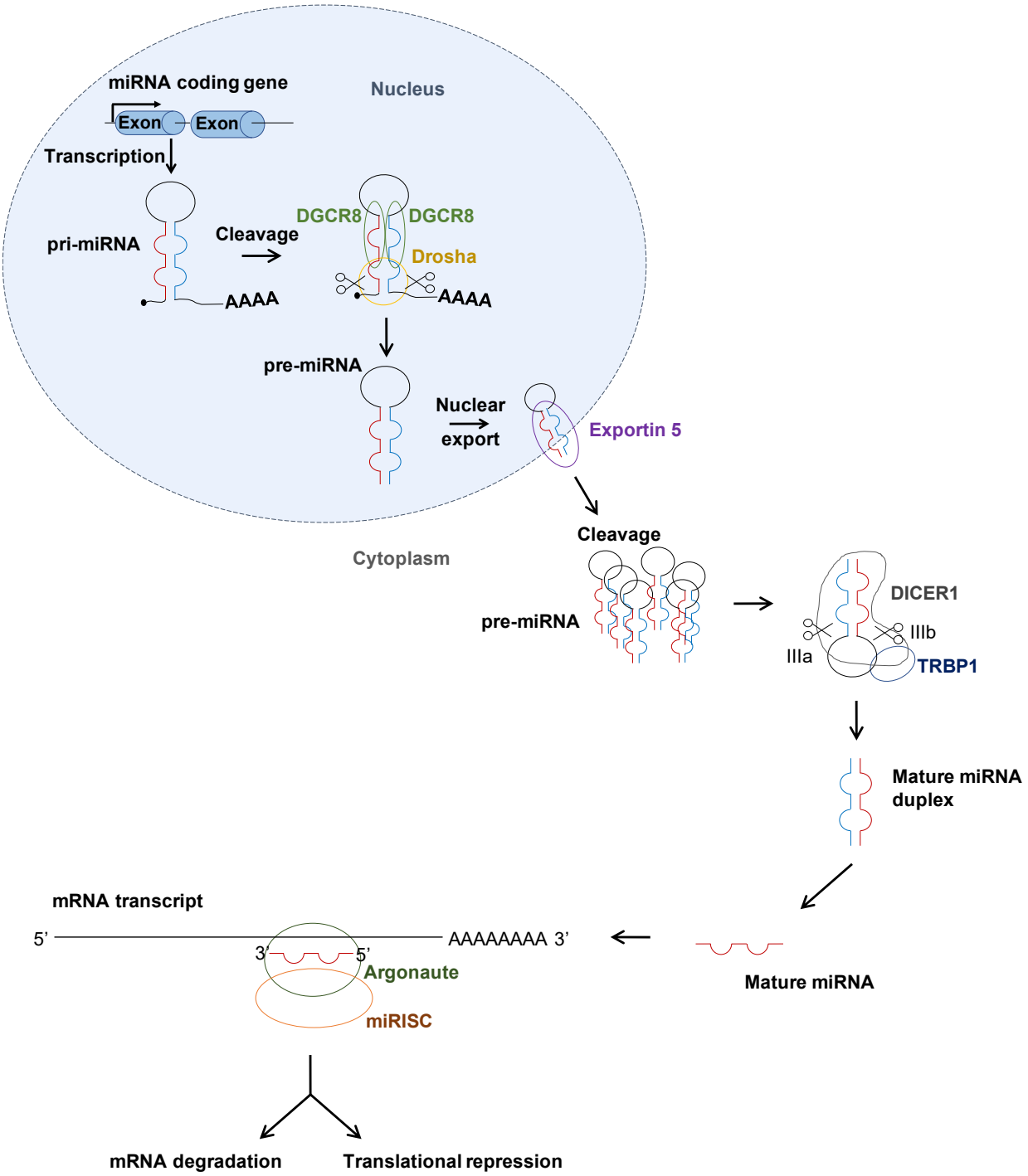

Figure 2: Graphical representation of the miRNA biogenesis pathway. Redrawn and adapted from Apellaniz-Ruiz *et al*, Genes Chromosomes and Cancer, 2020.

1.3. Endonuclease III conservation

Ribonuclease III (RNase III) enzymes are a class of highly conserved endonucleases that specifically cleave select double-stranded-RNAs (dsRNAs). RNase III enzymes can be subdivided into three different families. Class I, represented by the bacterial *Aquifex aeolicus* RNase III (*Aa*-RNase III), contain only a single catalytic endonuclease domain as well as one dsRNA binding domain (dsRBD). Class 2, represented by the Drosha enzyme, contain two endonuclease domains and one dsRBD and a long N-terminal segment. Class 3, represented by Dicer-like enzymes, contain two endonuclease domains, one dsRBD, a N-terminal helicase domain and a PAZ domain. RNase III enzymes not only have high conservation of the amino acid sequence but are also highly conserved in secondary and tertiary structures (21, 22). Sequence alignment studies of the RNase III domains have identified a stretch of conserved amino acid residues known as the RNase III signature motif, which encompass the catalytic residues of the enzyme ($_{37}$ERLEFLGD$_{44}$ in *Aa*-RNase III) (Figure 3). RNase III enzymes require divalent ions, namely Mg^{2+} or Mn^{2+} (23-26). Hs-Dicer is consistent with Mg^{2+}-dependent activity(4, 5, 27, 28). Studies have reported that class I enzymes form homodimers while class II and class III enzymes form intramolecular heterodimers. The DICER1 RNase IIIa and RNase IIIb domains form two catalytic cores through intramolecular dimerization(5, 28).

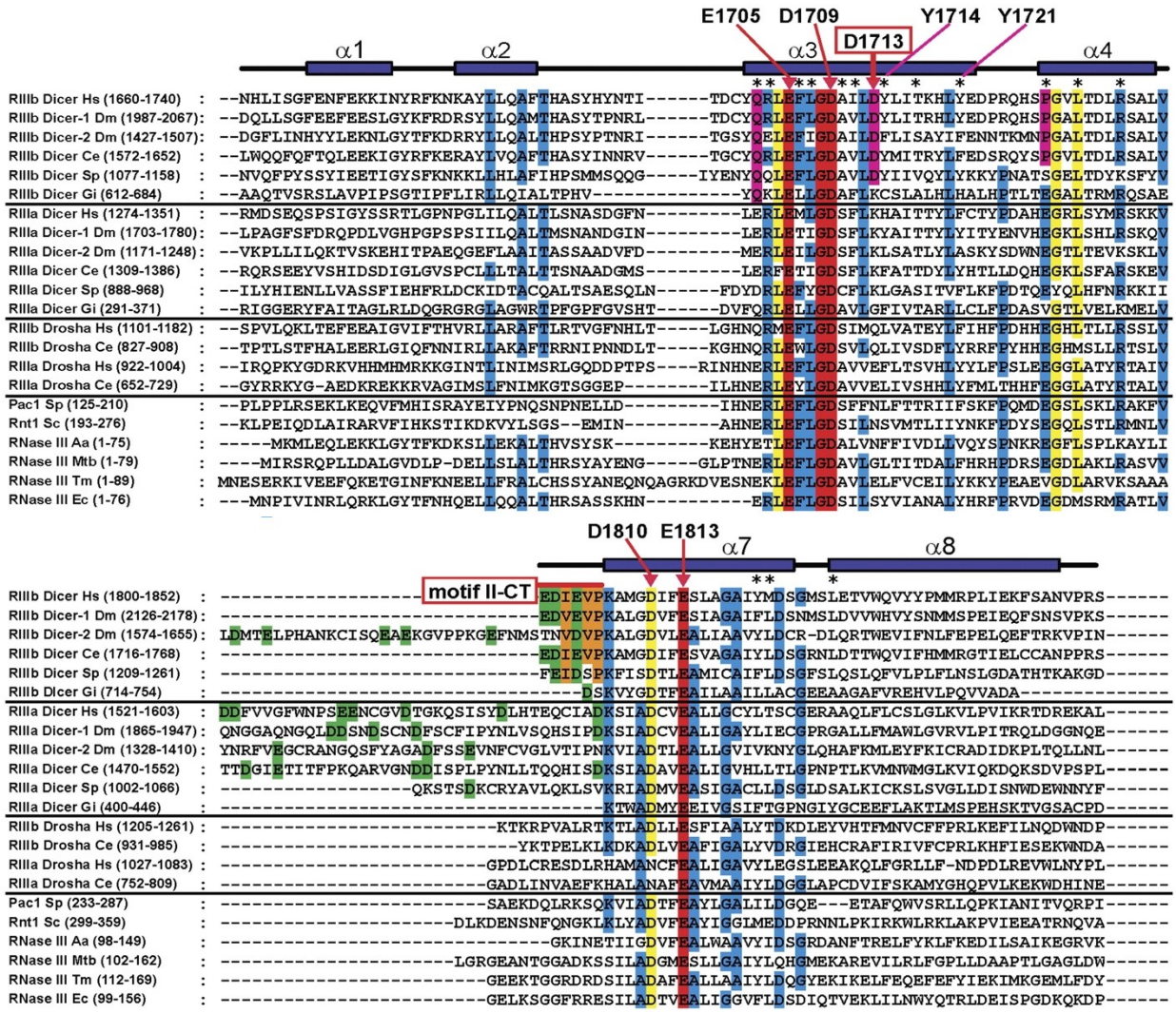

Figure 3: Sequence alignment of RNase III domains

Sequence alignments of three classes of the RNase III superfamily. Homo sapiens (Hs-Dicer, Hs-Drosha), Drosophila melanogaster (Dm-Dicer-1, Dm-Dicer-2), Caenorhabditis elegans (Ce-Dicer, Ce-Drosha), Schizosaccharomyces pombe (Sp-Dicer, Sp-Pac1), Giardia intestinalis (Gi-Dicer), Saccharomyces cerevisiae (Sc-Rnt1), Aquifex aeolicus (Aa-RNase III), Mycobacterium tuberculosis (Mtb-RNase III), Thermotoga maritima (Tm-RNase III), and Escherichia coli (Ec-RNase III). Residues shaded in red indicate invariant residues. Residues shaded in blue show 65% conservation and residues shaded in yellow demonstrate 85% conservation. Red arrows indicate the metal ion-

binding residues and asterisks (8) indicate the residues involved in RNase III dimerization. Residues unique to the RNase IIIb domains of Dicers are shaded in magenta. Squared residue D1713 indicates a metal-ion binding residue that does not interact directly with the Mg^{2+} ion. Modified from Takeshita et al. J Mol Biol, 2007.

1.4. "Ball and socket" junction model

Crystallographic and modelling studies of the *Aa*-RNase III show that it functions as a dimer and that the dimer is formed by hydrophobic interactions between two RNase III molecules stabilized by two "ball and socket" junctions(29). The "ball and socket" junctions model proposed by Blaszczyk et al. consists of two "ball and socket" junctions located at each end, with the "ball" being the side chain of a specific amino acid residue of one RNase III, and the "socket" being the cavity formed by the side chains of five amino acids located on the other RNase domain (Figure 4a). This leads to the formation of a valley between the dimer interface that can accommodate the double-stranded RNA substrate and which brings together six acidic side chains (E37, E40, D44, D107 and E110 from one RNase III and E64 from the other RNase III) needed to create the catalytic cores of the enzyme(29) (Figure 4b). Blaszczyk *et al*. have demonstrated that the catalytic active centers, containing two different RNA cleavage sites, E37/E64 and D44/E110. The catalytic active site of Aa-RNase III includes four metal-ion binding residues p.E40, p.D44, p.D107 and p.E110 (equivalent to p.E1316, p.D1320, p.D1561 and p.E1564 in RNase IIIa of Hs-DICER1 and p.E1705, p.D1709, p.D1810 and p.D1813 in the RNase IIIb of Hs-DICER1, respectively) (Figure 3). In Hs-Dicer, the metal-ion binding residues of the RNase IIIa domain are not observed in patient

samples, but *in vitro* studies have shown that the p.D1320A mutant cannot generate mature 3p miRNAs(21).

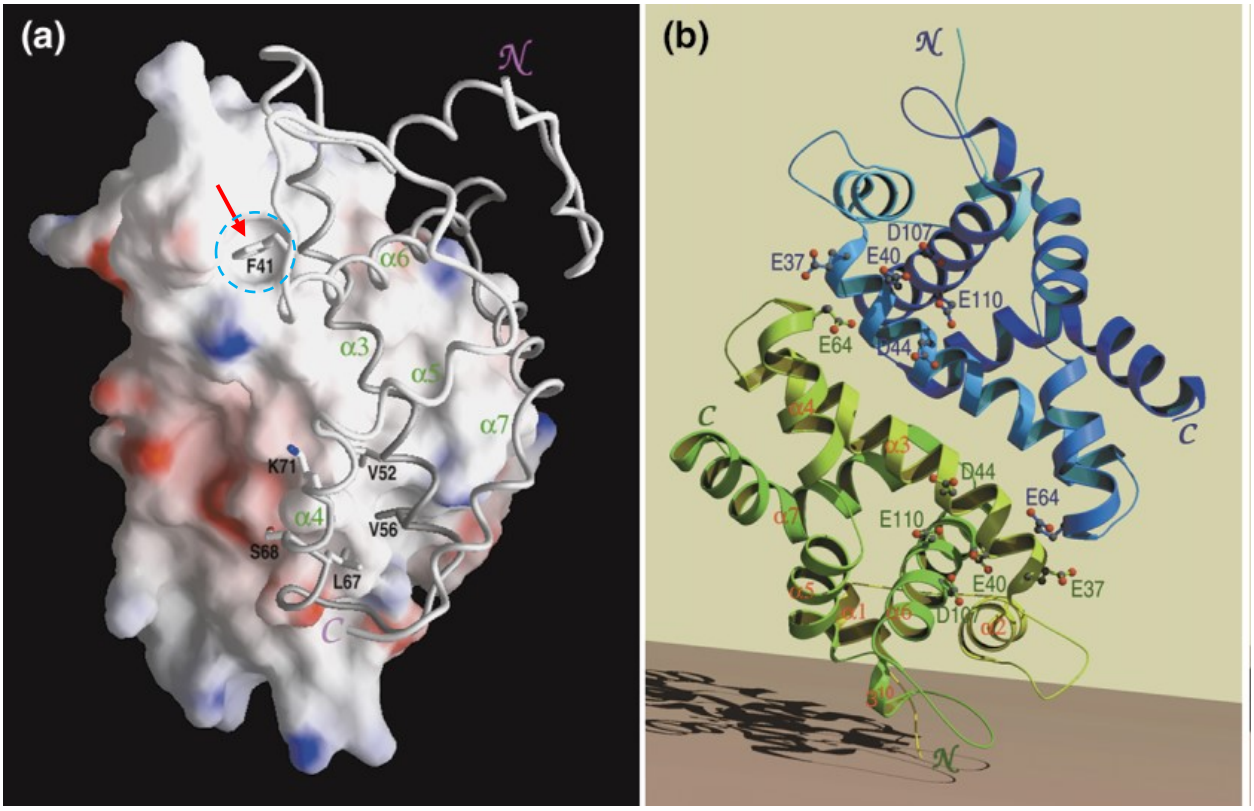

Figure 4: "Ball and socket" junction model of the Aa-RNase III and acidic residues of the catalytic active center.

Structure of the Aquifex aeolicus RNase III homodimer. a) Dimer interface of the Aa-RNase III illustrating Molecule A as surface representation and Molecule B as backbone "worm". "Ball and socket" residue side chains are illustrated in Molecule B as stick model. Red arrow indicates the "ball" residue, F41. Blue circle indicates "socket" in Molecule A formed by the side chains of V52, V56, L67, S68 and K71. b) Ribbon diagram of Aa-RNase III dimer with labelled metal ion-binding residues, E37, E40, D44, D107, E110 on one molecule and E64 on the opposing molecule,

illustrating the two catalytic centers of the RNase III dimer. Modified from Blaszczyk et al. Structure, 2001.

1.5. DICER1 Syndrome and phenotypes

DICER1 syndrome (OMIM 606241, 601200) is an autosomal dominant pleiotropic tumour predisposition syndrome that generally manifests in children, adolescents, and young adults. It is characterized by germline pathogenic variants (GPVs) in the *DICER1* gene, and the tumour phenotypes of the syndrome are manifested when obligatory second hits in *DICER1* occur. Its phenotype typically includes lesions such as pleuropulmonary blastoma (PPB), cystic nephroma (CN), ovarian Sertoli-Leydig cell tumour (SLCT), cervical embryonal rhabdomyosarcoma (cERMS) and multinodular goitre (MNG) (30) (Table 1). No founder variants have yet been described in the *DICER1* gene. *DICER1* syndrome tumours are characterized by an unusual mutation profile, whereby almost all tumours are associated with a germline loss of function (LOF) variant and a somatic hotspot variant localized to exons encoding the RNase IIIb domain of DICER1 (19). These RNase IIIb hotspot variants affect almost exclusively the metal-ion binding residues (p.E1705, p.D1709, p.G1809, p.D1810, p.E1813) that are critical for proper RNase IIIb nuclease activity and thus affect DICER1 cleavage of precursor microRNAs (pre-miRNA) into mature microRNA (miRNA) products (31) (Figure 5).

Table 1: DICER1-associated neoplasms. Taken from González *et al.* Modern Pathology, 2021

Pleuropulmonary blastoma (PPB) and PPB-like neoplasms
Pleuropulmonary blastoma, type I, IR, II, III
PPB-like Sertoli-Leydig cell tumor of lung
Pediatric cystic neoplasms and *DICER1*-sarcoma (anaplastic sarcoma of kidney)
Nasal chondromesenchymal hamartoma
Central nervous system sarcoma with rhabdomyosarcoma/PPB III-like features
Sertoli-Leydig cell tumor with and without heterologous features and type I PPB-like features
Peritoneal, ovarian and fallopian tube sarcoma with PPB-like features
DICER1-associated cystic hepatic neoplasm with type I PPB-like features
Cervical embryonal rhabdomyosarcoma
Teratoid and primitive neuroepithelial neoplasms
Cervical-thyroid teratoma
Malignant teratoid neoplasm of sacrococcygeal region
Ciliary body medulloepithelioma
Pituitary blastoma
Pineoblastoma
Embryonal tumor with multilayered rosettes
Thyroid
Multinodular hyperplasia (goiter)
Papillary thyroid carcinoma, invasive follicular variant
Follicular carcinoma, pediatric type
Poorly differentiated thyroid carcinoma, pediatric type
Intestine
Hamartomatous polyp with juvenile polyp-like features

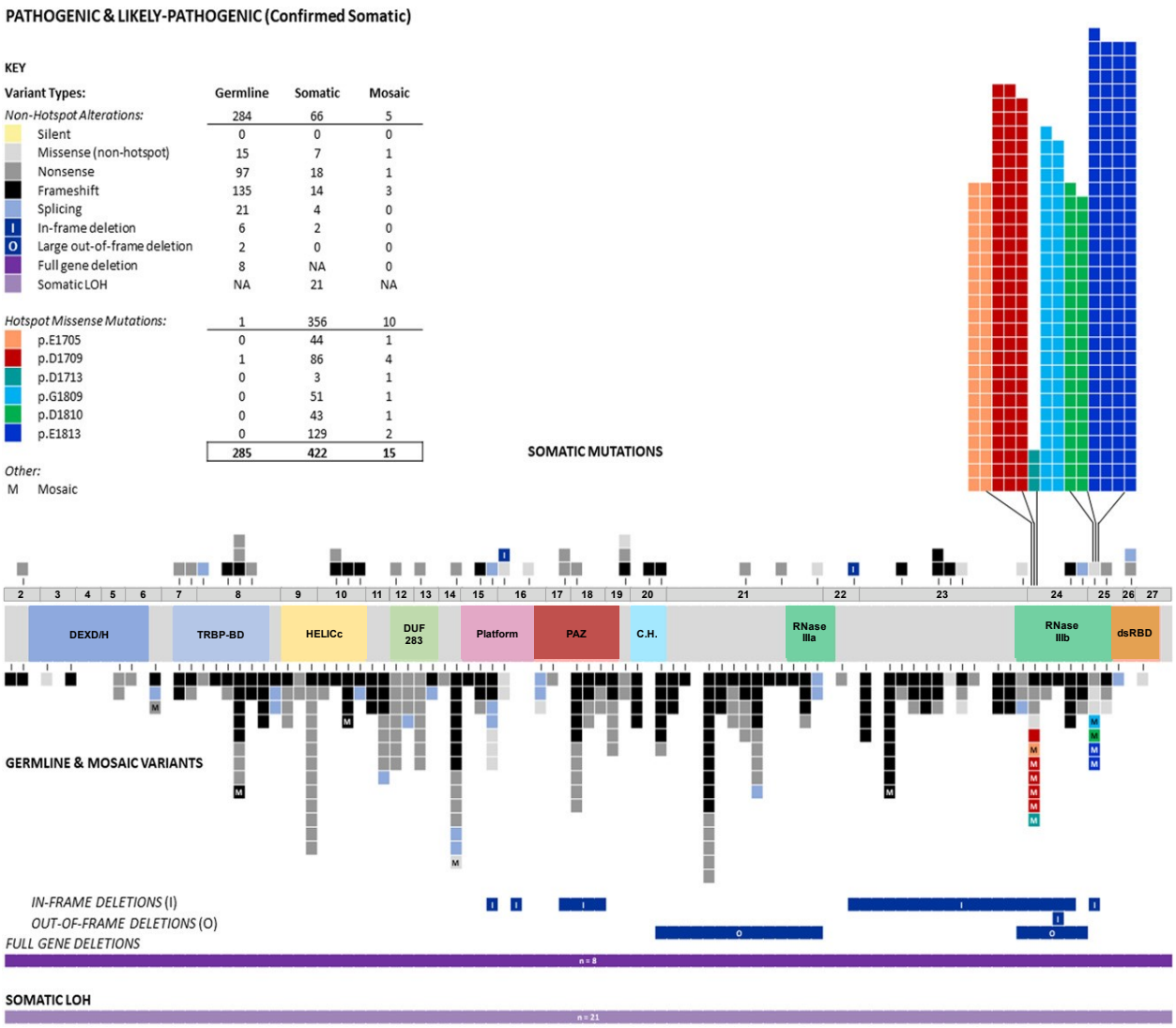

Figure 5: Plot of the pathogenic and likely pathogenic *DICER1* alterations published before January 31st, 2019. Taken from de Kock *et al.* Hum. Mutat., 2019.

LOH, loss of heterozygosity; NA, not applicable.

1.6. DICER1 alterations in the female reproductive tract (SLCT, aGCT, JGCT, ERMS)

DICER1 pathogenic variants (PVs) have been reported in various tumour types of the female reproductive tract such as Sertoli-Leydig cell tumours (SLCT), adult granulosa cell tumours (aGCT) and juvenile granulosa cell tumours (JGCT)(32-34), sex cord-stromal tumours not otherwise specified (SCST-NOS)(35) and embryonal rhabdomyosarcomas (ERMS) affecting the

genitourinary tract (36). SLCTs account for less than 0.5% of all ovarian cancer and can occur in all age groups, but generally occurring in young women with a mean age of 25 years)(37). The 2014 WHO classified them into 3 categories: poorly differentiated SLCTs (PD-SLCT), moderately differentiated SLCTs (MD-SLCT) and well-differentiated SLCTs (WD-SLCT). Retiform forms have also been reported. PD-SLCTs and MD-SLCTs can be seen with heterologous elements (cartilage, skeletal muscle enteric/intestinal epithelium, carcinoid tumour)(38, 39). SLCTs represent the most common ovarian neoplasm in *DICER1* syndrome, with *DICER1* GPVs having been reported at varying percentages (15%-97%)(32, 33, 35, 40, 41). Over 90% of JGCTs are diagnosed in the first three decades of life (mean age of 13 years)(42) whereas aGCTs occur in peri-menopausal or early post-menopausal women(43). Approximately 95% of aGCTs harbour the somatic missense, c.402C>G, p.C134W in the *FOXL2* gene(44). This *FOXL2* somatic PV has also been reported occasionally in JGCTs (32, 44) and in SLCTs (45). One study identified activating mutations in *AKT1* in 87.5% of JGCTs(46). The distinction between SLCTs and other OSCSTs can be difficult due to the high morphologic diversity of SLCTs and the lack of distinct immunohistochemical markers(47, 48) for SLCTs. As differential diagnosis of SLCTs have included aGCTs, molecular studies have been useful in distinguishing between these tumours. Karnezis et al. have reported that SLCTs can be subdivided into three molecular subtypes: *DICER1/FOXL2* wild-type, *DICER1*-mutated and *FOXL2*-mutated(49). *DICER1* PVs are only present in PD-SLCTs and MD-SLCTs and have not been reported in WD-SLCTs(30, 49). *FOXL2*-mutated SLCTs were reported in older patients (median age 79.5 years) compared to *DICER1*-mutated tumours (median age 24.5 years).

DICER1-associated sarcomas arise from many anatomical locations and show histological and morphological similarities to PPB, regardless of site of origin. Characteristics features of these tumours can include a subepithelial layer of malignant mesenchymal cells, rhabdomyoblastic differentiation (embryonal rhabdomyosarcoma) with myogenin and myoD1 positive staining, anaplasia, chondroid or chondrosarcomatous differentiation and foci of bone/osteoid(50, 51). Embryonal rhabdomyosarcomas (ERMS) are malignant mesenchymal tumours commonly seen in childhood(52). EMRS harbouring *DICER1* GPVs have been reported in ERMS of the uterine cervix (cERMS), of the ovary (oERMS) and of the fallopian tube (ftERMS)(2, 53-59). These *DICER1*-associated ERMS often exhibit the same features of the *DICER1*-associated sarcomas.

DICER1 syndrome also features a spectrum of central nervous system (CNS) lesions such as pituitary blastoma, pineoblastoma, *DICER1*-associated CNS sarcomas, ciliary body medulloepithelioma, ETMR-like infantile cerebellar embryonal tumour and PPB type II/III metastases to the CNS(60, 61). *DICER1* GPVs have been reported in other CNS tumours, but lack evidence of genetic association such as medulloblastoma (MB)(62, 63), neuroblastoma (NB)(64), intracranial medulloepithelioma(65), anaplastic meningeal sarcoma(66), and glioblastoma multiforme(67, 68).

1.7. DICER1 alterations in the lung (DICER1 and PPB, PB and WDFA)

PPB is the most common primary lung neoplasm in children and is probably the most common tumour seen in DICER1 syndrome(69). It generally manifests in children younger than 6 years. It is an aggressive sarcoma of mesenchymal origin that is classified into 4 subtypes: type I regressed

(type Ir), purely cystic (type I), mixed cystic and solid (type II), and purely solid (type III). PPBs progress over time (from type I to III). *DICER1* GPVs account for approximately 70% of PPBs (70), and biallelic tumour-specific *DICER1* PVs account for approximately 10% of PPB (70). Congenital pulmonary airway malformation (CPAM) are rare lung lesions affecting the fetal lung. Stocker pathologic classification subdivides CPAMs into five subtypes originating from different parts of the airways: Type 0, type 1, type 2, type 3, and type 4. CPAM type 4 is a peripheral cystic lesion with an epithelial layer of pneumocytes type I and II, which can be flat or cuboidal. PPB type I is also a peripherally cystic lesion where the cysts can be lined with cuboidal or columnar epithelium. PPB type I have a subepithelial layer of primitive round cells resembling the cambium layer of rhabdomyosarcoma and rhabdomyoblastic differentiation(71). Earlier reports have reported CPAMs as type I PPB and vice versa(72), given their histological similarities and indistinguishability by imaging(73).

Fetal lung adenocarcinoma (FLAC) is a rare tumour which accounts for approximately 0.1% - 0.5% of all lung neoplasms(74, 75). It is categorized into 2 subtypes: low-grade FLAC (L-FLAC) and high-grade FLAC (H-FLAC)(76). L-FLAC also known as well-differentiated fetal adenocarcinoma of the lung (WDFA) is commonly seen in patients in the third or fourth decade of life. It is characterized by a pure pattern, low nuclear atypia and morule formations, whereas H-FLAC presents at least 50% fetal morphology, lack morule formations and is often associated with conventional lung adenocarcinomas(76). Molecular profiling of L-FLACs and H-FLACs, have identified *DICER1* alterations(77-81) and *CTNNB1* variants in several cases of L-FLACs (75, 79-84), but not in H-FLACs. H-FLACs were found to harbour genetic alterations that are commonly seen in lung

adenocarcinomas, suggesting that H-FLACs might be specific subtype of lung adenocarcinoma (77).

Pulmonary blastoma (PB) is a biphasic tumour with malignant epithelial and mesenchymal components. Biallelic tumour-specific *DICER1* alterations have been reported in adult-onset pulmonary blastoma (PB)(78, 85). In their series, Sekine et al. showed that *CTNNB1* variants were always associated with PBs harbouring morules and that these PBs were predominantly epithelial(84) and suggest that these variants play a role in epithelial cell over-growth and morule formation. Studies of *DICER1*-related PBs have also shown associations with *CTNNB1* variants(78, 84, 86, 87) similarly to L-FLACs.

1.8. DICER1 and non-small cell lung cancer

Non-small cell lung cancer (NSCLC) accounts for approximately 85% of all lung cancers. It includes a variety of subtypes, with lung adenocarcinoma and squamous cell carcinoma being the most predominant ones. NSCLC most commonly contains somatic variants in *EGFR* (epidermal growth factor receptor), *KRAS* (Kirsten rat sarcoma virus), *FGFR1* (fibroblast growth factor receptor 1), *MET* (mesenchymal epithelial transition factor) and *PIK3CA* (Phosphatidylinositol-4,5-Bisphosphate 3-Kinase Catalytic Subunit Alpha) and chromosomal rearrangements affecting *ALK* (anaplastic lymphoma kinase), *RET* and *ROS1*.

1.9. DICER1 and trans-acting RNase III mutant, p.S1344L

As mentioned previously, *DICER1*-associated tumours have a specific mutation profile with *DICER1* somatic hotspot variants localized to exons encoding the RNase IIIb domain of DICER1. However, we have previously identified a patient with biallelic *DICER1* PVs in a Wilms tumour (WT) for which this was not the case. The patient harboured a germline LOF variant and the Wilms tumour harboured a somatic variant in the RNase IIIa domain (c.4031C>T, p.S1344L), instead of the canonical somatic hotspot variant in the RNase IIIb domain(88, 89). This variant has also been reported in the germline of a patient presenting with a severe subtype of *DICER1* syndrome(82). *In vitro* cleavage experiments have demonstrated that this variant behaves similarly to a RNase IIIb variant than an RNase IIIa variant (30, 90), i.e., generates an aberrant 5p-loop intermediate (Figure 6). In *Hs*-DICER1, the side chain of S1344 residue is a part of the "socket". Hs-DICER1 "ball and socket" junction residues are listed in Table 2.

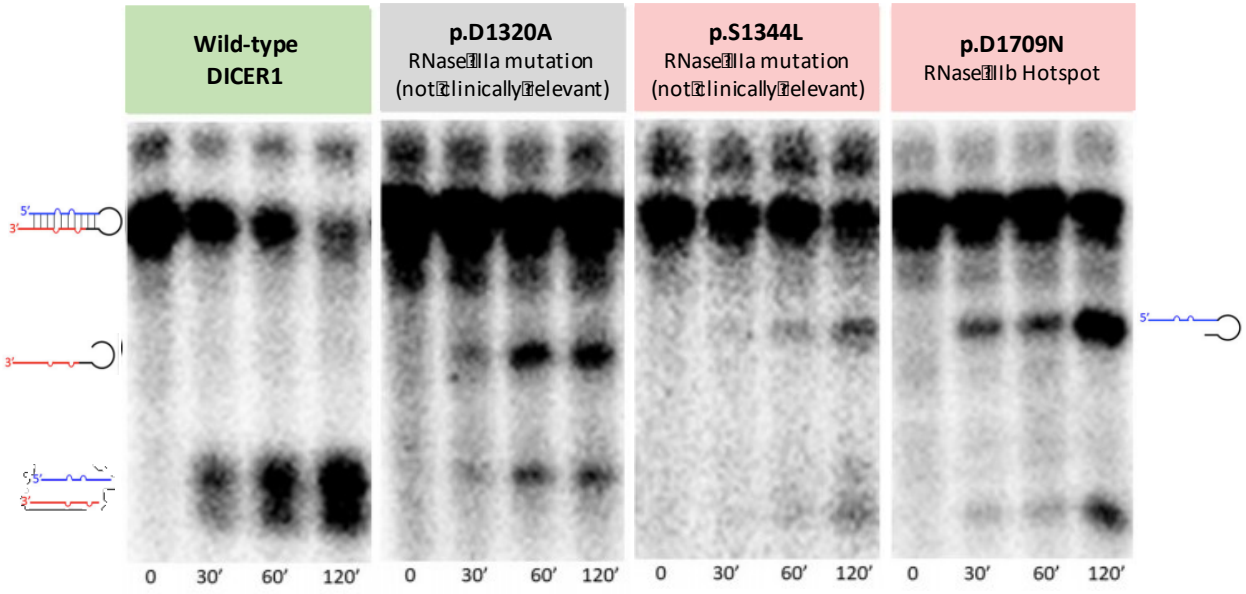

Figure 6: in vitro cleavage assays showing the effect of DICER1 RNase IIIa and RNase IIIb mutations on DICER1 cleavage of a radio-labeled pre-miR-122.

(From left to right) Representative autoradiograph of wild-type DICER1 cleavage pattern showing production of 5p and 3p microRNA (miRNA) species. Autoradiograph 2 illustrates the RNase IIIa variant, p.D1320A (has never been seen in clinical samples) which is unable to produce mature 3p miRNAs and instead produces 5p miRNA and 3p-loop products. Autoradiograph 3 for the RNase IIIa mutation, p.S1344L shows a cleavage pattern analogous to that of a pathogenic RNase IIIb hotspot mutation. Final autoradiograph shows cleavage products of the RNase IIIb hotspot mutation, p.D1709N. Mature 3p is produced. 5p-loop product is produces instead of mature 5p miRNA. Time points for all radiographs are 0-, 30-, 60-, and 120-min. Figure adapted from de Kock *et al*., Hum Mutat, 2019.

Table 2: "Ball and socket" junction amino acid residues in Hs-Dicer

Ball residue	**Socket residues**
M1317 (RNase IIIa)	T1717, Y1721, L1732, T1733, R1736 (RNase IIIb)
F1706 (RNase IIIb)	T1328, F1332, L1343, S1344, R1347 (RNase IIIa)

1.10. Hypotheses

1.10.1. *DICER1* sequencing can be used to resolve tumours with diagnostic uncertainty

I hypothesize that *DICER1* sequencing can be used to resolve diagnostic dilemmas for possible *DICER1*-associated tumours: i) with differential diagnoses, ii) with unusual diagnoses of the *DICER1* syndrome spectrum, iii) featuring undetermined same or separate origin and iv) featuring *DICER1* GPV in tumours not belonging to the *DICER1* syndrome spectrum.

Given the difficult distinction between aGCTs and SLCTs, I wished to validate or refute the findings by Karnezis *et al*.(49) and see if *FOXL2*-mutated SLCTs reported in older patients are in fact SLCTs and not aGCTs.

1.10.2. *DICER1* sequencing will identify new associations

Given that adult-onset PBs possess biallelic somatic PVs in *DICER1* but have never been reported to occur in DICER1 syndrome, we hypothesized that *DICER1* tumour-only variants could play a role in other adult-onset tumours, specifically lung cancers, that are not known to be part of *DICER1* syndrome. Given that non-small cell lung cancer (NSCLC) accounts for more than 85% of all lung cancer cases (91) and the similarities of certain *DICER1*-associated lung tumours with NSCLC, it would not be surprising to identify subset of NSCLCs harbouring *DICER1* PVs. Though no drug therapy exists for *DICER1* tumours at the moment, the identification of a subset of *DICER1*-associated NSCLCs would put forward the possibility of new drug therapies for these lung tumours if or when a targeted cancer therapy becomes available.

1.10.3. Other RNase III variants affecting the "ball and socket" junction exhibit trans effects similar to the p.S1344L variant

Sequencing of *DICER1* tumours have demonstrated the importance of specific RNase III variants in initiation and progression of DICER1-associated tumours(91) and crystallographic studies have demonstrated the importance of "ball and socket" junction residues located in the RNase IIIa and RNase IIIb domain to overall proper functioning of the DICER1 protein(29, 31, 92). Given previous studies on DICER1 "ball and socket" junction mutants and the trans-acting cleavage effect of the

DICER1 "ball and socket" junction residue p.S1344L, we hypothesized that other RNase III variants affecting the "ball and socket" junction might disrupt cleavage activity of their respective RNase III domain or show trans-acting effects like those of the p.S1344L mutant.

1.11. Objectives

Objectives (SECTION 1):

1) Resolving the 4 subtypes of "diagnostic uncertainty" by sequencing exons encoded in DICER1 RNase IIIa and RNase IIIb domains
2) Sequence a series of cases comprising SLCTs diagnosed in patients over 50 years of age for *DICER1* and *FOXL2* hotspot variants

Objection (SECTION 2):

1) Determine the frequency of *DICER1* hotspots in NSCLCs
2) Determine the prevalence of other *DICER1* alterations in NSCLCs with *DICER1* hotspots
3) Compare the mutational landscape of *DICER1*-mutated NSCLC with and without hotspots

Objective (SECTION 3):

To further the understanding of the role and interaction of DICER1 RNase III domains, I aimed to:

1) Evaluate the impact of specific *DICER1* variants affecting residues of the "ball and socket" junction on microRNA biogenesis by *in vitro* cleavage assay
2) Investigate the effect of DICER1 RNase III mutants which directly affect the DICER1 catalytic activity and the effect of trans-acting "ball and socket" mutants on miRNA expression profile

2. CHAPTER 2: MATERIALS AND METHODS

2.1. Material and Methods: SECTION 1

2.1.1. Collection of patient samples

I received 9 cases for *DICER1* testing all referred to us by physicians involved in the respective cases, which included 1 CPAM type (Table 3).

Table 3: Cases received for *DICER1* sequencing

Case	Age of diagnosis	Pathology	Reason for referral
1	11 months	CPAM type IV/ PPB type I	Differential diagnosis
2	6 years	OGCT/SLCT	Differential diagnosis
3	41 years	SCST-NOS/JGCT	Differential diagnosis
4	60 years	oERMS	Unusual case
5	19 years	subtle ERMS	Unusual case
6	7 years	SLCT	Interesting DICER1 germline variant
7*	7 years	Right SLCT	Bilateral SLCT case
8*	11 years	Left SLCT	Bilateral SLCT case
9	3 years	Medulloblastoma	Seen in a *DICER1* syndrome patient

* These cases are from a same patient with bilateral SLCT.

CPAM, congenital pulmonary abnormal malformation; ERMS, embryonal rhabdomyosarcoma; JGCT, juvenile granulosa cell tumour; oERMS, ovarian embryonal rhabdomyosarcoma; OGCT, ovarian granulosa cell tumour; PPB, pleuropulmonary blastoma; SCST-NOS, sex-cord stromal tumour not otherwise specified; SLCT, Sertoli-Leydig cell tumour.

For the second aim of Part 1, I received a series of 10 cases of SLCTs and SCST not otherwise specified (SCST-NOS) diagnosed in patients over 50 years of age for *DICER1* and *FOXL2* testing. The cases included 3 cases of PD/MD-SLCTs, 4 cases of MD-SLCT and 3 cases of SCST-NOS.

2.1.2. *DICER1* RNase III hotspot variant screening

The reference *DICER1* sequence used throughout this thesis investigation is NM_177438.2. Tumour DNA was extracted using QIAamp DNA FFPE Tissue Kit (Qiagen). Screening of the sequence encoding only the DICER1 RNase IIIa and IIIb domains for hotspot variants in formalin-fixed paraffin-embedded (FFPE) tumour-derived DNA was performed by PCR amplification using the primers in Table 3. For section 1 part II, all SLCTs were screened for the *FOXL2* hotspot variant, c.402C>G, p.C134W using primers in Table 4.

Table 4: Primers for the *DICER1* RNase III hotspot and *FOXL2* hotspot

Primer Name	**Forward Primer**	**Reverse Primer**
DICER1-SomVar10	CTTGAAATGCTTGGCGACTC	CAAACCACTTTCAGGCACACT
DICER1-SomVar1	GGGGATCAGTTGCTATGTGG	CGGGTCTTCATAAAGGTGCT
DICER1-SomVar2	ACTTCGGATCCCCTCAGATT	CGATGCAAAGATGGTGTTGT
DICER1-SomVar7	GGCCTTTTTGCTTACAAGTCAC	ATTAGTGGCCGCATCATGG
DICER1-SomVar7n	TGGCCTTTTTGCTTACAAGTC	TCTTTCTAAAGGGAGCCAACA
FOXL2_C132W_1	GAGAAGAGGCTCACGCTGTC	GGTAGTTGCCCTTCTCGAAC
FOXL2_C132W_1	CATCCGCCACAACCTCAGCC	CGGAAGGGCCTCTTCATGCGG

All PCR reactions were performed using 2.5 µL of 10X PCR buffer, 0.5 µL of 10 mM dNTPs, 0.25 µL of 25 mM $MgCl_2$, 1.4 µL of 20 µM primers and 0.2 µL Qiagen Hotstart Taq polymerase in a 25 µL PCR reaction. All PCR reactions were performed using approximately 50 ng of input DNA. PCR

amplification was done using a touchdown PCR program (95°C for 15 min, (95°C for 20s, 63°C for 20s, 72°C for 30s) for 16 cycles less 0.5°C per cycle, (94°C for 20s, 55°C for 20s, 72°C for 30s) for 28 cycles, 72°C for 7 min, and a 12°C hold) previously described (1, 35, 93).

All samples were Sanger sequenced by the McGill University and Genome Quebec Innovation Centre (MUGQIC).

2.1.3. Cloning experiment

To determine the phase of the variants identified in case 6, the region of interest was PCR amplified using Phusion High-Fidelity DNA Polymerase (New England BioLabs) with the following primer pairs: 5'-GGCCTTTTTGCTTACAAG -3' and 5'- TCTTTCTAAAGGGAGCCAACA-3'. The PCR fragment was TA cloned into pCR™4Blunt-TOPO (Invitrogen) following the manufacturer recommendations. DNA from 20 DNA clones was collected and Sanger sequenced.

2.1.4. Fluidigm Access Array and Whole Exome Sequencing (WES)

All cases that were negative for RNase IIIa and RNase IIIb hotspots were screened using a custom *DICER1* Fluidigm Access Array (94). For section 1 part II, all SLCTs harbouring no pathogenic variants in *DICER1* were screened by whole exome sequencing using previously described libraries on a MiSeq sequencer from Illumina (95).

2.1.5. Pathology review

Pathology review of the CPAM was done Dr Dorothée Bouron-Dal Saglio (DB-DS). Pathology review of SLCTs was done by the referring pathologist of the case Dr W. Glenn McCluggage (WGM), Dr Blaise Clarke (BC) and Dr Colin Stewart (CS).

2.2. Material and Methods: SECTION 2 (CARIS samples)

2.2.1. Collection of patient samples and *DICER1* screening

We received normal tissue-derived DNA from 14 FFPE tumours sequenced by CARIS Life Sciences (Phoenix, AZ) and which harboured biallelic *DICER1* variants (Table 5). Samples were screened for suspected germline and somatic *DICER1* variants by PCR and Sanger sequenced (93).

2.2.2. CARIS Life Sciences NSCLC data annotation and analysis

To further investigate the association of *DICER1* and NSCLC, we received tumour sequencing data for 778 *DICER1*-positive NSCLC cases from the CARIS Life Sciences database containing a total of 12,147 NSCLCs (09/03/2019) sequenced using the Agilent SureSelect XT panel consisting of 592 genes. All *DICER1* variants were then classified applying the classification of de Kock *et al*.(30), created to identify cases with *DICER1* predicted pathogenic variants (PPV). Variant population frequency was not evaluated. NSCLC cases were broken down according to number of *DICER1* PPV and mutation type (truncating variant, hotspot missense, non-hotspot missense and splice site variant) (Figure 7). Variants characterized as truncating included nonsense and frameshift variants and splice site variants were those affecting consensus splice sites.

Table 5: *DICER1* biallelic cases from CARIS Life Sciences

Case	Age	Sex	Submitting Histology	Primary Site	***DICER1* variants observed**	
					Hotspot variant	**Suspected germline variant**
Case 1	22	F	SLCT	Ovary	E1813V	c.2180delA, p.D727fs
Case 6	56	F	SLCT	Ovary	E1813K	p.E1532*
Case 9	53	F	Endometrioid adenocarcinoma, NOS	Endometrium	D1709N	p.K1486fs
Case 10	64	F	Endometrioid adenocarcinoma, NOS	Endometrium	E1813Q	p.R937H
Case 14	43	F	Carcinosarcoma, NOS	Endometrium	D1709N	p.S520I
Case 20	39	F	Adenocarcinoma	Lung	E1813D	p.Q1580*
Case 21	74	F	Adenocarcinoma	Lung	E1813Q	p.Q1614*
Case 22	60	M	Adenocarcinoma	Ascending colon	D1810V	p.R201H
Case 24	47	F	Sarcoma	Uterus	D1709N	c.5095+2T>A
Case 26	55	F	Sarcoma	Vagina	D1810Y	p.S1076fs
Case 27	39	F	Adenosarcoma	Endometrium	E1813G	p.K1123*
Case 28	74	F	Adenosarcoma	Uterus	D1810Y	p.R1060H; p.R821H
Case 32	27	F	Carcinoma, anaplastic, NOS	Thyroid gland	E1813D	c.4047_4050 +5delinsTT
Case 37	17	F	Yolk sac tumour (Extragonadal)	Endometrium	D1810Y	p.T350fs

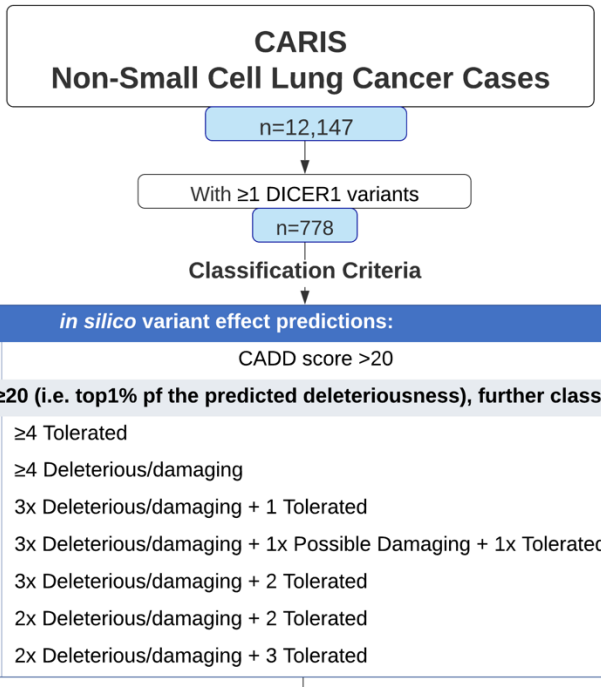

in silico variant effect predictions:		Classification
CADD	CADD score >20	**B**
If CADD score ≥20 (i.e. top1% pf the predicted deleteriousness), further classified as follows:		
	≥4 Tolerated	**B**
SIFT	≥4 Deleterious/damaging	**P**
PolyPhen2	3x Deleterious/damaging + 1 Tolerated	**LP**
FATHMM	3x Deleterious/damaging + 1x Possible Damaging + 1x Tolerated	**LP**
PROVEAN	3x Deleterious/damaging + 2 Tolerated	**VUS**
M-CAP	2x Deleterious/damaging + 2 Tolerated	**VUS**
	2x Deleterious/damaging + 3 Tolerated	**VUS**

Figure 7: Filtering of *DICER1*-positive NSCLCs from the CARIS Life Sciences database

2.2.3. OncoPrint

OncoPrint analysis explored the mutational landscape of the *DICER1*-hotspot positive and *DICER1*-hotspot negative NSCLC cases from CARIS Life Sciences. OncoPrint included 84 genes (including *DICER1*). Other gene hotspots were classified as such if reported in http://www.cancerhotspots.org/.

2.2.4. Immunohistochemistry of β-catenin

Immunohistochemistry was performed at the Segal Cancer Centre Research Pathology Facility (Jewish General Hospital) by Naciba Benlimame. Tissue samples were cut at 4-µm, placed on SuperFrost/Plus slides (Leica) and dried overnight at 37°C, before IHC processing. The slides were then loaded onto the Discovery XT Autostainer (Ventana Medical System). All solutions used for

automated immunohistochemistry were from Ventana Medical System (Roche) unless otherwise specified. Slides underwent de-paraffinization, heat-induced epitope retrieval (CC1 prediluted solution Ref: 950-124, standard protocol). Immunostaining for β-Catenin was performed online using a heat protocol. Briefly, Mouse Monoclonal anti-β-Catenin (Clone 14, Roche) prediluted, was auto-applied for 32 minutes at 37°C then followed by the appropriate detection kit (OmniMap anti-Mouse-HRP, Ref: 760-4310 and ChromoMap-DAB Ref: 760-159). A negative control was performed by the omission of the primary antibody. Slides were counterstained with Hematoxylin for 12 minutes, blued with Bluing Reagent for 4 minutes, removed from the autostainer, washed in warm soapy water, dehydrated through graded alcohols, cleared in xylene, and mounted with Eukitt Mounting Medium (Eukitt, Fluka Analytical). Sections were analyzed by conventional light microscopy and analyzed by Dr Paul Thorner (or scanned at 20X using the Aperio AT Turbo Scanner (Leica Biosystems)).

2.3. Materials and Methods: SECTION 3

2.3.1. DICER1 *in vitro* cleavage assay

The DICER1 *in vitro* cleavage assay was used to identify the impact of specific *DICER1* variants of the RNase IIIa and RNase IIIb domains on cleavage of pre-miRNA(95).

The *DICER1* mutations that were selected for the assay affect "ball and socket" junction residues and have never been reported in the literature or any human population or tumour database. The list of mutations evaluated by *in vitro* cleavage is listed in Table 6.

Table 6: *DICER1* mutations evaluated by in vitro cleavage assay

Mutation	Forward primer	Reverse Primer
Wild-type	---	---
c.3959A>C; p.D1320A	GAAATGCTTGGCGCCTCCTTTTTAAAGC	GCTTTAAAAAGGAGGCGCCAAGCATTTC
c.5437G>A; p.E1813K	GGCCATGGGGGATATTTTTAAGTCGCTTGCTGGTG	CACCAGCAAGCGACTTAAAAATATCCCCCATGGCC
c.3949_3950ATdelinsGC, p.M1317A	GCGGCTTGAAGCGCTTGGCGACTCCTTTTTAAAGCA	AGTCGCCAAGCGCTTCAAGCCGCTCCAGGTTAAATCCA
c.3982A>G, p.T1328A	GCATGCCATCGCCACATATCTATTTTGCACTTACCCTGAT	ATAGATATGTGGCGATGGCATGCTTTAAAAAGGAGTCGC
c.3994_3995TTdelinsGC, p.F1332A	CACATATCTAGCTTGCACTTACCCTGATGCGCATGAGGGC	GGGTAAGTGCAAGCTAGATATGTGGTGATGGCATGCTTTA
c.4031G>T, p.R1347L	GCCTTTCATATATGTTAAGCAAAAAGGTCAGCAACTGTAATC	CTTTTTGCTTAACATATATGAAAGGCGGCCCTCATGC
c.5116_5117TTdelinsGC, p.F1706A	CAGCGCTTAGAAGCCCTGGGAGATGCGATTTTGGACTAC	CATCTCCCAGGGCTTCTAAGCGCTGGTAACAATCAGTG
c.5149A>G, p.T1717A	CTACCTCATAGCCAAGCACCTTTATGAAGACCCGCGGC	AGGTGCTTGGCTATGAGGTAGTCCAAAATCGCATCTCCC
c.5161_5162TAdelinsGC, p.Y1721A	AACCAAGCACCTTGCTGAAGACCCGCGGCAGCACTCCCCG	GCGGGTCTTCAGCAAGGTGCTTGGTTATGAGGTAGTCCAA
c.5197_5198CdelinsCT, p.T1733L	GGGGGTCCTGCTAGACCTGCGGTCTGCCCTGGTCAA	ACCGCAGGTCTAGCAGGACCCCCGGGGAGTGCTGCCGC
c.5207G>T, p.R1736L	GACAGACCTGCTGTCTGCCCTGGTCAACAACACCATCTT	ACCAGGGCAGACAGCAGGTCTGTCAGGACCCCCGGG

2.3.2. Introduction of mutations in pQCXIB-FLAG-DICER1 by site-directed mutagenesis

All point mutations were generated by site-directed mutagenesis (SDM). Briefly, PCR (95°C for 5 minutes, (95 °C for 30 seconds, 60°C for 1 minute, 68°C for 20 minutes) x5, (94°C for 30 seconds, 66°C for 1 minute, 72°C for 20 minutes) x 11, 72°C for 7 minutes, 10°C hold) using the pQCXIB-FLAG-DICER1 construct as a template according to Wu (96). The SDM primers are listed in Table 6. Four 50 µL-PCR reactions were performed for each mutation. The PCR products were digested with 1 µL DpnI restriction enzyme (New England Biolabs) per PCR reaction at 37°C for 4 hours to remove the bacterial template. PCR products were pooled and column-concentrated by adding 1 volume of isopropanol and 5 volumes of PE buffer (10 mM Tris-HCl pH 7.5, 80% ethanol), transferring to a DNA column (Bio Basic), spinning at 13,000 rpm for 1 minute, discarding the flow-through, washing the column with 750 µL PE buffer, centrifuging at 13,000 rpm for 1 minute, discarding the flow-through, centrifuging at 13,000 rpm for 1 minute to dry and eluting in 50 µL dH2O.

10 µL of the SDM concentrated PCR product was used to transform 100 µL of One Shot™ TOP10 competent *E. coli* (Invitrogen) by heat-shock (incubate on ice for 30 minutes, 42°C for 45 seconds, on ice for 2 minutes, add 250 µL SOC medium (Invitrogen) and incubate with shaking at 37°C for 60 minutes, centrifuge at full speed for 1 minute, remove the most of the supernatant, resuspend the pellet in the remaining supernatant, plate on LB + ampicillin plates and incubate at 37°C overnight. Clones of the pQCXIB FLAG-DICER1 constructs were inoculated, mini-prepped using the QiaPrep Spin Miniprep Kit (Qiagen) and Sanger sequenced to confirm that the desired variant was obtained.

2.3.3. Generation of stable HEK293 cell lines expressing FLAG-DICER1 protein mutants

pQCXIB constructs were then used to generate retroviruses for transduction of HEK 293 (human embryonic kidney cells) cells to generate FLAG-tagged DICER1 protein. Virus was generated in HEK 293T cells grown to ~25% confluence in a 6-well plate according to protocol described by Wu (96): 2 µg of pQCXIB construct + 200 µL Optimem (LifeTechnologies) + 2 µg of pUMVC + 1 µg VSV-G and 24 µL polyethylenimine (1 mg/mL) were added together and incubated at room temperature (RT) for 5 minutes. 1000 µL of Optimem was added to the construct mixture and incubated for 10 minutes at RT. Media was removed from HEK 293T cells, replaced with 500 µL of the construct mix, and incubated at 37°C for 5 hours. Construct mix was removed and replaced with 2 ml DMEM (Wisent) supplemented with 10% FBS (Wisent) and 1% penicillin/streptomycin (LifeTechnologies) and incubated at 37°C for 48 hours. Supernatant was collected and filtered (0.45 µm) and added dropwise to infect HEK 293 cells grown to ~ 25% confluence in a 6-well plate with 2 µL polybrene (4 mg/mL). HEK 293 cells were infected a second time the following day. HEK 293 cells were selected for virus retention using blasticidin (10 µg/mL) and propagated in culture.

2.3.4. Immunoprecipitation of DICER1-FLAG tagged mutant protein

DICER1 protein used in the *in vitro* cleavage was isolated by FLAG immunoprecipitation. HEK 293 cells were grown to near confluence in 15 cm dishes, rinsed twice with PBS, scrapped, centrifuged at 1200xg for 3 minutes. Supernatants were discarded and the cell pellets were frozen at -80°C. Cells were lysed in 5 pellet volumes of NP-40 lysis buffer (20 mM Tris-HCl pH7.6, 150 mM NaCl, 1 mM EDTA, 0.4% (v/v) NP-40, complete protease inhibitors (Roche), vortexed, placed on a rotator

for 1 hour at 4°C, vortexed again, centrifuged at max speed for 15 minutes. Pre-cleared lysates were incubated with 50 µL of washed FLAG M2 agarose resin (Sigma) overnight at 4°C. FLAG-M2 slurry was washed 2x with NP-40 lysis buffer, then washed 2x with IP wash buffer (20 mM Tris-HCl pH7.6, 300 mM NaCl, 1 mM EDTA ,0.4% NP-40, and then washed 2x with DICER1 storage buffer (20 mM Tris-HCl pH7.6, 50 mM NaCl, 20% Glycerol). FLAG-DICER1 protein was eluted from the slurry by addition of 3X FLAG peptide solution (5 ug/µL) to 50 µL DICER1 storage buffer/sample with complete protease inhibitors and incubated on rotator for 1 hour at 4°C. Immunoprecipitated protein was transferred to new microfuge tubes. The amount of FLAG-DICER1 used for the *in vitro* cleavage assay was determined by comparing IP amounts by western blot (WB).

2.3.5. *In vitro* cleavage assay

The DICER1 p.E1813K mutant was used as a control for an RNase IIIb mutant and the DICER p.D1320A mutant was used as a control for an RNase IIIa mutant for the assay since it is known to not produce 3p miRNAs (21). However, this variant has never been reported in any human variant population or tumour database. FLAG immunoprecipitant from HEK 293 infected with pQCXIB construct was used as a negative control in the *in vitro* cleavage assay.

2.3.5.1. Generation of the radio-labelled pre-miRNA

The precursor substrate selected for this work was pre-miRNA 122 (pre-miR-122) since it has been previously used in *in vitro* cleavage assays to evaluate cleavage activity of DICER1 mutants(30, 96, 97) as has been shown to produce distinguishable cleavage products after being

resolved on a denaturing PAGE. Cleavage products include 3p and 5p and intermediate cleavage products 3p+loop and 5p+loop.

The pre-miR-122 template was synthesized using a three-primer PCR method. The forward primer 5'-TATTTAGTGTGATAATGGCGTTTGATAGTTTAGAC-3' and reverse primer 5'-TAATACGACTCACTATAG-3' were used to amplify a template primer 5'-ATAGTTTAGACACAAACACCATTGTCACACTCCACTATAGTGAGTCGTATTA-3'. The thermocycler conditions were as follows: 94°C for 2 minutes, (94°C for 30 sec, 54°C for 30 sec, 72°C for 30 sec) x 25, 72°C for 10 minutes, 4°C hold) using 10% DMSO and Phusion® High-Fidelity DNA Polymerase (New England BioLabs). Six PCR reaction products were pooled, column-concentrated, gel purified (QIAquick Gel Extraction Kit, Qiagen) and eluted in 50 µL dH_2O) and then stored at -20°C. The radiolabeled pre-miR 122 was generated by T7 in vitro transcription (MAXIscript T7 Transcription kit, Invitrogen) of 5 µL of pre-miR-122 template and 8 µL of radioactive UTP ([α-32P]-800 ci/mmol). The *in vitro* transcribed product was treated with 1 µL DNase at 37°C for 30 minutes (Ambion) and then column-purified on a mini Quick Spin column (Roche) with elution in 50 µL ddH_2O and stored at -20°C in the radioactivity room.

2.3.5.2. *in vitro* cleavage reaction conditions and resolving cleavage products

Radio-labelled pre-miR-122 (used within 1 week of preparation) was diluted (10^4 cpm), heated and slow-cooled to produce hairpins using the following conditions :95°C for 3 minutes, 75°C for 3 minutes, RT until reaction began. One PCR-strip tube was labelled per time point of the assay (0 minutes, 60 minutes, 120 minutes, and 180 minutes). Reactions were prepared for each time point as follows: 2.4 µL 25 mM $MgCl_2$, 2 µL 0.1 M DTT, 0.25 µL RNase inhibitor and a pre-

determined amount of FLAG-DICER1 IP (see above) and DICER1 storage buffer with protease inhibitors (see above) to a volume of 20 µL. All incubations were conducted at 37°C in a thermocycler. A wild-type FLAG-DICER1, FLAG-DICER1 E1813K and FLAG-DICER1 D1320A set of reactions were conducted as positive controls with each batch of *in vitro* cleavage reactions. Reactions were stopped by addition of 20 µL formamide loading dye (Invitrogen) and storage on ice after 0 minutes, 60 minutes, 120 minutes, and 180 minutes of incubation at 37°C.

Samples were boiled for 5 minutes and then resolved via denaturing 7M Urea PAGE (4.2 g urea + 4.5 ml 40% 19:1 Acrylamide/Bis solution (BioRad) + 1 ml 10x TBE melted in a 50 ml Falcon tube at 50°C for 3 minutes, vortexed and topped to 10 ml with ddH_2O with addition of 80 µL 10% APS + 8 µL TEMED (BioRad)). Samples were run for 2 hours at 200V in 1x TBE. Gels were wrapped in saran wrap and exposed to a storage phosphor screen (GE Healthcare) for 24 hours at 4°C. Autoradiographs were generated using phosphorimager (GE Storm 840, GE Healthcare) and used to determine the effect of FLAG-DICER1 mutants on 3p and 5p production.

Characterization of cleavage patterns was done according to categories previously described by Wu(96) with :

- DICER1 variants that cleave pre-miR-122 as efficiently as wildtype DICER1 = 5p + 3p
- DICER1 variants incapable of cleaving pre-miR-122 within 120 minutes = no cleavage
- DICER1 variants that produce 3p and 5p + loop = 5p with loop + 3p
- DICER1 variants that produce 3p + loop and 5p = 3p with loop + 5p

- DICER1 variants that have both reduced and delayed production of both 5p and 3p miRNAs = Delayed 5p and 3p, Reduced 5p and 3p

2.3.6. NanoString assay

To further investigate the impact of the "ball and socket" mutants on the overall expression of miRNAs, we generated 5 DICER1 mutant rescue cell lines in *Dicer1*$^{-/-}$ mouse mesenchymal stromal cells (MSC) previously generated by Wu(96), in which *Dicer1* exon 23 is removed.

2.3.6.1. Generation of stable mouse MSC *Dicer1* KO cell lines expressing FLAG-DICER1 mutant protein and selection of monoclonal lines

Generation of the stable cell lines followed the same protocol described above. Virally infected MSCs were single-cell sorted into a 96-well plate and then expanded with antibiotic selection (blasticidin 10 µg/ml) to 10 cm plates. DICER1 expression levels were evaluated by WB. Clones selected for the nanoString assay were determined to have similar expression of FLAG-DICER1 protein compared to *Dicer1*$^{flox/flox}$ by Western blot. MSC lines included DICER1 E1813K, D1320A, S1344L, T1733L and F1332A. Controls included parental *Dicer1*$^{flox/flox}$, *Dicer1*$^{-/-}$ and the DICER1 wild-type rescue.

2.3.6.2. RNA extractions

RNA extractions from mouse MSC were done using the mirVana miRNA Isolation Kit (Ambion) according to manufacturer's instructions. RNA extractions were done from 3 different replicates for each DICER1 cell line.

2.3.6.3. nCounter miRNA expression panel

miRNA differential expression profile using the NanoString nCounter Mouse v1.5 miRNA Expression Assay (Nanostring Technologies) according to the manufacturer's instructions was done using NanoString technology at the LDI Molecular Pathology Research Core. Approximately 100 ng purified total RNA was used for miRNA sample preparation (miRNA tagging following an annealing, ligation, and purification protocol). Next, using the miRNA CodeSet hybridization protocol, denatured samples were hybridized with the reporter and capture probes at 65°C for 16 hours. The samples were then processed with the nCounter Preparation Station to purify the hybridized targets and affix them to the cartridge for imaging using the nCounter Digital Analyzer (CCD camera). Barcodes were counted for each target molecule at maximum resolution 555 fields of view (FOV). The CodeSet incorporated 577 miRNAs based on miRbase v21, as well as 33 murine-associated viral miRNAs, 6 positive controls, 8 negative controls, 6 ligation controls, 5 spike-in controls, and 4 mRNA housekeeping controls (*ACTB*, *B2M*, *GAPDH* and *RPL19)*. Initial data QC and extraction of raw data was performed using the nSolver Analysis Software v4.0 (NanoString Technologies). Sample-by-sample unsupervised hierarchical clustering was performed based on Z-score transformation of miRNAs, using the 105 miRNAs that were expressed at levels above the background.

3. CHAPTER 3: RESULTS

3.1. Results SECTION 1: Resolving *DICER1*-associated tumours

3.1.1. SECTION 1 part I: *DICER1* sequencing in tumours with diagnostic uncertainty

Case 1 consisted of a lung lesion diagnosed in a 11-month-old female. Multiplex ligation-dependent probe amplification (MLPA) of the germline DNA did not reveal any large exon deletions or insertions in the *DICER1* gene. Sequencing of the tumour did not reveal a *DICER1* hotspot variant. Given the lack of *DICER1* hotspot, the case was reviewed by an expert pathologist (DB-DS) and was re-diagnosed as a CPAM type IV from its original diagnosis as a type I PPB.

Case 2 was referred to us as an "ovarian GCT" diagnosed in a 6-year-old female with a germline *DICER1* splice variant (c.5527+3A>G). However, review of the ovarian GCT by a specialist gynaecologic pathologist (WGM) resulted in a re-diagnosis of retiform SLCT. Tumour sequencing identified a *DICER1* RNase IIIb hotspot (c.5439G>T, p.E1813D) and targeted sequencing confirmed the presence of the germline in the tumour, thus confirming the suspicion of differential diagnosis by WGM. Cycloheximide treatment of the germline cDNA (performed by Nelly Sabbaghian) shows that the splice variant leads to exon 25 skipping (Figure 8).

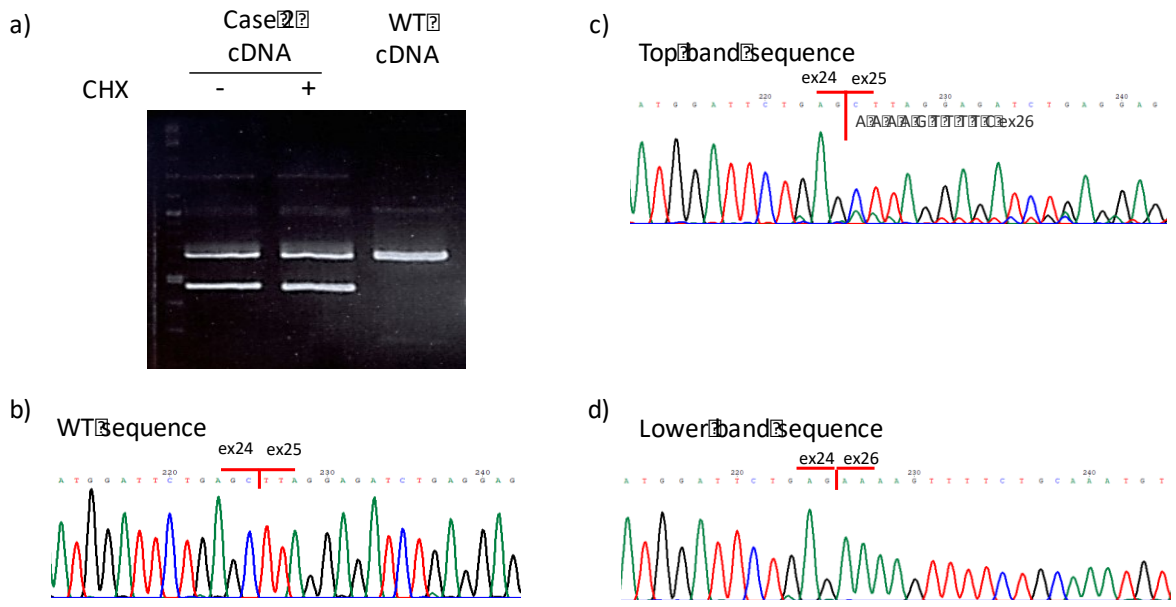

Figure 8: Cycloheximide treatment of the germline cDNA from case 2 with WT cDNA as control a) Agarose gel of cDNA from case 2 treated and untreated with cycloheximide (CHX). b) Chromatogram of wild-type (WT) sequence cDNA. c) Chromatogram sequence of the top band from case 2 cDNA treated with CHX shows wild-type and mutant sequence (exon 25 skipping). d) Sequencing for the lower band shows exon 24-exon-26 junction, producing an exon 25-skipping cDNA product. Figure provided by Nelly Sabbaghian.

Case 3 was diagnosed in a 41-year-old patient and was referred to us as a recurrent SCST-NOS. Review of the recurrent SCST-NOS tumour by WGM favoured a diagnosis of JGCT. *DICER1* germline sequencing and tumour sequencing of the RNase III hotspots was negative. Previous *FOXL2* screening of the tumour did not reveal the presence of a mutation, suggesting that the tumour was not an aGCT.

Case 4 was referred for *DICER1* sequencing due to the unusual diagnosis of an oERMS in a 60-year-old woman. A *DICER1* RNase IIIb hotspot missense (c.5438G>C, p.D1810H) and loss-of-heterozygosity (LOH) at the D1810H variant were identified. Germline sequencing was performed at the Royal Marsden Hospital, London and did not identify an underlying constitutional *DICER1* variant. Therefore, identified *DICER1* PVs are tumour-specific(2). This case was published in *American Journal of Surgical Pathology*(2).

Case 5 was published in *International Journal of Gynecological Pathology* and consisted of a subtle ERMS identified in a 19-year-old female(3). The features of the tumour were those of a conventional endocervical polyp, but showed positive immunoreactivity for myoD1 and myogenin, immunohistochemical markers for RMS(98). Sanger sequencing of *DICER1* exon 24 identified the presence of c.5125G>A, p.D1709N hotspot missense.

Case 6 was a SLCT identified in a 7-year-old girl harbouring a *DICER1* germline missense (c.5441C>T), which was shown to generate two protein products, the missense variant p.S1814L and the p.E1788fs*41 variant resulting from exon 25 skipping (95, 99). It is not known which product is dominant. Sanger sequencing of the SLCT revealed the presence of a somatic hotspot, c.5437G>A, (p.E1813K), located only one amino acid residue away from the germline variant. Cloning experiments confirmed that the presence of the germline mutation and the somatic hotspot in *trans* (Figure 9).

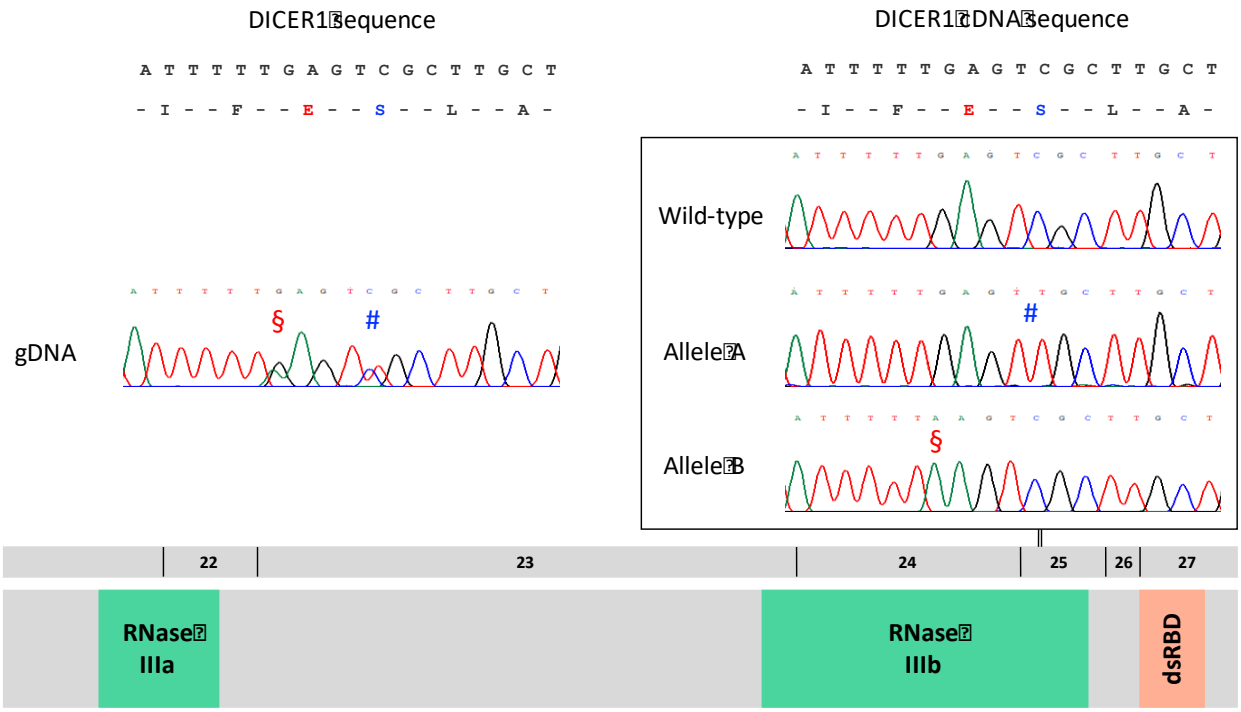

Figure 9: Graphic depiction of the biallelic nature of the *DICER1* variants identified in the case 6 SLCT

DICER1 gDNA sequencing for case 6 on the left side. Panel on the right depicts the wild-type cDNA sequence and corresponding amino acid sequence at the top. Wild-type chromatogram depicts the expected sequence. Allele A illustrates sequence observed in 10 clones out 24 for case 6, which harboured the germline hit c.5441C>T, p.[S1814L,E1788fs*41] (indicated by # in blue). Allele B harboured the somatic hit p.E1813K (indicated by § in red).

Cases 7 and 8 consisted of two SLCTs diagnosed in the same patient that were published in *Histopathology*(1). The right and left SLCTs were found to harbour hotspot missenses, *DICER1* c.5439G>T, p.E1813D and *DICER1* c.5438A>C, p.E1813A, respectively. The identification of two different hotspot variants confirms the idea that the two SLCTs represent distinct primary SLCTs and not metastasis from one ovary to another(1).

For the final case, Fluidigm sequencing revealed the presence of a DICER1 GPV (c.1870C>T, p.R624*) in the MB (case 9), which was diagnosed in a 3-year-old boy. No *DICER1* RNase III somatic hotspot missense was identified in the tumour, suggesting that MB is not part of the *DICER1* syndrome spectrum. LOH was also not observed.

All *DICER1* sequencing results are summarized in Table 7.

Table 7: *DICER1* sequencing results for cases with diagnostic uncertainty

Case	Pathology	***DICER1* sequencing**		Final diagnosis
		Germline	Somatic	
1	CPAM type IV/ PPB type I	Negative	Negative	CPAM type IV
2	OGCT/SLCT	c.5527+3A>G	c.5439G>T, p.E1813D	retiform SLCT
3	JGCT/SCST-NOS	Negative	Negative	JGCT
4	oERMS	Negative	c.5438G>C, p.D1810H and LOH	No change
5	subtle ERMS	Not known	c.5125G>A, p.D1709N	No change
6	Primary SLCT	c.5441C>T, p.[S1814L,E1788fs*41]	c.5437G>A, p.E1813K	No change
7*	Right primary SLCT	Not known	c.5439G>T, p.E1813D	Primary SLCT
8*	Left primary SLCT	Not known	c.5438A>C, p.E1813A	Primary SLCT
9	Medulloblastoma	c.1870C>T, p.R624*	Negative	No change

* These two cases are from a same patient with bilateral SLCT.

All somatic missenses were observed in heterozygosis, except in case 4.

CPAM, congenital pulmonary abnormal malformation; ERMS, embryonal rhabdomyosarcoma; JGCT, juvenile granulosa cell tumour; oERMS, ovarian embryonal rhabdomyosarcoma; OGCT,

ovarian granulosa cell tumour; PPB, pleuropulmonary blastoma; SCST-NOS, sex-cord stromal tumour not otherwise specified; SLCT, Sertoli-Leydig cell tumour.

3.1.2. SECTION 1 part II: *DICER1* sequencing in SLCTs and SCST-NOS over 50 years of age

DICER1 hotspot mutations were identified in 2 MD-SLCTs and the *FOXL2* hotspot was identified in 2 SLCTs. All remaining SLCTs were negative for *DICER1* and *FOXL2* mutations as well as the 3 SCST-NOS cases. *DICER1* and *FOXL2* sequencing results are described in Table 8. The whole *DICER1* gene was not assessed for cases harbouring a somatic hotspot since *DICER1* GPV was not suspected given patient history and age of diagnosis (mean age of diagnosis = 12.7 years in *DICER1* carriers)(71).

Table 8: *DICER1* and *FOXL2* sequencing results for SLCTs/SCST-NOS diagnosed in patients over 50 years of age

Case	Age of diagnosis	Pathology	***DICER1* results**		***FOXL2* results**
			Germline	**Somatic**	
1	64	MD-SLCT	n/a	c.5439G>T, p.E1813D	Negative
2	56	MD-SLCT	n/a	c.5127T>G, p.D1709E	Negative
3	56	MD-SLCT	Negative	Negative	Negative
4	48	MD-SLCT	n/a	Negative	Negative
5	62	PD/MD-SLCT	Negative	Negative	Negative
6	63	SCST, NOS	Negative	Negative	Negative
7	71	SCST, NOS	Negative	Negative	Negative
8	51	SCST, NOS	Negative	Negative	Negative
9	50	SLCT	n/a	Negative	c.402C>G, (p.C134W)
10	74	PD/MD-SLCT	n/a	Negative	c.402C>G, (p.C134W)

3.2. Results SECTION 2: The identification of *DICER1* variants in NSCLC

3.2.1. Sequencing of normal tissue from CARIS Life Sciences tumours suggests somatic biallelic *DICER1* cases

None of the *DICER1* variants observed in the CARIS tumours was identified in the matched tissue normal (Table 9), thereby showing that the observed mutations are tumour-specific. This confirms the possible role of *DICER1* tumour-only variants in adult-onset tumours that exist outside of the *DICER1* syndrome spectrum.

Table 9: *DICER1* mutation status observed in the tumour and matched normal of 14 tumours from CARIS Life Sciences

Case	Age	Sex	Submitting Histology	***DICER1* variants observed in the tumour**		***DICER1* variants observed in the normal**	
				Suspected germline mutation	**Hotspot mutation**	**Suspected germline mutation**	**Hotspot mutation**
Case 1	22	F	SLCT	D727fs	E1813V	Neg	Neg
Case 6	56	F	SLCT	E1532*	E1813K	Neg	Neg
Case 9	53	F	UAC	K1486fs	D1709N	Neg	Neg
Case 10	64	F	UAC	R937H	E1813Q	Neg	Neg
Case 14	43	F	UCS	S520I	D1709N	Neg	Neg
Case 20	39	F	LUAD	Q1580*	E1813D	Neg	Neg
Case 21	74	F	LUAD	Q1614*	E1813Q	Neg	Neg
Case 22	60	M	COAD	R201H	D1810V	Neg	Neg
Case 24	47	F	Uterine sarcoma	c.5095+2T>A	D1709N	Neg	Neg
Case 26	55	F	Vaginal sarcoma	S1076fs	D1810Y	Neg	Neg
Case 27	39	F	UAS	K1123*	E1813G	Neg	Neg
Case 28	74	F	UAS	R821H, R1060H	D1810Y	Neg	Neg
Case 32	27	F	THCA	c.4047_4050 +5delinsTT	E1813D	Neg	Neg
Case 37	17	F	YST	T350fs	D1810Y	Neg	Neg

COAD, colon adenocarcinoma; EAC, endometrioid adenocarcinoma; LOF; loss-of-function; LUAD, lung adenocarcinoma; Neg, negative; SLCT, Sertoli-Leydig cell tumour; THCA, thyroid carcinoma; UAS; uterine adenosarcoma; UCS, uterine carcinosarcoma; YST, yolk sac tumour

3.2.2. *DICER1* NSCLC Final breakdown and *CTNNB1*

To establish the occurrence of biallelic *DICER1* tumour-only variants in adult-onset tumours, we tested normal tissue DNA from 14 adult-onset tumours sequenced by CARIS Life Sciences (Phoenix, AZ) for the suspected *DICER1* LOF and hotspot mutations. Eight of the tumours (cases 1, 6, 24, 26, 27, 28, 32, 37, (Table 9)) represent already known phenotypes of *DICER1* syndrome, whereas six tumours, which included two lung adenocarcinomas (cases 20 and 21), have not been reported to occur in *DICER1* syndrome. Sanger sequencing of all 14 normal tissue DNA samples did not reveal any *DICER1* variants, thereby confirming that the identified *DICER1* variants were confined to the tumour.

Because of our prior reports of somatic-only *DICER1* PVs in PB(78), we focused on NSCLC, specifically the NSCLCs from the CARIS Life Sciences database. We identified 236 (1.9%) NSCLC cases harbouring one or more *DICER1* PPV after classification from a total of 12,147 NSCLC cases. Of those 236 cases, 225 were single-hit *DICER1* cases (95.3%) and 11 were two-hit *DICER1* cases (4.7%). Of the 11 *DICER1* two-hit cases, seven cases were found to harbour a truncating *DICER1* pathogenic variant and a RNase IIIb hotspot, following the two-hit model of tumourigenesis seen in other *DICER1*-related lesions. Two additional hotspot-positive cases were present in the *DICER1* single-hit cases, giving a total of 9 *DICER1* hotspot-positive cases (3.8%) (Table 10). No

significant differences were observed for age, smoking status and tumour histology between the *DICER1* hotspot-positive and hotspot negative groups.

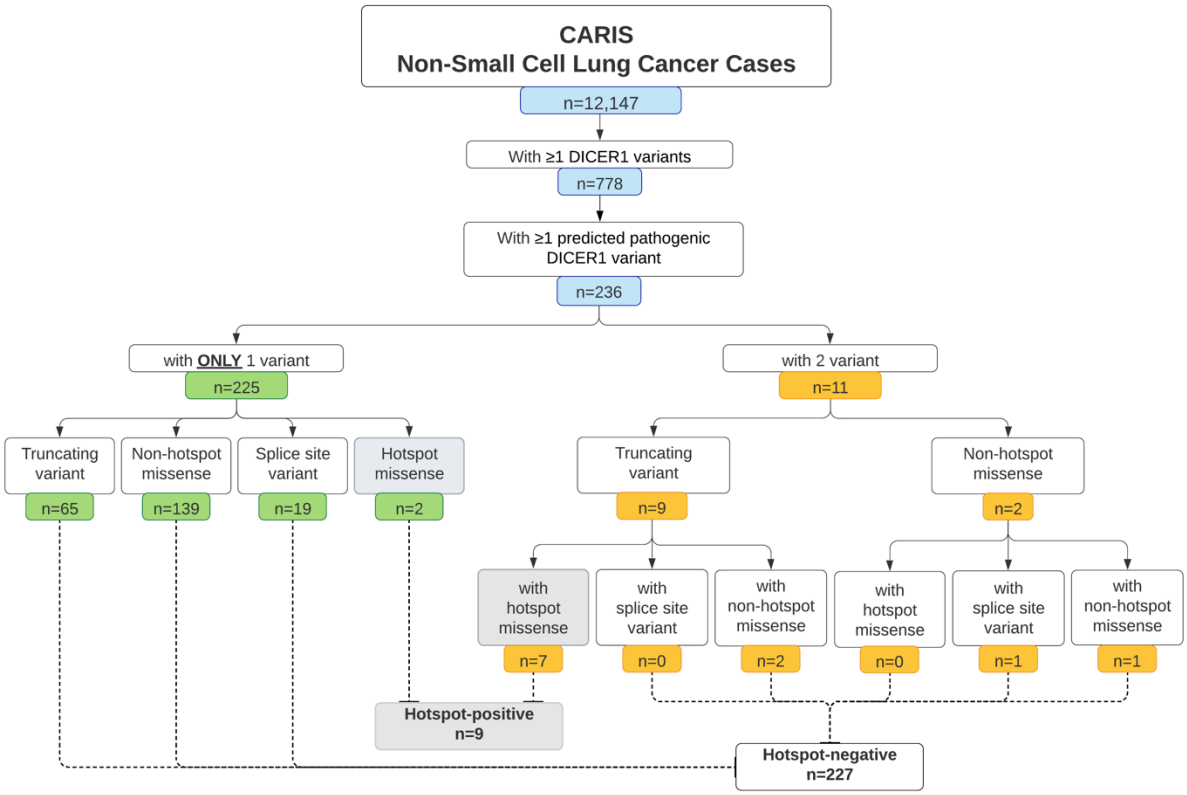

Figure 10: Breakdown of *DICER1*-positive NSCLC cases from CARIS Life Sciences

CARIS Life Sciences database of 12,147 NSCLCs was queried for all NSCLC cases harboring one or more *DICER1* variants. NSCLC cases harboring *DICER1* nonsense, frameshift, canonical splice site, or *DICER1* RNase IIIa and RNase IIIb hotspot missense variants were classified as predicted pathogenic variants. All *DICER1* non-hotspot missense variants were assessed using 6 in silico variant effect prediction tools as described by de Kock *et al.* (100). Cases with *DICER1* predicted pathogenic variants were then subdivided according to number of DICER1 variants and then

further subdivided according to type of *DICER1* variant harbored (i.e., hotspot missense, truncating variant, non-hotspot missense and splice site variant.)

Table 10: *DICER1*-hotspot positive NSCLC cases

Case	Diagnosis	*CTNNB1*	*DICER1*	Other genes
Case 20	Adenocarcinoma, metastatic, NOS	p.D32Y	p.Q1580* p.E1813D	*APC* p.R1640fs
Case 21	Adenocarcinoma, NOS		p.Q1614* p.E1813Q	*CDKN2A* p.E88*; *KRAS* p.G12I; *STK11* p.G171fs
Case 102	Adenocarcinoma, NOS		p.Q1614* p.E1813Q	*CDKN2A* p.E88*; *KRAS* p.G12I; *STK11* p.G171fs
Case 327	Adenocarcinoma, metastatic, NOS		p.E1813Q	*TP53* p.R306*
Case 397	Adenocarcinoma, metastatic, NOS	p.T41A	p.E194* p.D1810Y	*TP53* p.R158H
Case 467	Carcinoma, metastatic, NOS	p.S37F	p.W400* p.D1810Y	
Case 723	Adenocarcinoma, NOS	p. H36_S37delinsRF p.S33C	p.W1831* p.D1709N	*STK11* p.D68fs; *U2AF1* p.S34F
Case 751	Malignant tumour, spindle cell type		p.D1810Y	*APC* p.G871*; *TP53* p.R273L
Case 789	Mucinous adenocarcinoma	p.D32Y	p.W1506* p.E1705K	*PIK3CA* p.E418K, p.E453K; *TP53* p.R282W

Comparison between the mutational landscape of *DICER1* hotspot-positive and hotspot-negative cases revealed a higher frequency of *CTNNB1* mutations occurring in the hotspot-positive cases compared to the hotspot-negative cases (5/9 versus to 2/227; $p<0.00001$, respectively) (Figure 11). The top 5 mutated genes included *TP53*, *KRAS*, *STK11*, *CDKN2A* and *ARID1A*, with *TP53* and *KRAS* mutations showing significant mutual exclusivity ($p<0.001$) (Figure 11) (and Appendix I) for all mutated genes). The overall total of non-*DICER1* mutations per sample in the *DICER1*

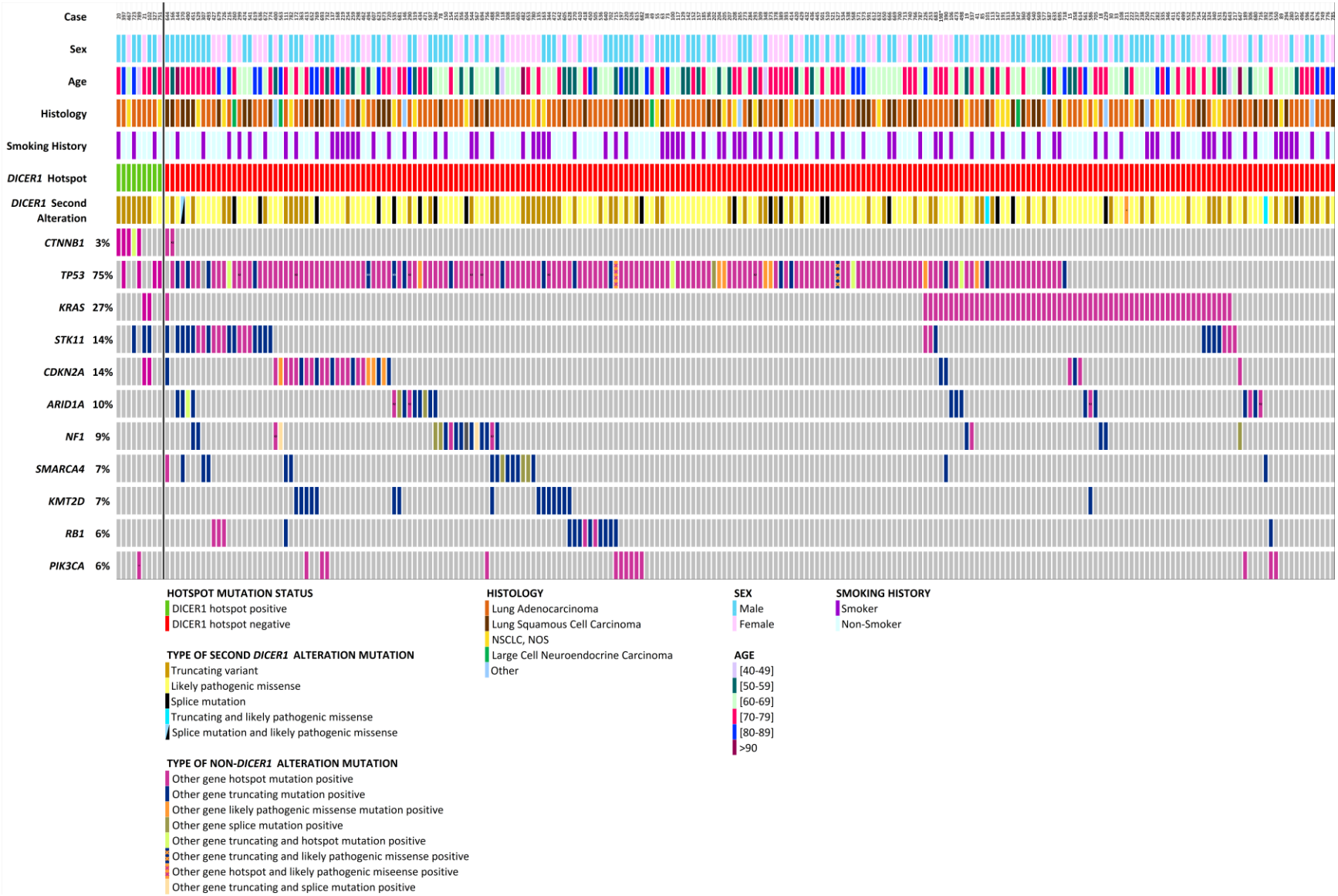

Figure 11: OncoPrint of CTNNB1 and top 10 mutated genes in DICER1-mutated NSCLCs from CARIS Life Sciences

hotspot-positive and *DICER1* hotspot-negative groups showed no significant difference. However, the two groups showed a significant difference in the variance between the *DICER1* hotspot-positive and *DICER1* hotspot-negative cases (F-test, $F_{(224,8)} = 4.281$, $p = 0.0314$), suggesting a significant difference in the distribution/spread of the samples given their overall total of non-*DICER1* variants.

To establish if *CTNNB1* mutations are a feature of other *DICER1*-related tumours, we performed β-catenin immunohistochemistry on the *DICER1* TMAs. The only tumour showing positive nuclear staining was PB, with all three cases positive, and showing stronger nuclear staining in the epithelial component compared to the mesenchymal component (Figure 12). These three PBs, previously published by de Kock *et al.* (78), have been shown to harbour *CTNNB1* PVs. Notably, none of the *DICER1*-mutated PPBs demonstrated nuclear positivity (Figure 10D and E). Many lesions showed normal membranous staining of epithelial cells, with weaker membranous or cytoplasmic staining of mesenchymal cells, including the PBs. This staining was not considered significant with respect to a *CTNNB1* variant. Thus, nuclear staining correlated with the presence of a *CTNNB1* mutation, as expected, and was not related simply to a *DICER1* variant.

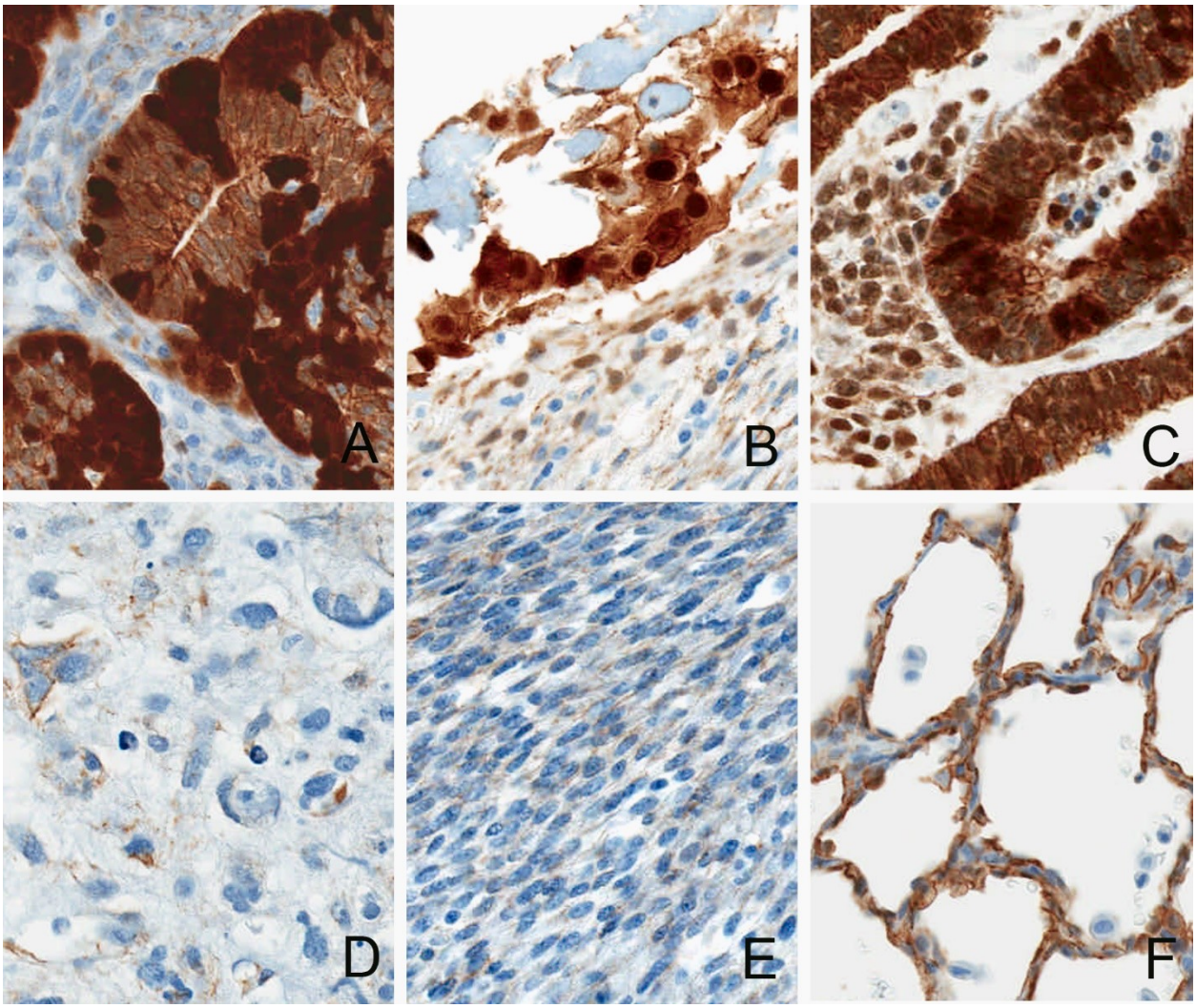

Figure 12: Expression of β-catenin by immunohistochemistry.

(A-C) Three cases of pulmonary blastoma with *CTNNB1* mutations show strong nuclear staining for β-catenin in a significant proportion of epithelial cells, as well as less intense staining in some stromal cells in B and C. In addition, there is diffuse membranous staining of epithelial cells (normal). (D&E) Two cases of pleuropulmonary blastoma type III that lack *CTNNB1* mutations show only membranous staining for β-catenin (focal in D and more diffuse but weak in E). (F) Normal lung shows diffuse membranous staining of alveolar epithelial cells but no nuclear staining. (Original magnifications: A-F x200). Figure produced by Paul Thorner.

3.3. Results SECTION 3: Crosstalk between RNase IIIa and RNase IIIb domains of DICER1

3.3.1. *in vitro* cleavage results

In vitro cleavage reactions of the radiolabelled pre-miR-122 by DICER1 WT showed appropriate cleavage producing both 3p and 5p miRNA species (Figure 13b panel I). Cleavage by RNase IIIb canonical mutant (p.E1813K) showed aberrant cleavage of the 5p strand, producing a mature 3p miRNA product and intermediate 5p+loop product (Figure 13b panel II) and cleavage by the RNase IIIa canonical mutant (p.D1320A) showed aberrant cleavage of the 3p strand, generating a 5p and 3p+loop intermediate product (Figure 13b panel III). Four DICER1 mutants (p.M1317A, p.R1347L, p.F1706A and p.R1736L) were shown to behave similarly to wild-type protein, producing 5p and 3p cleavage products (Figure 13c and 13d panel I and V). Two mutants showed no cleavage activity whatsoever (p.F1332A and p.Y1717A) (Figure 13c panel III and 13d panel II) and two showed delayed or reduced activity (p.T1328A and p.Y1721A) (Figure 13c panel II and 13d panel III). The RNase IIIb mutant p.T1733L was shown to behave like a RNase IIIa mutant, producing an aberrant 3p+loop intermediate and 5p (Figure 13d panel IV). The cleavage products generated by each mutant are summarized in Table 11.

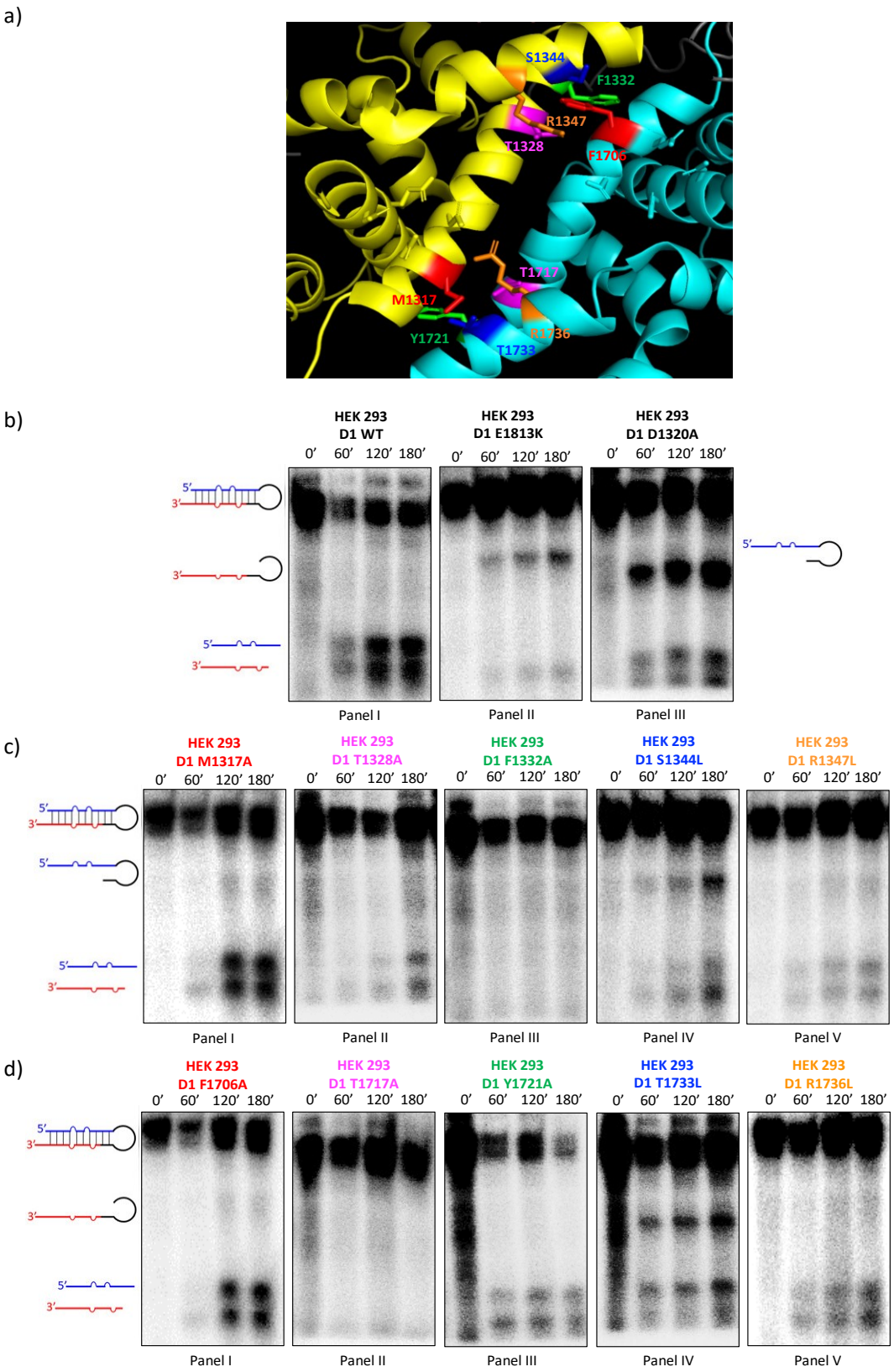

Figure 13: in vitro cleavage of Hs-DICER1 “ball and socket” residue mutants

a) “Ball and Socket” junction amino acid residues of the RNase IIIa and RNase IIIb domains in Hs-DICER1. “Ball” residues are labelled in red. “Socket” residues are labelled in magenta, green, blue and orange. Equivalent residues of the RNase IIIa and IIIb domain are labelled in the same colour. Illustration was done using Hs-DICER1 cryo-EM structure 5ZAK published by Liu et al. in Cell (2018). b) *in vitro* cleavage of radio-labeled precursor-miRNA-122 by DICER1 WT and RNase IIIa and RNase IIIb canonical mutants. A representative cleavage pattern of DICER1 WT shows production of 3p and 5p miRNAs. RNase IIIb mutant E1813K shows aberrant cleavage of the 5’ strand of pre-miRNA, generating mature 3p and a 5p+loop intermediate. RNase IIIa mutant D1320A generates 3p+loop intermediate cleavage products and mature 3p and 5p miRNA. c) Autoradiographs for *in vitro* cleavage of DICER1 RNase IIIa mutants. d) Autoradiographs for *in vitro* cleavage of DICER1 RNase IIIb mutant.

Table 11: *in vitro* cleavage products of DICER1 RNase IIIa and RNase IIIb mutants

Type of DICER1 variant	*DICER1* mutation	Cleavage products
CONTROLS	Wild-type	5p + 3p
	c.5437G>A, p.E1813K	5p with loop + 3p
	c.3959A>C, p.D1320A	3p with loop + 5p
RNase IIIa	c.3949_3950ATdelinsGC, p.M1317A	5p + 3p
	c.3982A>G, p.T1328A	Delayed 5p and 3p
	c.3994_3995TTdelinsGC, p.F1332A	No cleavage
	c.4031C>T, p.S1344L	5p with loop + 3p
	c.4031G>T, p.R1347L	5p + 3p
RNase IIIb	c.5116_5117TTdelinsGC, p.F1706A	5p + 3p
	c.5149A>G, p.T1717A	No cleavage
	c.5161_5162TAdelinsGC, p.Y1721A	Reduced 5p and 3p
	c.5197_5198CdelinsCT, p.T1733L	3p with loop + 5p
	c.5207G>T, p.R1736L	5p + 3p

Review of various population and tumour databases show few reports of variants affecting the "ball and socket" junction residues, except for p.S1344, where the p.S1344L variant is now recognized as a canonical hotspot variant(90). For the most part, reported variants affecting the "ball and socket" residues are synonymous mutations (Table 12), suggesting a selective pressure ensuring specific "ball and socket" residue interactions to maintain proper DICER1 cleavage and thereby suggesting that missense variants at these sites are likely to affect DICER1 activity.

Table 12: List of variants affecting "ball and socket" junction residues observed in population and tumour database

"Ball and socket" residues	cBioportal	TCGA	COSMIC	Clinvar	gnomAD	ExAC
M1317	--	--	--	--	p.M1317V (x1) (germline)	
T1328	--	p.T1328= (x1)	--	--	--	
F1332	--	--	--	--	--	
L1343		p.L1343= (x1)	p.L1343F (x1)			
S1344	p.S1344L (x5)† p.S1344T(x1)†	p.S1344= (x1) p.S1344L (x5)† p.S1344T (x1)†	p.S1344L (x5)‡	p.S1344L (x1) p.S1344X (x1)	p.S1344= (x2)	
R1347	--	--			--	
F1706	--	p.F1706= (x1)§	p.F1706= (x1)§ p.F1706L (x1)	p.F1706L (x1) (germline)	--	--
T1717	--	--	--	p.T1717= (x2)	--	
Y1721	--	--	--	p.Y1721= (x2) p.Y1721C (x1) p.Y1721X (x1)	p.Y1721= (x3)	p.Y1721= (x1)
L1732				p.L1732= (x2)		
T1733	--	--	--	p.T1733= (x2)	--	
R1736	--	p.R1736W(x1) (germline)	p.R1736L (x2) p.R1736Q (x2)	p.R1736= (x3)	p.R1736= (x3)	

† cBioportal cases are the same as those reported in TCGA

‡ Excluded the cases already reported in TCGA and Clinvar

§ Indicates same case reported in both TCGA and COSMIC database

3.3.2. NanoString Results

Nanostring analysis was performed on RNA isolated from five mouse Dicer1$^{-/-}$ cell lines that expressed either wild-type DICER1 or a variety of *DICER1* mutations (i.e., E1813K, D1320A, S1344L, T1733L and F1332A). Dicer1$^{flox/flox}$ and Dicer1$^{-/-}$ were included as positive and negative controls, respectively. Clustering of miRNA expression indicated that RNase IIIa and IIIb canonical mutants (E1813K and D1320A) clustered more closely with the Dicer1$^{-/-}$, while DICER1 T1733L

and S1344L clustered more closely to Dicer1$^{flox/flox}$ and DICER1 WT (Figure 14). miRNA profiling of the different DICER1 mutants identified 98 differentially expressed miRNAs (n = 39 3p miRNAs; n = 59 5p miRNAs) that showed a maximum read count above 50 and where the Dicer1$^{-/-}$ KO and WT results showed appropriate directionality, with miRNA expression levels being downregulated in the Dicer1$^{-/-}$ KO and miRNA expression being up in the Dicer1$^{flox/flox}$ and DICER1 WT cell lines (Figure 16a). The DICER1 F1332A was observed to cluster together with the Dicer1 $^{-/-}$ KO, showing low expression levels for the majority of 5p (89.8%) and 3p miRNAs (89.7%). These included miRNAs like the members of the mmu-let-7 family, mmu-miR-181a, mmu-miR-149, mmu-miR-152 and mmu-miR-132(Figure 14a). Cells expressing the DICER1 E1813K mutant displayed lower levels of 98.3% of expressed 5p miRNAs, whereas cells expressing the D1320A mutant displayed lower levels for 94.8% of differentially expressed 3p miRNAs (Figure 15). The RNase IIIa S1344L mutant was observed to negatively impact only a select number of 5p miRNAs (n = 32) such as mmu-miR-106b, mmu-let-7b, mmu-let-7i, mmu-miR-20a and mmu-miR-99a (Figure 15). The RNase IIIb T1733L mutant altered the expression of both 3p (e.g., mmu-miR-152, mmu-miR-148a, mmu-miR-221 and mmu-miR-23b) and 5p miRNAs (e.g., mmu-miR-872, mmu-miR-30b and mmu-miR-145) (Figure 15), however affecting more 3p miRNAs compared to 5p miRNAs. A large proportion of differentially expressed miRNAs (70.4%) can be divided into 4 main groups based on expression patterns and mutation status, if excluding the F1332A mutant: 1) only affected by DICER1 E1813K (DICER1 E1813K-only), 2) affected by only DICER1 E1813K and S1344L (DICER1 E1813K/S1344L), 3) only affected by DICER1 D1320A (DICER1 D1320A-only) and 4) affected by only DICER1 D1320A and T1733L (DICER1 D1320A/T1733L) (Figure 16b and c). The differential expression analysis showed that 14 out of 59 5p miRNAs are downregulated by the

DICER1 E1813K-only and 21 miRNAs are downregulated by E1813K/S1344L group (Table 13). The remaining miRNAs (29.6%) are affected by other combination of the mutants (Figure 15).

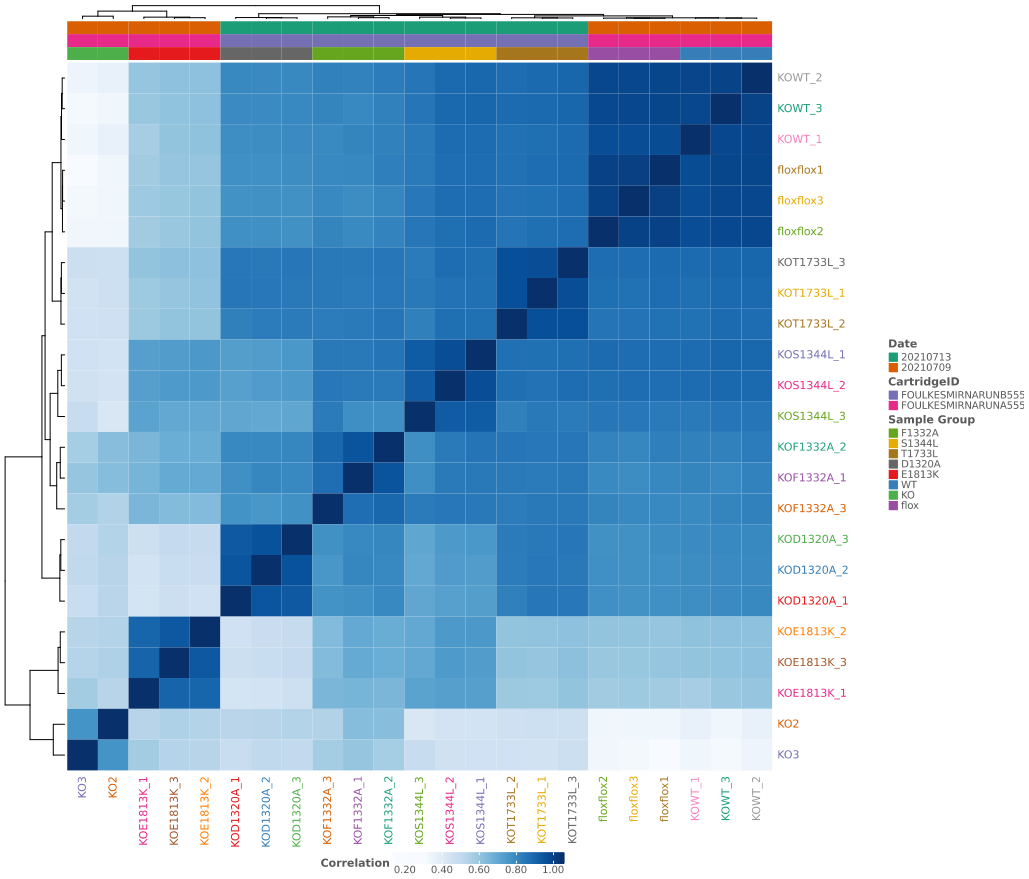

Figure 14: Clustering of miRNA expression in 8 DICER1 mouse cell lines by the ROSALIND®

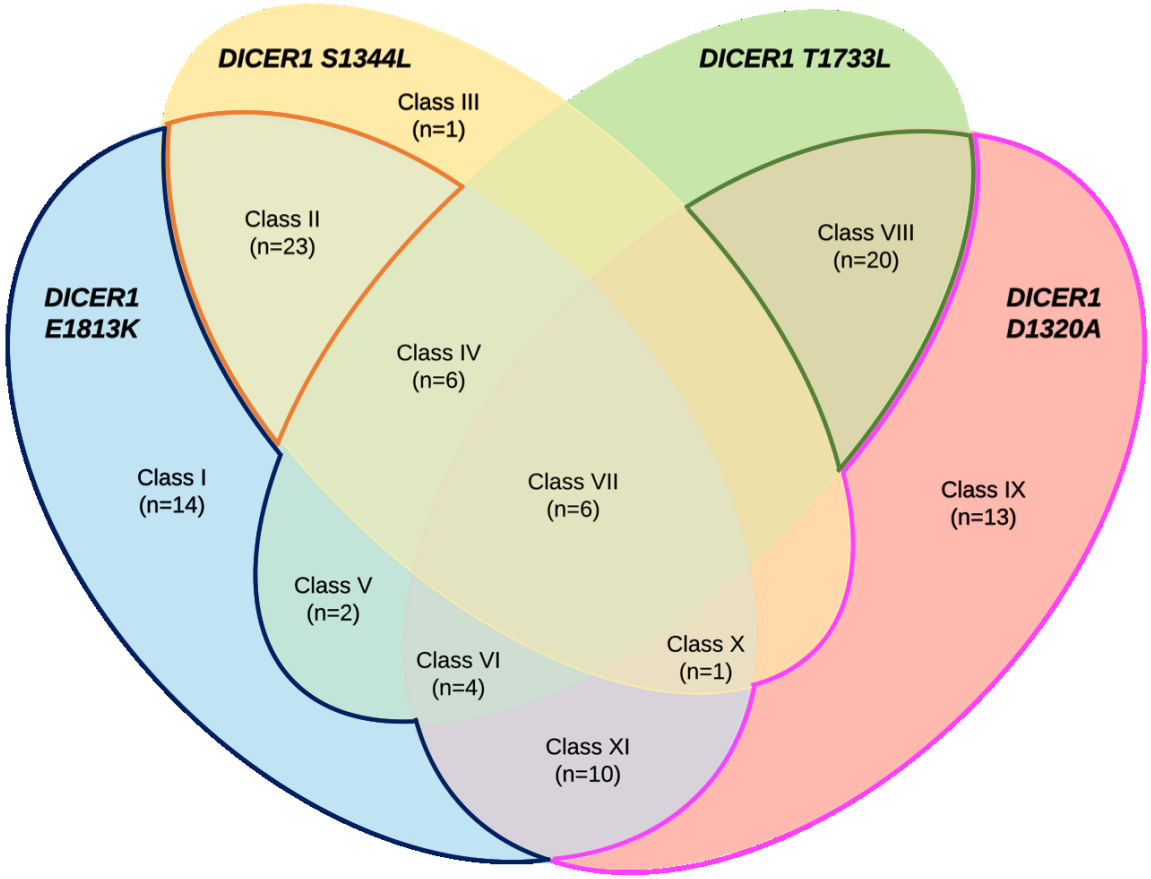

Figure 15: Breakdown of miRNAs downregulated by the DICER1 mutants

The DICER1 E1813K-only group highlighted by the dark blue line. DICER1 E1813K/S1344L group highlighted by the orange outline. DICER1 D1320A-only group is outlined in the magenta and DICER1 D1320A/T1733L group outlined in green. List of miRNAs in each class in Appendix II.

Table 13: Summary of downregulated 3p and 5p miRNAs seen in the four miRNA expression groups

miRNA expression group	Total number of differentially expressed 3p miRNAs (n = 39)	Total number of differentially expressed 5p miRNAs (n = 59)
	Downregulated 3p miRNAs	Downregulated 5p miRNAs
DICER1 E1813K-only	0	14
DICER1 E1813K/S1344L	0	21
DICER1 D1320A-only	13	0
DICER1 D1320A/T1733L	20	0
Other combinations	6	24

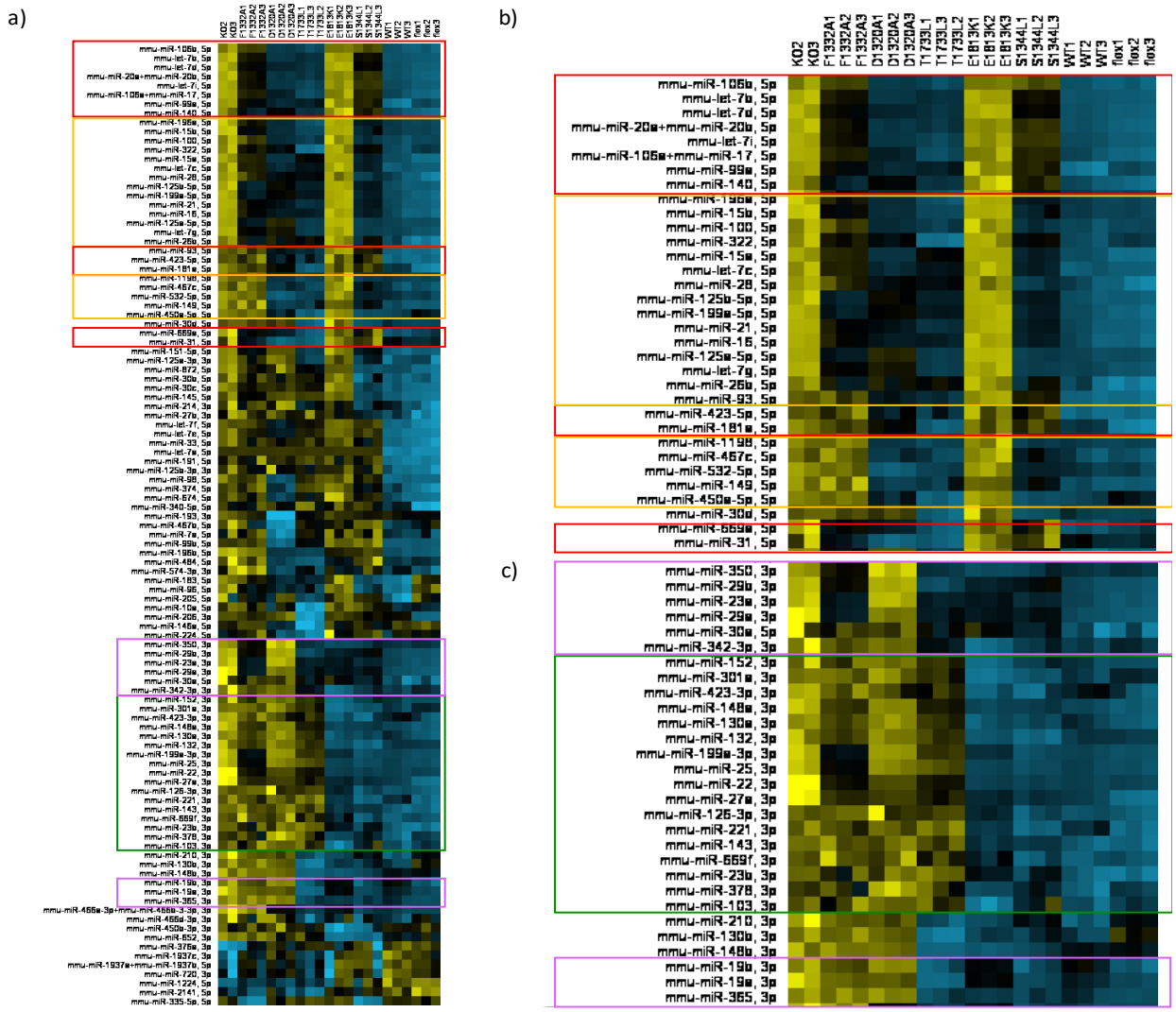

Figure 16: 105 differentially expressed miRNAs based on nanoString data from 8 DICER1 mmuMSC cell lines (Dicer1$^{flox/flox}$, Dicer1$^{-/-}$ KO, DICER1 WT, DICER1 E1813K, DICER1 D1320A, DICER1 S1334L, DICER1 T1733L and DICER1 F1332A)

a) Heatmap of all 105 differentially expressed miRNAs. Red rectangles indicate miRNAs affected by the DICER1 E1813K-only group. Yellow rectangles highlight miRNAs affected by the DICER1 E1813K/S1344L group. Purple rectangles show miRNAs affected by the D1320A-only group. Green box indicates miRNAs affected by DICER1 D1320A/T1733L. b) Heatmap focuses on the

miRNAs affected by the DICER1 E1813K-only and DICER1 E1813K/S1344L groups. c) Heatmap focuses on the miRNAs affected by the DICER1 D1320A-only and DICER1 D1320A/T1733L groups.

4. CHAPTER 4: DISCUSSION

4.1. Discussion of results SECTION 1: The value of *DICER1* sequencing in elucidation of rare and challenging presentations of *DICER1* neoplasms

DICER1 sequencing has allowed the elucidation of various tumours with rare and difficult diagnoses. The CPAM type IV, retiform SLCT and JGCT cases emphasize the value of *DICER1* sequencing in determining the correct diagnosis. CPAMs are developmental abnormalities affecting the fetal lung, with more than 70% of cases undergoing a wait and see strategy(101) as surgical resection is recommended in symptomatic patients and observation recommended in asymptomatic ones(102, 103). However, PPBs can readily transition from cystic to solid to metastatic lesions, surgery is recommended before possible progression of the tumour. Approximately 70% of PPBs harbour GPVs(70), and no clear genetic predisposition exists for CPAMs(104). Therefore, *DICER1* sequencing is crucial in determining the proper diagnosis, since CPAM type IV and PPB type I are indistinguishable on imaging, but also in determining appropriate clinical management.

Both aGCTs and JGCTs are sex cord-stromal tumours like SLCTs, which for the most part are molecularly distinct entities from each other and from SLCTs. As mentioned previously, approximately 95% of aGCTs harbour a somatic *FOXL2* PV (c.402C>G, p.C134W)(44) and approximately 85% of JGCTs harbour in-frame duplication in *AKT1*(46), while a large proportion of SLCTs harbour *DICER1* PVs(32, 33, 35, 40, 41). One study has also identified hotspot activating *GNAS* PVs (at position 201) in nine out of 30 JGCT(105). Although *DICER1* mutations have been reported in JGCT(32-34) and SCST-NOS(35), these are very few and there are some important differences in treatment of these tumours. Given that recurrence or metastasis is quite common

in aGCTs(106), fertility-sparing surgery is the mainstay of treatment. Recurrence in JGCTs(42) is rare, however fertility-sparing surgery seems to be the only proven treatment for stage 1A JGCT(107). PD-SLCTs, MD-SLCTs and retiform SLCTs are often aggressive and therefore adjuvant chemotherapy is recommended in addition to surgery(108-110). Once more, correct diagnosis allows for proper clinical management. Furthermore, surveillance guidelines have been reported for patients with a GPV as they are at risk for developing other *DICER1* syndrome-related tumours such as CN, MNG and SLCTs(111, 112). It has been reported that in patients with a GPV the risk of developing a tumour before the age of 10 is 5.3% and before the age of 60 is 31.5%(113).

The case of the ovarian ERMS represents the second oERMS reported associated with a *DICER1* PV(2). The first case was identified in a 6-year-old girl and the tumour was found to harbour two *DICER1* variants (c. 1196_1197dupAG and c.5435G<A)(114). The oERMS presented in this work harboured two *DICER1* alterations, c.5438G>C coupled with LOH and was published by McCluggage *et al*.(2). The first case was identified in a 6-year-old girl and the oERMS was found to harbour two *DICER1* PVs (c. 1196_1197dupAG and c.5435G<A)(114). ERMS arising from the ovary are especially rare as they usually arise from the uterine corpus and the cervix(55, 115). The pathological diagnosis of ERMS of the female genital tract can be difficult as it exhibits significant morphological overlap with other tumour types, especially adenosarcoma which can exhibit rhabdomyoblastic differentiation. A review of ERMS and adenosarcoma illustrated the difficulties in distinguishing between the two tumour types (no consensus for 28%)(116). The presence of cartilage favours the diagnosis of ERMS as no *DICER1*-associated adenosarcomas contained cartilage(116). Pathological review of the tumour showed the presence of cartilage

like the previously reported *DICER1*-associated oERMS(114) and similarly to other *DICER1*-associated uterine ERMS, where cartilage was present in approximately 50% of cases (36, 53). *DICER1* PVs have also been reported in a case of ectomesenchymoma, an RMS with mesenchymal and neuroectodermal components, which presented at an uncharacteristic age and anatomic location(117). Similar to the oERMS presented in this work, the ectomesenchymoma also exhibited cartilage formation, suggesting that ERMS arising from unusual sites and showing presence of cartilage or bone are more likely to be associated with *DICER1* PVs.

Case 5 is a subtle ERMS reported in 19-year-old female without a history of DICER1 syndrome(3). cERMS represents one of the two most common tumour types that affects the female reproductive system in DICER1 syndrome(55, 59, 116, 118, 119). This case represents one of two cases of subtle ERMS published by Yoon *et al*(3). Both cases resembled conventional endocervical polyps with absence of phyllodes-like architecture, but showed positive immunoreactivity for myoD1 and myogenin, immunohistochemical markers for RMS(98). The lack of phyllodes-like architecture ruled out the differential diagnosis of adenosarcoma. Though no *DICER1* GPV was identified in the subtle EMRS presented in this work, the second case of subtle ERMS found to harbour a second somatic mutation (c.5428G>T; p.D1810Y) was diagnosed in a 21-year-old female with a DICER1 GPV (c.3907_3908delCT; p.Leu1303Valfs*4)(3). The identification of the second somatic mutation in this second case was helpful in raising suspicion of the possibility of "early" cervical ERMS for the case presented in this work. These two cases, which represent the earliest discernable cERMS, emphasize the idea that "subtle" ERMS may arise from within conventional endocervical polyps with positive staining for myogenin and

myoD1 and that *DICER1* sequencing plays a considerable role in determining the proper diagnosis of these subtle tumours. Furthermore, the identification of somatic *DICER1* mutations suggest the existence of possible *DICER1* GPVs, which are important to recognize for the same reasons stated above regarding clinical management of DICER1 syndrome patients.

Case 6 represents an interesting *DICER1* case of a female diagnosed with a SLCT at 7 years and MNG at 12 years(89, 95). *DICER1* germline sequencing was done previously and identified a missense (c.5441C>T, p.[S1814L,E1788fs*41]). This variant was also previously identified in a family of six first-degree relatives with MNGs(99). This variant is unusual as it is in the RNase IIIb domain and is not predicted to be truncating. Sequencing of the SLCT identified a hotspot missense mutation (c.5437G>A, p.E1813K) located just one amino acid away from the germline variant. Although the p.E1813K and p.[S1814L,E1788fs*41] variants are only one amino acid away, they cause very different phenotypes when seen in the germline(70, 120, 121). The typical hotspot mutation such as p.E1813K, when occurring in the germline, is only seen in the mosaic state since it directly affects one of the critical metal ion binding residues of the RNase IIIb, thus affecting miRNA processing and causes a much more severe phenotype such as multiple disease foci at significantly younger ages(70, 120, 121) and a sub-type of DICER1 syndrome that has been referred to as GLOW (**G**lobal development delay, **L**ung cysts, **O**vergrowth and **W**ilms tumour)(120). The S1814 residue, on the other hand is not a critical metal ion binding residue. Moreover, even though the p.S1814L variant is not predicted to be truncating, exon cassette experiments have demonstrated that it causes exon 25 skipping, producing the p.E1788fs*41 product(95) and *in vitro* cleavage experiments by Wu has demonstrated that the mutant cause

aberrant DICER1 pre-miRNA cleavage, generating 5p with loop + “less” 5p + “less” 3p cleavage products(96). This might explain why the p.[S1814L,E1788fs*41] phenotype is more consistent with typical *DICER1* syndrome (MNG and SLCT).

Cases 7 and 8 are SLCTs diagnosed in the same patient but arising from separate ovaries (published by McCluggage *et al*.)(1). *DICER1* somatic sequencing revealed two separate *DICER1* hotspot missenses c.5439G>C, p.E1813D and c.5438A> C, p.E1813A in right and left ovary, respectively. The identification of distinct hotspot mutations provides conclusive molecular evidence of independent contralateral neoplasms, which is of clinical significance since it excludes diagnosis of metastasis or of recurrence, which indicate adverse prognosis, and which require different clinical management. Though many reports of bilateral SLCTs exist(1), germline *DICER1* sequencing has only been investigated in nine cases and all nine cases were found to have a germline *DICER1* mutation(62, 99, 122, 123), suggesting that the identification of two distinct hotspot missenses is indicative of a *DICER1* germline variant in patients with bilateral SLCTs. Although the identification of distinct *DICER1* hotspots variants confirms the occurrence of independent tumours, the identification of a same hotspot variant however does not necessarily preclude the possibility of independent neoplasms. For tumours harbouring the same *DICER1* hotspot variant, molecular tumour profiling by NGS-based approaches (e.g. WES or Comprehensive Genomic Profiling (Illumina)), DNA methylation profiles and subclonality evolution analyses can be used to distinguish between metastatic disease/recurrence and second primary cancers(124-126).

Case 9 is a MB diagnosed in a patient carrying a *DICER1* GPV c.1870C>T, (p.R624*). Pedigree of the patient showed a family history of MB, suggesting the involvement of *DICER1* in MB. MB has not previously been reported as part of the DICER1 syndrome spectrum, therefore we questioned the status of MB as a *DICER1*-related tumour. *DICER1* sequencing of the MB was negative for a somatic DICER1 variant and sequencing of the parents' germline DNA revealed that the *DICER1* GPV segregating in the non-MB side of the family. This indicated that the MB was not related to DICER1 at all. A study by Pugh *et al*. investigated the spectrum of mutations in 92 MBs(127). They performed whole-exome sequencing (WES) of matched tumours and normal DNA for every case and did not identify any *DICER1* variant(127), further emphasizing that *DICER1* does not play a role in MB development.

Another type of CNS neoplasm which has been occasionally reported in DICER1 syndrome is neuroblastoma. We previously identified a 14-year-old female who presented with MNG, NB and CN(64). Sequencing revealed the presence of a *DICER1* GPV c.4566_4570dupCTTTG, p.V1524fs*38 and of somatic RNase III hotspot mutations in the MNG and CN of the patient. No RNase III somatic variant was identified in the NB, suggesting that this tumour might not be DICER1-related(64). We also recently sequenced another case of a seven-year-old with a *DICER1* germline VUS (c.4891T>G, p.S1631A) that was diagnosed with NB and anaplastic sarcoma of the kidney (ASK)(128). Sanger sequencing of both tumours revealed the presence of a somatic hotspot missense in the ASK, but not in the NB. Another study by Pugh *et al.* investigated the genetic landscape of 240 NBs by performing WES of matched and normal DNA for every case. They did not identify any *DICER1* variants(129). Therefore, the lack of *DICER1* hotspot missense

in the MB and both NBs suggest that *DICER1* does not seem to contribute to development of these tumour types and that they may be connected to the *DICER1* syndrome via non-canonical mechanisms or simply due to chance, as these types of tumours are not rare.

Previous research by Karnezis *et al.* showed that *FOXL2*-mutated SLCTs were diagnosed in older patients of peri-/post-menopausal age (median age of 79.5 years, range 51 to 90 years)(49), thereby exhibiting some overlap with the age of diagnosis of aGCTs (median age between 50 and 54 years)(130). In the series of SLCTs/SCST-NOS diagnosed in patients over 50 years of age, I identified two SLCTs with *DICER1* mutations, two SLCTs with *FOXL2* mutations and six SLCTs/SCST-NOS without mutations in either of the two genes, corroborating the findings of Karnezis *et al*. describing three molecular subtypes of PD-/MD-SLCTs (*DICER1*-mutated, *FOXL2*-mutated and *DICER1/FOXL2*-wild-type). Karnezis *et al.* did not identify a *DICER1*/*FOXL2*-mutant subtype, which is consistent with previous findings by Goulvent *et al.*, which observed that *DICER1* and *FOXL2* mutations are mutually exclusive(32) and it is not known why the two genes are mutually exclusive. Given the difficulties in differentiating aGCTs and SLCTs, *DICER1* and *FOXL2* sequencing were crucial in determining proper pathology of the *FOXL2*-mutated samples.

A proposed algorithm for DICER1 analysis for tumours with diagnostic uncertainty is summarized in Figure 17.

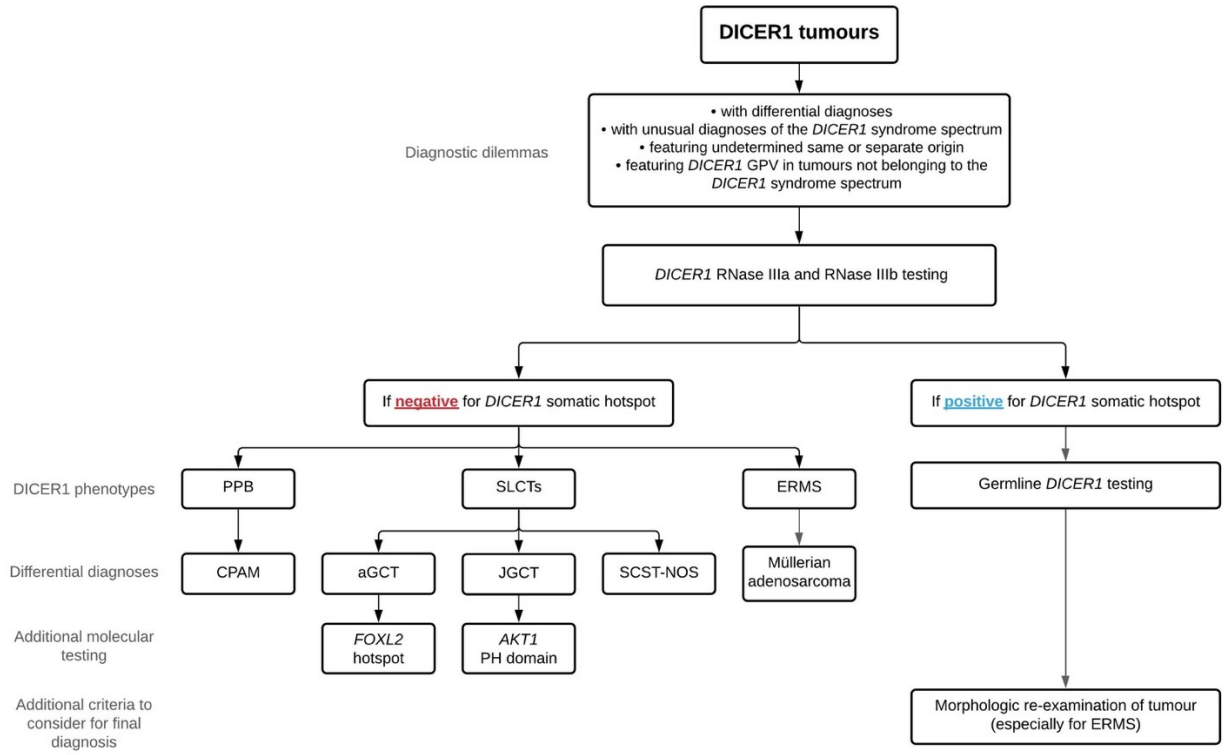

Figure 17: Proposed algorithm for DICER1 analysis strategy of tumours posing diagnostic dilemmas

4.2. Discussion of results SECTION 2: *DICER1* mutations in the lung demonstrate tight relationship with CTNNB1

We report a prevalence of 1.9% NSCLC in adults with a *DICER1* PPV and a prevalence of 0.06% NSCLC with biallelic *DICER1* alterations.

The majority of *DICER1* hotspot-positive cases harboured a second LOF PPV and sequencing of the normal tissue DNA from the 14 biallelic *DICER1* cases established that the *DICER1* biallelic PVs arose due to somatically, similarly to biallelic *DICER1* mutations seen in adult-onset PBs (78, 85).

DICER1 hotspot-negative NSCLC cases harboured a typical mutational landscape of NSCLC with the most frequently mutated genes being *TP53, KRAS, STK11, CDKN2A and ARID1A* (131-133).

Although, the total number of non-*DICER1* mutations in *DICER1* hotspot-positive cases compared with hotspot-negative tumours was not significant, the difference in variance is worth investigating further since the difference in sample size between the two groups (9 vs 225, respectively) was large. The identification of additional *DICER1* hotspot-positive NSCLCs is needed to get a more accurate view of the mutational landscape of *DICER1*-hotspot NSCLCs.

The analysis revealed a strong co-occurrence of *CTNNB1* mutations in *DICER1* hotspot-positive NSCLCs compared to NSCLCs without *DICER1* hotspot missenses. *CTNNB1* mutations have previously been reported in *DICER1*-associated L-FLACs (77, 79, 81), PPB (134), PB (78) and *DICER1* thyroid nodules(135). PB are biphasic carcinosarcomas consisting of malignant mesenchyme and epithelium(136), with *CTNNB1* mutations present in both epithelial and mesenchymal components. The exclusivity of β-catenin staining in the PB and the presence of *CTNNB1* mutations in *DICER1* hotspot-positive L-FLACs and NSCLCs suggests a tight relationship between *CTNNB1* and these *DICER1*-associated lung tumours. *CTNNB1* mutations have previously been reported in a subset of lung adenocarcinomas and were shown to affect residues of the GSK-3β phosphorylation site and lead to constitutive activation of Wnt pathway signalling (137). *CTNNB1* mutations have also been seen in *DICER1*-mutated endometrioid adenocarcinomas, but do not show significant co-occurrence in *DICER1* hotspot-positive cases compared to hotspot-negative cases. This further emphasizes a relationship between *DICER1* and *CTNNB1*. The DICER1-associated rare lung neoplasms PPB, PB and L-FLAC share interesting relationships regarding origin of the malignancy, with PPB being an exclusively mesenchymal tumour(136), L-FLAC being an epithelial tumour and PB being a biphasic with both malignant epithelial and mesenchymal components. Though *CTNNB1* mutations of the lung tumours have

been reported in both mesenchyme and epithelium, the *CTNNB1* mutation reported in the L-FLAC by de Kock *et al.* was found to be exclusive to the L-FLAC epithelium(79), which suggests that the DICER1 and *CTNNB1* relationship might be more specific to the lung epithelium as three out of four *DICER1*-associated neoplasms involve malignant epithelium (PB, L-FLAC and lung adenocarcinoma).

CTNNB1 mutations with *DICER1* somatic hits have also been identified in thyroid nodules(135). Both digestive and respiratory systems are derived from a common embryonic origin, the anterior foregut. In mouse, the anterior foregut then separates into a ventral anterior foregut endoderm and dorsal anterior foregut endoderm, with the ventral anterior foregut endoderm giving rise to the thyroid, lung, liver and pancreas(138) (Figure 18). Therefore, the co-occurrence of *DICER1* and *CTNNB1* mutations in organs of same embryonic origin suggests the possible role of Wnt signalling in adult-onset DICER1-associated lesions.

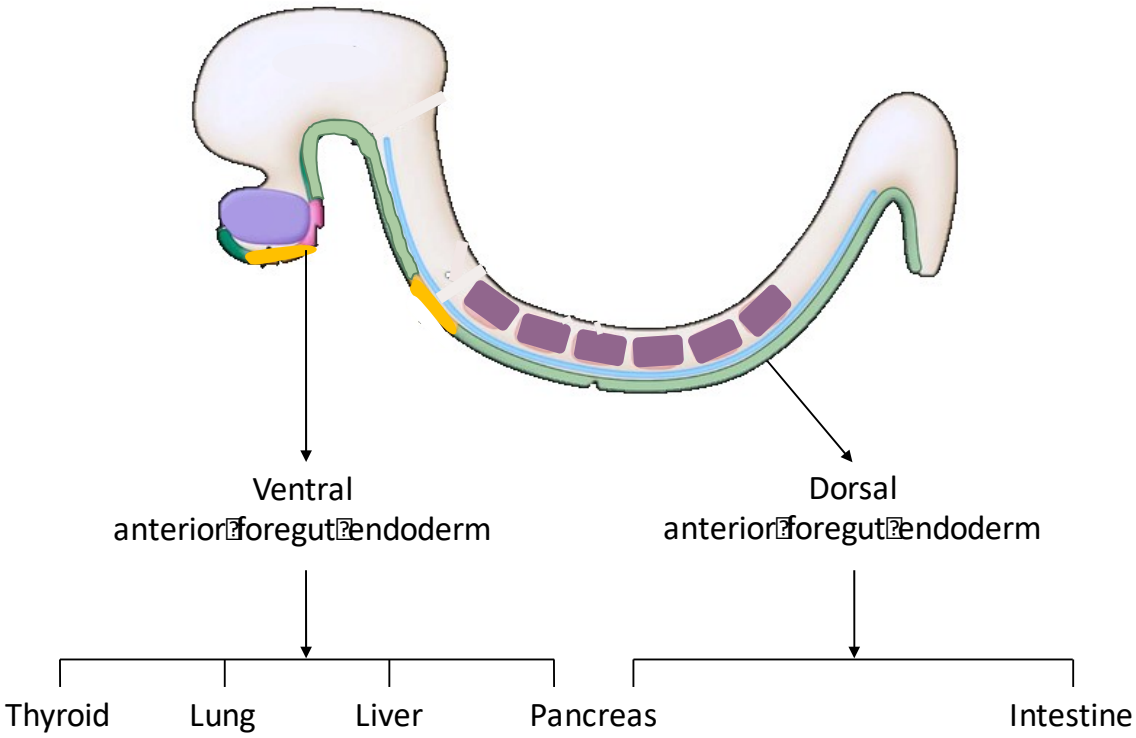

Figure 18:Embryonic development of the foregut endoderm. Adapted from Zaret *et al,* Sicence, 2009

Wnt signaling plays a key role in lung development, with β -catenin being responsible for initiation of respiratory development. Inactivation β-catenin in the epithelium of the lung has been shown to lead to aberrant branching and proximal-distal patterning after lung budding in mice(139, 140). In the thyroid, the relationship between Wnt signalling and thyroid hormone (TH) signalling is believed to have antagonizing effects, with TH stimulation leading to Wnt pathway signalling silencing through interactions of TH receptor-β and β-catenin(141, 142).

4.3. Discussion of results SECTION 3: The interdependency of RNase domain crosstalk for synchronization

Homologous mutant residues exhibited similar cleavage activity, generating one of the three cleavage patterns (wild-type, abnormal and trans-acting). Both "ball" residue mutants, p.M1317A and p.F1706A and the homologous arginine "socket" residue mutants showed wild-type DICER1 cleavage. "Socket" residue mutants p.T1328A and p.F1332A and their homologs p.T1717A and Y1721A, respectively, showed no cleavage activity whatsoever or reduced/delayed activity. Homologous mutants p.S1344L and T1733L exhibited trans-acting cleavage effects, generating opposite cleavage patterns to the canonical mutant of their respective RNase III domains (Table 14). The observation of similar cleavage effects from homologous residues of the RNase IIIa and RNase IIIb domain emphasizes the importance of the "ball and socket" junction interactions in *Hs*-DICER1 *in vitro*.

Table 14: Similar cleavage patterns exhibited by homologous residues of the RNase IIIa and RNase IIIb domains

		Ball residue	Cleavage products		Socket residues	Cleavage products
"Ball and socket" junction 1	RNase IIIa	M1317A	5p + 3p (wild-type)	RNase IIIb	T1717A	No cleavage
					Y1721A	Reduced 5p and 3p
					L1732	---- (not assessed)
					T1733L	3p with loop + 5p
					R1736L	5p + 3p (wild-type)
"Ball and socket" junction 2	RNase IIIb	F1706A	5p + 3p (wild-type)	RNase IIIa	T1328A	Delayed 5p and 3p
					F1332A	No cleavage
					L1343	---- (not assessed)
					S1344L	5p with loop + 3p
					R1347L	5p + 3p (wild-type)

Equivalent residues are labelled in the same colour.

The mutants of the "ball" residues p.M1317A and p.F1706A did not affect DICER1 cleavage activity. Previous experiments by Blaszczyk *et al*. in the *Escherichia coli* RNase III (*Ec*-RNase III) evaluated five different mutants of the "ball" p.F40 (p.F40G, p.F40D, p.F40R, p.F40M and p.F40W), where p.F40 in *Ec*-RNase IIII corresponds to RNase IIIa p.M1317 and RNase IIIb p.F1706 in *Hs*-DICER1. They concluded that the mutations to the "ball' residue leading to absence of a side chain (p.F40G) or charged side chains (p.F40D and p.F40R) lead to defective RNase III activity, thereby demonstrating that the "ball" socket plays a critical role in proper enzyme function. They also concluded that the "ball" residue requires a hydrophobic side chain since p.F40M and p.F40W mutants showed no defective RNase activity(29). The change of the p.F40 residue to

methionine corresponds to the *Hs*-DICER1 RNase IIIa p.M1317 residue. Both methionine and tryptophan changes retain the large hydrophobic side chain structures like the original phenylalanine residue, suggesting the need for large hydrophobic side chains in proper 'ball and socket' interactions. Conservation analysis of the "ball" residue across the RNase III superfamily also supported this idea, with most preserving the phenylalanine and the others changing to residues with sizeable side chains (e.g., leucine, isoleucine, and threonine)(143). Therefore, the DICER1 "ball" residue mutants in this work looked to evaluate whether the size of the hydrophobic side chain contributes to proper "ball and socket" interactions for functional RNase III activity. Cleavage results of the DICER1 "ball" residue mutants DICER1 p.M1317A and p.F1706A further conclude that any hydrophobic side chain no matter the size is enough to maintain proper 'ball and socket" interactions and proper RNase function as the DICER1 "ball" residues in this work were mutated to alanine, i.e., bearing the smallest hydrophobic side chain. This suggest that the reported germline mutations affecting the "ball" residues in DICER1 (p.M1317V in gNOMAD and p.F1706L in Clinvar) most probably do not affect DICER1 enzyme activity.

Homologous "socket" residue mutants, p.R1347L and p.R1736L showed no effects on cleavage activity. The p.R1736 residue is highly conserved as a basic amino acid, either arginine or lysine, and interacts with the main-chain carboxyl group of the opposing "ball" residue as well as side-chain of hydroxyl group of p.T1717 and side-chain carboxyl group of the opposing p.D1320(143), implying the possible importance of hydrogen bond interactions in the "ball and socket" junctions. In this work, these "socket" residues were modified to leucine with the thinking that

the removal of the positively charged side chain would lead to disruption of cleavage activity. However, cleavage results showed that that is not the case. The change to leucine still retained a large non-polar side chain suggesting that perhaps the hydrogen bond interactions are not as essential as the hydrophobic interactions between the "ball and "socket" residues. Population and tumour database search identified a p.R1736L variant in one case of lung squamous cell carcinoma, a p.R1736Q variant in one gastric adenocarcinoma and one cholangiocarcinoma and a p.R1736W variant identified in the germline. Both p.R1736L and p.R1736Q were identified in tumours harbouring driver mutations in other more relevant genes such as *CDKN2A* in the lung tumour and *CTNNB1* in the cholangiocarcinoma, supporting the idea that these mutations are most likely benign given large preserved hydrophobic side chain. The p.R1736W also retains a large hydrophobic group, suggesting that this variant might also be benign.

The cleavage results of the majority of "socket" residue mutants exhibited aberrant cleavage of both the 3p' arm 5'p arm, i.e., defects in both RNase IIIa and RNase IIIb catalytic activity. This suggests that DICER1 cleavage activity may require synchronization of RNase IIIa and RNase IIIb catalytic activity in order to properly cut, showing interdependency of the interactions between RNase III domains. A study by Gan *et al.*(27) described a stepwise model of double-stranded RNA cleavage in the bacterial Aa-RNase III consisting of three conformational steps – 1) the "minor conformation" consisting of conformation of the catalytic site immediately after the phosphoryl transfer (Figure 19C), 2) the "major conformation" consisting of the first step towards release of the cleaved RNA substrate with the 5' phosphate of the RNA substrate having moved away from the catalytic center (Figure 19D) and 3) the "product release" with the 3' end-processed RNA

having moved far away from the catalytic center (figure 19E)(27). Given the evolutionary conservation of RNase III enzymes in eukaryotes, it is reasonable to predict that this stepwise model would also apply to *Hs*-DICER1. Specifically, that support interdependency of RNase III domains in DICER1 would be required for synchronization of cleavage events by the two catalytic centers. In the absence of such a system, the absence of synchronization would imply that as one arm of the pre-miRNA is being cleaved, the mature miRNA would withdraw away from the catalytic site ("product release") and that the remaining loop+strand intermediate would also start distancing itself from the catalytic center ("major conformation") thereby possibly affecting the positioning of the pre-miRNA substrate for proper cleavage of the other pre-miRNA arm.

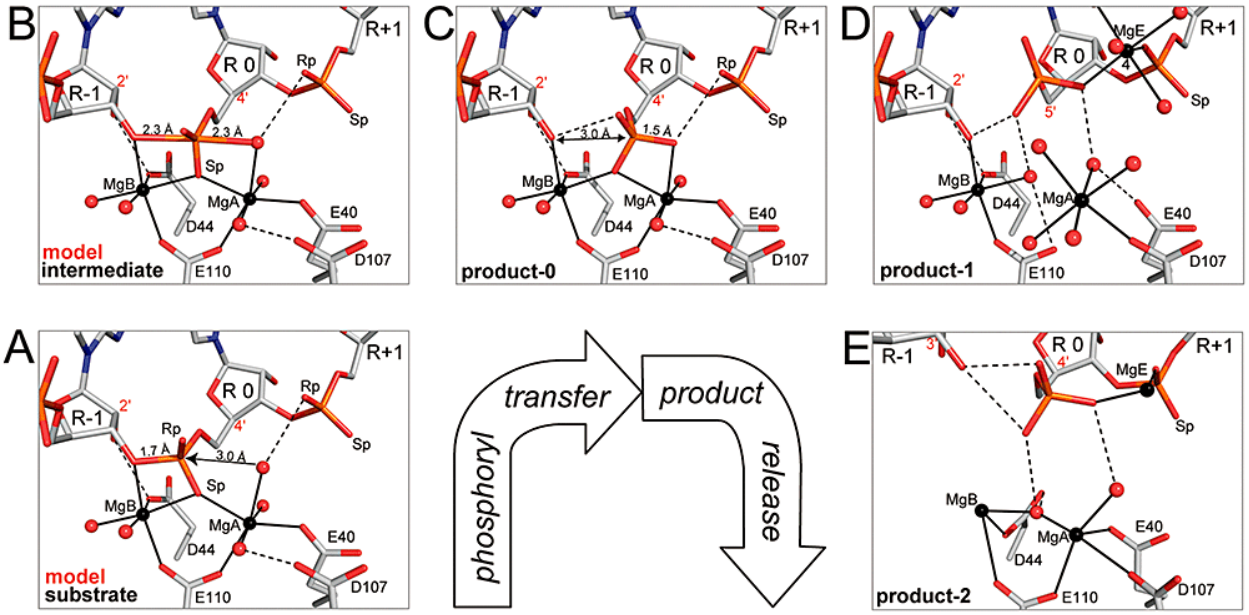

Figure 19: Stepwise model of RNa cleavage by Aa-RNase III

A) Molecular model for the Aa-RNase III/RNA complex. Shows nucleophilic attack of the 5' phosphorus. B) Molecular model of the Aa-RNase III/RNA reaction complex intermediate (transition state). C)"Minor conformation" of the Aa-RNase III-MgRNA9 substrate. It shows the

cleavage site assembly immediately after cleavage of the scissile bond/phosphodiester bond of the dsRNA. D) "Major conformation" of the Aa-RNase III-MgRNA9 substrate. It illustrates the first step towards product release with 5' phosphate having moved away from the cleavage site. E) The "product release" of the Aa-RNase III-MgRNA8 structure. 3'end-product has also moved away from the cleavage site. Taken from Gan *et al.* Molecular Microbiology, 2007.

4.3.1. miRNA differential expression profiling

Notwithstanding that the *in vitro* cleavage assay was limited by the evaluation of different DICER1 mutants in the context of only one pre-miRNA (pre-miR-122), miRNA expression profiling of cells expressing different DICER1 mouse MSC mutants corresponded with the DICER1 cleavage effects observed in the *in* vitro cleavage assays. The miRNA profiling revealed 98 differentially expressed miRNAs that showed a maximum read count above 50 and where the $Dicer1^{-/-}$ and WT results showed appropriate directionality, with $Dicer1^{-/-}$ miRNA expression levels being downregulated and $Dicer1^{flox/flox}$ and DICER1 WT miRNA expression being up.

The mouse MSC DICER1 E1813K mutant was shown to negatively affect all differentially expressed 5p miRNAs, which is consistent with the role of the RNase IIIb p.E1813 residue in cleavage of the 5p arm and the mouse MSC DICER1 D1320A mutant showed downregulation of almost all differentially expressed 3p miRNAs (94.8%), also consistent with the role of the RNase IIIa p.D1320 residue in cleavage of the 3p arm of the pre-miRNA. We also observe lower levels of select 5p miRNAs in the DICER1 p.D1320A expressing cells such as mmu-miR-30b, mmu-miR-

145, mmu-let-7a. This is consistent with cleavage findings by Gurtan *et al.* which suggested that the DICER1 p.D1320A mutant negatively affects the efficiency of RNase IIIb processing (21). Gurtan *et al.* also performed small RNA-sequencing of *Dicer1*$^{-/-}$ cells and showed no recovery of 3p miRNAs miRNA and partial recovery of 5p expression in DICER1 p.D1320A expression cells (21) further emphasizing the effect of p.D1320A on RNase IIIb processing. The downregulation of 3p miRNAs and of select 5p miRNAs demonstrates that DICER1 p.D1320A has a broader negative impact on miRNA expression compared to the RNase IIIb canonical mutant. This in combination with the absence of RNase IIIa metal-ion binding residue mutants in human samples suggests that mutating the active residues of the RNase IIIa may be too damaging – maybe incompatible with life.

miRNA expression profiling of the DICER1 p.F1332A mutant showed downregulation of almost all differentially expressed 3p and 5p miRNAs similarly to the expression profile seen in the DICER1 KO. The miRNA expression profile observed corresponded with the *in vitro* cleavage assay results that showed no DICER1 cleavage activity at all in the p.F1332A mutant. Both the p.F1332A mutant and its homolog p.Y1721A showed aberrant cleavage. These residues are highly conserved as aromatic residues as they are not only involved in formation of the "ball and socket" junctions, but are also involved in the dimerization of the RNase III domains via hydrophobic interactions with p.R1314 and p.H1325 for p.Y1721 and p.R1703 and L1707 for p.F1332 (143). Therefore, removal of the large side chain not only disrupts the "ball and socket", but also the dimerization, thereby having a two-fold effect on the positioning of the metal ion-binding residues of the opposing catalytic center.

4.3.2. The trans-acting DICER1 variants – p.S1344L and p.T1733L

The trans-acting cleavage effect of the p.T1733L mutant indicates that the p.T1733 is likely coupled to the RNase IIIa catalytic center similar to the p.S1344 and the RNase IIIb catalytic site, as was previously suggested by Vedanayagam *et al*.(90). Crystal modelling of Aa-RNase III D44N/dsRNA complex by Gan *et al*. demonstrated the role of p.S68 (equivalent to p.S1344 in Hs-DICER1) in forming a hydrogen bond with the nucleotide in the cleavage site and indicated its role in determining substrate specificity and selection of the phosphodiester bond for cleavage(92). Modeling of the p.S1344L mutant by Vedanayagam *et al.* demonstrated that the mutant residue is closer to the active site of RNase IIIb domain compared to the wild-type S1344 residue (19.60 ± 2.62 Å vs 11.7 ± 2.0 Å distance)(90). This may suggest that the change from threonine to leucine in p.T1733L may also bring the residue closer to the active site of RNase IIIa. Evolutionary coupling studies that identify pairs of residues that are evolutionarily constrained as interacting pairs not only showed higher coupling scores between the RNase IIIb p.T1733 residue and the RNase IIIa metal ion-binding residues (p.E1316, p.D1320, p.D1561, p.E1564) compared to those of the RNase IIIa p.S1344 and the RNase IIIb metal-ion binding residues (p.E1705, p.D1709, p.D1810 and p.E1813), but also showed coupling of p.T1733 and p.E1705 in the top ranked pair, indicating possible greater functional coordination of p.T1733 and the RNase IIIb catalytic center. This is further supported by the miRNA profiling of the p.T1733L mutant which showed downregulation of a subset of 5p miRNAs. The p.S1344 did not show any significant coupling to the RNase IIIa active residues. The broader effect of the DICER1 p.T1733L on miRNA expression of both 3p and 5p miRNAs compared to the p.S1344L suggest that the p.T1733 might be more important for RNase III catalytic processing compared to the p.S1344

residue. This may also serve to explain why no missense mutations affecting p.T1733 have not been reported in any population or tumour database compared to its homolog p.S1344 (see Table 10).

The differentially expressed miRNAs showed four main expression patterns depending on DICER1 mutation status, if excluding the p.F1332A mutant: 1) miRNAs only affected by DICER1 p.E1813K (DICER1 p.E1813K-only), 2) miRNAs affected by DICER1 p.E1813K and p.S1344L (DICER1 p.E1813K/p.S1344L), 3) miRNAs only affected by DICER1 p.D1320A (DICER1 p.D1320A-only) and 4) miRNAs affected by DICER1 p.D1320A and p.T1733L (DICER1 p.D1320A/T1733L) (Figure 16b) and c)). Although the DICER1 p.E1813K mutant was shown to affect all 5p miRNAs, only 14 5p miRNAs were shown to be negatively affected by exclusively by the DICER1 p.E1813K mutant and approximately 20 being affected by the DICER1 p.E1813K/p.S1344L group (Figure 15). Similar numbers of negatively impacted 3p miRNAs were observed in the DICER1 p.D1320A-only group (n = 13) and the DICER1 p.D1320A/T1733L group (n = 20), however these represent a higher proportion of the differentially expressed 3p miRNAs, suggesting that the impact of the DICER1 p.D1320A and p.T1733L mutants is more severe on 3p miRNA expression compared to 5p miRNA expression. Outside of these four main groupings, some 3p miRNAs were seen to be affected not only by the canonical RNase IIIa, but also by the canonical RNase IIIb mutant, suggesting a possible direct role of the RNase IIIb catalytic center on processing of these miRNAs or indirect effects due to genetic ripple (i.e. changes in 5p miRNA impacting a transcription factor which in turn affects select 3p levels (Figure 15). The same was also seen for a subset of 5p miRNAs.

DICER1 germline RNase IIIb hotspot mutations are only seen in mosaic form(70, 120, 121), with one exception(144, 145), as DICER1 germline mutations affecting RNase IIIb hotspots in considered to be incompatible with life since the mutations directly affect the critical metal ion binding residues of the RNase IIIb, thereby affecting miRNA processing. Patients harbouring a mosaic hotspot mutation occurring at p.E1813 present with a much more severe phenotype with includes a greater number of lesions occurring at significantly younger ages(121) and features of GLOW(120) compared to patients harbouring *DICER1* GPV or mosaic LOF mutations. The DICER1 RNase IIIa p.S1344L mutant has been recently reported in the germline of a patient presented with complex "DICER1 syndrome plus" phenotype which included multiple tumours (PPB, CN, WT and L-FLAC) as well as various physical anomalies and intellectual disabilities. The DICER1 RNase IIIa p.S1344L mutant was also reported in the germline in another case with a similar phenotype presented at a paediatric pneumology association meeting in Vienna(146). This "DICER1 syndrome plus" phenotype is believed to be a more severe, but distinct phenotype compared to that of DICER1 RNase IIIb mosaics. Though giving rise to a worse phenotype, the existence of the p.S1344L variant in the germline suggests that it may be less damaging compared to the RNase IIIb p.E1813K mutant which has never been reported in the germline, indicating that this variant may be incompatible with life. The absence of the DICER1 p.E1813K mutant in the germline also suggests that the 5p miRNAs exclusively downregulated by the p.E1813K may be more critical compared to those that are shared by regulating general aspects of cell physiology, whereas the miRNAs (e.g. members of the let-7 family) affected by both the DICER1 p.E1813K and p.S1344L mutants may play a more vital role in tumorigenesis(147). The miRNA expression profiling showed that although some matching effects were observed in p.S1344L and p.E1813K

which supports the trans-acting effect of p.S1344L on the RNase IIIb catalytic processing, the DICER1 p.S1344L mutant had a more limited effect on miRNA expression compared to the DICER1 p.E1813K mutant, which may explain the reasoning behind the differences in clinical presentation of patients with mosaic RNase IIIb hotspot compared to patients with germline DICER1 p.S1344L, but also genetic inheritance of these RNase III mutants.

5. CHAPTER 5: CONCLUSION AND FUTURE DIRECTIONS

5.1. SECTION 1 and 2: Unifying diagnoses

In this work, *DICER1* mutation analysis was used to evaluate a series of nine cases presenting with various diagnostic dilemmas, a series of SLCTs/SCST-NOS diagnosed in older patients and a series of biallelic DICER1 tumours. For the series of nine cases, *DICER1* sequencing was critical for final determination of tumour pathology with *DICER1* hotspot testing representing a simple genetic test that can be done in a molecular pathology laboratory since absence of a hotspot is indicative of the tumour most likely not being *DICER1*-related. With respect to the SLCTS/SCST-NOS series, *DICER1* sequencing validated findings by Karnezis *et al.* describing three molecular subtypes of SLCTs. Here, the correct classification of DICER1-related lesions has clear implications on clinical management as identification of somatic hotspots suggests the existence of *DICER1* GPVs. Future studies of the *DICER1*/*FOXL2* wild-type SLCTs/SCST-NOS include WES analysis to get a better understanding of the molecular basis of this group.

Sequencing of the biallelic tumours *DICER1* pathogenic variants are present in approximately 2% of NSCLCs, suggesting a potential broader role of *DICER1* in NSCLC. The *DICER1* hotspot-positive NSCLCs co-occurring with *CTNNB1* variants do not harbour variants in the main driver genes of NSCLC (*EGFR* and *KRAS*), suggesting a possible synergistic role of *DICER1* and *CTNNB1* variants in driving this subset of NSCLCs. As previously discussed, of this relationship in this subset of NSCLCs proposes novel avenues for possible drug therapies. Pathology review and β-catenin staining of the *DICER1* hotspot-positive NSCLCs would provide additional details for characterization of this subset of NSCLCs.

Similar to the work in this thesis, the recent characterization of *DICER1*-related sarcomas has also emphasized the utility of *DICER1* mutation analysis in correctly classifying *DICER1*-related sarcomas(148). It has also demonstrated the use of DNA methylation arrays in further defining these tumours, suggesting a possible tool for deeper characterization of *DICER1*-associated NSCLCs.

5.2. SECTION 3: RNase interdomain interactions are required for the activation of synchronized cleavage of pre-miRNAs by each RNase domain

Ten DICER1 variants affecting the residues of the "ball and socket" junctions were assessed with respect to their ability to cleave the pre-miR-122 by *in vitro* cleavage experiments. Of these ten, one was previously evaluated - p.S1344L. Of the remaining nine variants, four variants, which included the "ball" residue mutants, showed no effects on cleavage function. As discussed above, a minimal side chain at the "ball" residue may be sufficient for "ball and socket" junction interaction. The two other variants were homologous arginine residues of the "socket" and as discussed previously, amino acid change to a leucine suggested a more significant role for hydrophobic interactions in the "ball and socket" junction compared to hydrogen bonding. Four more variants, also affecting homologous residues of the RNase IIIa and RNase IIIb, showed aberrant cleavage effects affecting both 3p and 5p miRNA generation, suggested an interdependency of the RNase III domains in synchronizing cleavage of 3'p and 5'p arms of the pre-miRNA. The remaining variant p.T1733L was the only mutant that exhibited trans-acting cleavage patterns similar to p.S1344L and, as discussed previously, the observed trans-acting effects may be due to proximity of these residues to the catalytic active sites of the opposing

RNase III domain in the intramolecular dimer. miRNA differential expression profiling of these trans-acting variants and canonical RNase III variants revealed four different miRNA expression patterns, which showed that the trans-acting mutants have similar, but not identical effects on 3p and 5p expression compared to their RNase III counterparts, providing insights into the lack of RNase IIIa hotspots and germline occurrences of the p.S1344L variant.

Conservation of both amino acid sequence and secondary structure of RNase III and findings by identifying somatic Hs-DROSHA hotspots at residues analogous to *Hs*-DICER1 p.E1705 and p.D1709 (97, 149) suggests that cleavage effects seen in *Hs*-DICER1 may be expanded to other RNase III of the miRNA biogenesis pathway, namely *Hs*-DROSHA (Figure 20). Therefore, it suggests that similar crosstalk interaction may be required to synchronize pri-miRNA stem-loop cleavage by Hs-DROSHA and that trans-acting RNase III activity may not be limited to *Hs*-DICER1, but is also be observed in *Hs*-DROSHA.

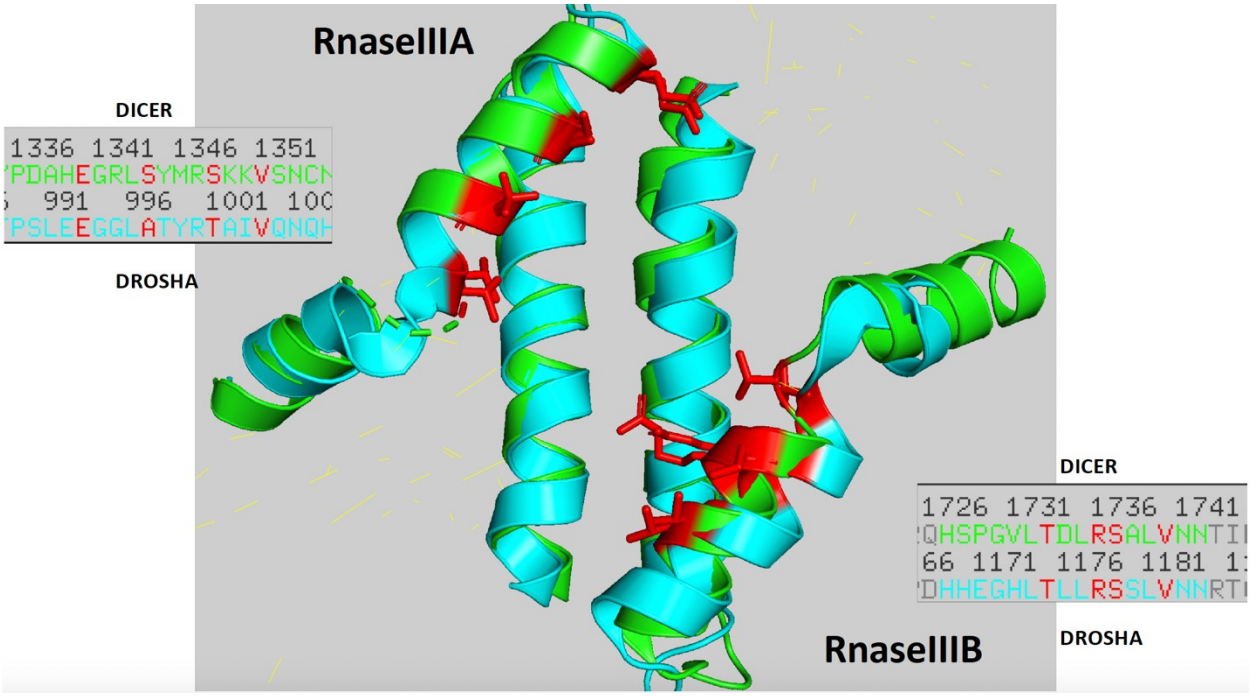

Figure 20: Alignment of Hs-DROSHA and Hs-DICER1 RNase III domains

DICER1 RNase III domains are coloured in green. DROSHA RNase III domains coloured in cyan. Figure produced by Marc Fabian.

5.3. Future directions

Regarding the "ball and socket" residues, future *in vitro* cleavage studies involving mutation of the p.R1736 residue to glycine or alanine are needed to assess the importance of the hydrophobic side chain. The nanoString miRNA findings also need to be validated by RT-qPCR of a select number of mature miRNAs belonging to each of the four miRNA profile groups and by luciferase reporter assays involving both 3p and 5p reporter constructs. Further analysis of pre-miRNA structure and sequence is needed understand why only certain subsets of miRNAs are affected

by the trans-acting mutants. Small RNA-sequencing might also be considered to see the specific effects

As for exploration of the RNase III domain crosstalk in Hs-DROSHA, future studies include *in vitro* cleavage of a pri-miRNA substrate by equivalent residues of the trans-acting variants and canonical RNase IIIa and RNase IIIb variants in Hs-DROSHA. Given the high conservation of the RNase III domains between Hs-DROSHA and Hs-DICER1, it may be interesting to design a fusion DICER1-DROSHA construct, with interchange of RNase III domains to evaluate whether the RNase III domains of Hs-DROSHA can be used to cleave pre-miRNAs by *in vitro* cleavage.

6. CHAPTER 6: REFERENCES

1. McCluggage WG, Chong AL, de Kock L, Foulkes WD. Somatic tumour testing establishes that bilateral DICER1-associated ovarian Sertoli-Leydig cell tumours represent independent primary neoplasms. Histopathology. 2020;77(2):223-30.

2. McCluggage WG, Apellaniz-Ruiz M, Chong AL, Hanley KZ, Velazquez Vega JE, McVeigh TP, et al. Embryonal Rhabdomyosarcoma of the Ovary and Fallopian Tube: Rare Neoplasms Associated With Germline and Somatic DICER1 Mutations. Am J Surg Pathol. 2020;44(6):738-47.

3. Yoon JY, Apellaniz-Ruiz M, Chong AL, Slim Z, Salfinger SG, Clarke BA, et al. The Value of DICER1 Mutation Analysis in "Subtle" Diagnostically Challenging Embryonal Rhabdomyosarcomas of the Uterine Cervix. Int J Gynecol Pathol. 2021;40(5):435-40.

4. Carmell MA, Hannon GJ. RNase III enzymes and the initiation of gene silencing. Nat Struct Mol Biol. 2004;11(3):214-8.

5. Lau PW, Guiley KZ, De N, Potter CS, Carragher B, MacRae IJ. The molecular architecture of human Dicer. Nat Struct Mol Biol. 2012;19(4):436-40.

6. Liu Z, Wang J, Cheng H, Ke X, Sun L, Zhang QC, et al. Cryo-EM Structure of Human Dicer and Its Complexes with a Pre-miRNA Substrate. Cell. 2018;173(5):1191-203 e12.

7. Tian Y, Simanshu DK, Ma JB, Park JE, Heo I, Kim VN, et al. A phosphate-binding pocket within the platform-PAZ-connector helix cassette of human Dicer. Mol Cell. 2014;53(4):606-16.

8. Macrae IJ, Zhou K, Li F, Repic A, Brooks AN, Cande WZ, et al. Structural basis for double-stranded RNA processing by Dicer. Science. 2006;311(5758):195-8.

9. Carthew RW, Sontheimer EJ. Origins and Mechanisms of miRNAs and siRNAs. Cell. 2009;136(4):642-55.

10. Denli AM, Tops BBJ, Plasterk RHA, Ketting RF, Hannon GJ. Processing of primary microRNAs by the Microprocessor complex. Nature. 2004;432(7014):231-5.

11. Kim VN. MicroRNA precursors in motion: exportin-5 mediates their nuclear export. Trends Cell Biol. 2004;14(4):156-9.

12. Lund E, Guttinger S, Calado A, Dahlberg JE, Kutay U. Nuclear export of microRNA precursors. Science. 2004;303(5654):95-8.

13. Bohnsack MT, Czaplinski K, Gorlich D. Exportin 5 is a RanGTP-dependent dsRNA-binding protein that mediates nuclear export of pre-miRNAs. RNA. 2004;10(2):185-91.

14. Yoda M, Kawamata T, Paroo Z, Ye X, Iwasaki S, Liu Q, et al. ATP-dependent human RISC assembly pathways. Nat Struct Mol Biol. 2010;17(1):17-23.

15. Schwarz DS, Hutvagner G, Du T, Xu Z, Aronin N, Zamore PD. Asymmetry in the assembly of the RNAi enzyme complex. Cell. 2003;115(2):199-208.

16. Khvorova A, Reynolds A, Jayasena SD. Functional siRNAs and miRNAs exhibit strand bias. Cell. 2003;115(2):209-16.

17. Bartel DP. Metazoan MicroRNAs. Cell. 2018;173(1):20-51.

18. Jonas S, Izaurralde E. Towards a molecular understanding of microRNA-mediated gene silencing. Nat Rev Genet. 2015;16(7):421-33.

19. Foulkes WD, Priest JR, Duchaine TF. DICER1: mutations, microRNAs and mechanisms. Nat Rev Cancer. 2014;14(10):662-72.

20. Kim VN, Han J, Siomi MC. Biogenesis of small RNAs in animals. Nat Rev Mol Cell Biol. 2009;10(2):126-39.

21. Gurtan AM, Lu V, Bhutkar A, Sharp PA. In vivo structure-function analysis of human Dicer reveals directional processing of precursor miRNAs. RNA. 2012;18(6):1116-22.

22. Court DL, Gan J, Liang Y-H, Shaw GX, Tropea JE, Costantino N, et al. RNase III: Genetics and function; structure and mechanism. Annu Rev Genet. 2013;47:405-31.

23. Sun W, Pertzev A, Nicholson AW. Catalytic mechanism of Escherichia coli ribonuclease III: kinetic and inhibitor evidence for the involvement of two magnesium ions in RNA phosphodiester hydrolysis. Nucleic Acids Res. 2005;33(3):807-15.

24. Sun W, Jun E, Nicholson AW. Intrinsic double-stranded-RNA processing activity of Escherichia coli ribonuclease III lacking the dsRNA-binding domain. Biochemistry. 2001;40(49):14976-84.

25. Yang W, Lee JY, Nowotny M. Making and breaking nucleic acids: two-Mg2+-ion catalysis and substrate specificity. Mol Cell. 2006;22(1):5-13.

26. Ji X. The mechanism of RNase III action: how dicer dices. Curr Top Microbiol Immunol. 2008;320:99-116.

27. Gan J, Shaw G, Tropea JE, Waugh DS, Court DL, Ji X. A stepwise model for double-stranded RNA processing by ribonuclease III. Mol Microbiol. 2008;67(1):143-54.

28. Macrae IJ, Li F, Zhou K, Cande WZ, Doudna JA. Structure of Dicer and mechanistic implications for RNAi. Cold Spring Harb Symp Quant Biol. 2006;71:73-80.

29. Blaszczyk J, Tropea JE, Bubunenko M, Routzahn KM, Waugh DS, Court DL, et al. Crystallographic and modeling studies of RNase III suggest a mechanism for double-stranded RNA cleavage. Structure. 2001;9(12):1225-36.

30. de Kock L, Wu MK, Foulkes WD. Ten years of DICER1 mutations: Provenance, distribution, and associated phenotypes. Hum Mutat. 2019.

31. Zhang H, Kolb FA, Jaskiewicz L, Westhof E, Filipowicz W. Single processing center models for human Dicer and bacterial RNase III. Cell. 2004;118(1):57-68.

32. Goulvent T, Ray-Coquard I, Borel S, Haddad V, Devouassoux-Shisheboran M, Vacher-Lavenu MC, et al. DICER1 and FOXL2 mutations in ovarian sex cord-stromal tumours: a GINECO Group study. Histopathology. 2016;68(2):279-85.

33. Heravi-Moussavi A, Anglesio MS, Cheng SW, Senz J, Yang W, Prentice L, et al. Recurrent somatic DICER1 mutations in nonepithelial ovarian cancers. N Engl J Med. 2012;366(3):234-42.

34. Lim D, Oliva E. Ovarian sex cord-stromal tumours: an update in recent molecular advances. Pathology. 2018;50(2):178-89.

35. Witkowski L, Mattina J, Schonberger S, Murray MJ, Choong CS, Huntsman DG, et al. DICER1 hotspot mutations in non-epithelial gonadal tumours. Br J Cancer. 2013;109(10):2744-50.

36. Li RF, Gupta M, McCluggage WG, Ronnett BM. Embryonal rhabdomyosarcoma (botryoid type) of the uterine corpus and cervix in adult women: report of a case series and review of the literature. Am J Surg Pathol. 2013;37(3):344-55.

37. Kurman RJ CM, Herrington CS, Young RH. World Health Organization Classification of Tumours of Female Reproductive Organs. 2014;Lyon: International Agency for Research on Cancer.

38. Prat J, Young RH, Scully RE. Ovarian Sertoli-Leydig cell tumors with heterologous elements. II. Cartilage and skeletal muscle: a clinicopathologic analysis of twelve cases. Cancer. 1982;50(11):2465-75.

39. Young RH, Prat J, Scully RE. Ovarian Sertoli-Leydig cell tumors with heterologous elements. I. Gastrointestinal epithelium and carcinoid: a clinicopathologic analysis of thirty-six cases. Cancer. 1982;50(11):2448-56.

40. Kato N, Kusumi T, Kamataki A, Tsunoda R, Fukase M, Kurose A. DICER1 hotspot mutations in ovarian Sertoli-Leydig cell tumors: a potential association with androgenic effects. Hum Pathol. 2017;59:41-7.

41. Conlon N, Schultheis AM, Piscuoglio S, Silva A, Guerra E, Tornos C, et al. A survey of DICER1 hotspot mutations in ovarian and testicular sex cord-stromal tumors. Mod Pathol. 2015;28(12):1603-12.

42. Young RH, Dickersin GR, Scully RE. Juvenile granulosa cell tumor of the ovary. A clinicopathological analysis of 125 cases. Am J Surg Pathol. 1984;8(8):575-96.

43. Young RH, Scully RE. Endocrine tumors of the ovary. Curr Top Pathol. 1992;85:113-64.

44. Shah SP, Kobel M, Senz J, Morin RD, Clarke BA, Wiegand KC, et al. Mutation of FOXL2 in granulosa-cell tumors of the ovary. N Engl J Med. 2009;360(26):2719-29.

45. Al-Agha OM, Huwait HF, Chow C, Yang W, Senz J, Kalloger SE, et al. FOXL2 is a sensitive and specific marker for sex cord-stromal tumors of the ovary. Am J Surg Pathol. 2011;35(4):484-94.

46. Bessiere L, Todeschini AL, Auguste A, Sarnacki S, Flatters D, Legois B, et al. A Hot-spot of In-frame Duplications Activates the Oncoprotein AKT1 in Juvenile Granulosa Cell Tumors. EBioMedicine. 2015;2(5):421-31.

47. Cathro HP, Stoler MH. The utility of calretinin, inhibin, and WT1 immunohistochemical staining in the differential diagnosis of ovarian tumors. Hum Pathol. 2005;36(2):195-201.

48. Zhao C, Vinh TN, McManus K, Dabbs D, Barner R, Vang R. Identification of the most sensitive and robust immunohistochemical markers in different categories of ovarian sex cord-stromal tumors. Am J Surg Pathol. 2009;33(3):354-66.

49. Karnezis AN, Wang Y, Keul J, Tessier-Cloutier B, Magrill J, Kommoss S, et al. DICER1 and FOXL2 Mutation Status Correlates With Clinicopathologic Features in Ovarian Sertoli-Leydig Cell Tumors. Am J Surg Pathol. 2019;43(5):628-38.

50. McCluggage WG, Foulkes WD. DICER1-associated sarcomas: towards a unified nomenclature. Mod Pathol. 2021;34(6):1226-8.

51. Warren M, Hiemenz MC, Schmidt R, Shows J, Cotter J, Toll S, et al. Expanding the spectrum of dicer1-associated sarcomas. Mod Pathol. 2020;33(1):164-74.

52. Siegel RL, Miller KD, Fuchs HE, Jemal A. Cancer Statistics, 2021. CA: A Cancer Journal for Clinicians. 2021;71(1):7-33.

53. de Kock L, Yoon JY, Apellaniz-Ruiz M, Pelletier D, McCluggage WG, Stewart CJR, et al. Significantly greater prevalence of DICER1 alterations in uterine embryonal rhabdomyosarcoma compared to adenosarcoma. Mod Pathol. 2020;33(6):1207-19.

54. Bean GR, Anderson J, Sangoi AR, Krings G, Garg K. DICER1 mutations are frequent in mullerian adenosarcomas and are independent of rhabdomyosarcomatous differentiation. Mod Pathol. 2019;32(2):280-9.

55. Dehner LP, Jarzembowski JA, Hill DA. Embryonal rhabdomyosarcoma of the uterine cervix: a report of 14 cases and a discussion of its unusual clinicopathological associations. Mod Pathol. 2012;25(4):602-14.

56. de Kock L, Boshari T, Martinelli F, Wojcik E, Niedziela M, Foulkes WD. Adult-Onset Cervical Embryonal Rhabdomyosarcoma and DICER1 Mutations. J Low Genit Tract Dis. 2016;20(1):e8-e10.

57. de Kock L, Rivera B, Revil T, Thorner P, Goudie C, Bouron-Dal Soglio D, et al. Sequencing of DICER1 in sarcomas identifies biallelic somatic DICER1 mutations in an adult-onset embryonal rhabdomyosarcoma. British Journal of Cancer. 2017;116(12):1621-6.

58. Doros L, Yang J, Dehner L, Rossi CT, Skiver K, Jarzembowski JA, et al. DICER1 mutations in embryonal rhabdomyosarcomas from children with and without familial PPB-tumor predisposition syndrome. Pediatr Blood Cancer. 2012;59(3):558-60.

59. Tomiak E, de Kock L, Grynspan D, Ramphal R, Foulkes WD. DICER1 mutations in an adolescent with cervical embryonal rhabdomyosarcoma (cERMS). Pediatr Blood Cancer. 2014;61(3):568-9.

60. Chong AS, Han H, Albrecht S, Weon YC, Park SK, Foulkes WD. DICER1 syndrome in a young adult with pituitary blastoma. Acta Neuropathol. 2021.

61. de Kock L, Priest JR, Foulkes WD, Alexandrescu S. An update on the central nervous system manifestations of DICER1 syndrome. Acta Neuropathologica. 2020;139(4):689-701.

62. Slade I, Bacchelli C, Davies H, Murray A, Abbaszadeh F, Hanks S, et al. DICER1 syndrome: clarifying the diagnosis, clinical features and management implications of a pleiotropic tumour predisposition syndrome. J Med Genet. 2011;48(4):273-8.

63. Priest JR, Watterson J, Strong L, Huff V, Woods WG, Byrd RL, et al. Pleuropulmonary blastoma: a marker for familial disease. J Pediatr. 1996;128(2):220-4.

64. Saskin A, de Kock L, Sabbaghian N, Apellaniz-Ruiz M, Bozkurt C, Bouron-Dal Soglio D, et al. A case of neuroblastoma in DICER1 syndrome: Chance finding or noncanonical causation? Pediatr Blood Cancer. 2018;65(1).

65. Cross SF, Arbuckle S, Priest JR, Marshall G, Charles A, Dalla Pozza L. Familial pleuropulmonary blastoma in Australia. Pediatr Blood Cancer. 2010;55(7):1417-9.

66. de Kock L, Sabbaghian N, Druker H, Weber E, Hamel N, Miller S, et al. Germ-line and somatic DICER1 mutations in pineoblastoma. Acta Neuropathol. 2014;128(4):583-95.

67. Priest JR, Williams GM, Hill DA, Dehner LP, Jaffe A. Pulmonary cysts in early childhood and the risk of malignancy. Pediatr Pulmonol. 2009;44(1):14-30.

68. Aksoy BA, Jacobsen A, Fieldhouse RJ, Lee W, Demir E, Ciriello G, et al. Cancer-associated recurrent mutations in RNase III domains of DICER1. bioRxiv. 2014:005686.

69. Stewart DR, Best AF, Williams GM, Harney LA, Carr AG, Harris AK, et al. Neoplasm Risk Among Individuals With a Pathogenic Germline Variant in DICER1. Journal of Clinical Oncology. 2019;37(8):668-76.

70. Brenneman M, Field A, Yang J, Williams G, Doros L, Rossi C, et al. Temporal order of RNase IIIb and loss-of-function mutations during development determines phenotype in pleuropulmonary blastoma / DICER1 syndrome: a unique variant of the two-hit tumor suppression model. F1000Res. 2015;4:214.

71. Gonzalez IA, Stewart DR, Schultz KAP, Field AP, Hill DA, Dehner LP. DICER1 tumor predisposition syndrome: an evolving story initiated with the pleuropulmonary blastoma. Mod Pathol. 2021.

72. Vandewalle RJ, Easton JC, Burns RC, Gray BW, Rescorla FJ. Review of Early Postoperative Metrics for Children Undergoing Resection of Congenital Pulmonary Airway Malformations and Report of Pleuropulmonary Blastoma at a Single Institution. Eur J Pediatr Surg. 2019;29(5):417-24.

73. Feinberg A, Hall NJ, Williams GM, Schultz KA, Miniati D, Hill DA, et al. Can congenital pulmonary airway malformation be distinguished from Type I pleuropulmonary blastoma based on clinical and radiological features? J Pediatr Surg. 2016;51(1):33-7.

74. Ricaurte LM, Arrieta O, Zatarain-Barron ZL, Cardona AF. Comprehensive review of fetal adenocarcinoma of the lung. Lung Cancer (Auckl). 2018;9:57-63.

75. Wu Y, Chen D, Li Y, Bian L, Ma T, Xie M. DICER1 mutations in a patient with an ovarian Sertoli-Leydig tumor, well-differentiated fetal adenocarcinoma of the lung, and familial multinodular goiter. Eur J Med Genet. 2014;57(11-12):621-5.

76. Zhang J, Sun J, Liang X-L, Lu J-L, Luo Y-F, Liang Z-Y. Differences between low and high grade fetal adenocarcinoma of the lung: a clinicopathological and molecular study. J Thorac Dis. 2017;9(7):2071-8.

77. Li Y, Xi SY, Yong JJ, Wu XY, Yang XH, Wang F. Morphologic, Immunohistochemical, and Genetic Differences Between High-grade and Low-grade Fetal Adenocarcinomas of the Lung. Am J Surg Pathol. 2021.

78. de Kock L, Bah I, Brunet J, Druker H, Astigarraga I, Bosch-Barrera J, et al. Somatic DICER1 mutations in adult-onset pulmonary blastoma. Eur Respir J. 2016;47(6):1879-82.

79. de Kock L, Bah I, Wu Y, Xie M, Priest JR, Foulkes WD. Germline and Somatic DICER1 Mutations in a Well-Differentiated Fetal Adenocarcinoma of the Lung. J Thorac Oncol. 2016;11(3):e31-3.

80. Fu Y, Wu Q, Su F, Tang Y, Lin Y, Wang W, et al. Novel gene mutations in well-differentiated fetal adenocarcinoma of the lung in the next generation sequencing era. Lung Cancer. 2018;124:1-5.

81. Liu S, Wang J, Luo X, Li X, Miao Y, Wang L, et al. Coexistence of Low-Grade Fetal Adenocarcinoma and Adenocarcinoma in situ of the Lung Harboring Different Genetic Mutations: A Case Report and Review of Literature. Onco Targets Ther. 2020;13:6675-80.

82. Ponten E, Frisk S, Taylan F, Vaz R, Wessman S, de Kock L, et al. A complex DICER1 syndrome phenotype associated with a germline pathogenic variant affecting the RNase IIIa domain of DICER1. J Med Genet. 2020.

83. Nakatani Y, Masudo K, Miyagi Y, Inayama Y, Kawano N, Tanaka Y, et al. Aberrant nuclear localization and gene mutation of beta-catenin in low-grade adenocarcinoma of fetal lung type: up-regulation of the Wnt signaling pathway may be a common denominator for the development of tumors that form morules. Mod Pathol. 2002;15(6):617-24.

84. Sekine S, Shibata T, Matsuno Y, Maeshima A, Ishii G, Sakamoto M, et al. Beta-catenin mutations in pulmonary blastomas: association with morule formation. J Pathol. 2003;200(2):214-21.

85. de Kock L, Fahiminiya S, Fiset PO, Astigarraga I, Nguyen VH, Albrecht S, et al. Infantile Pulmonary Teratoid Tumor. N Engl J Med. 2018;378(23):2238-40.

86. Nakatani Y, Miyagi Y, Takemura T, Oka T, Yokoi T, Takagi M, et al. Aberrant nuclear/cytoplasmic localization and gene mutation of beta-catenin in classic pulmonary blastoma: beta-catenin immunostaining is useful for distinguishing between classic pulmonary blastoma and a blastomatoid variant of carcinosarcoma. Am J Surg Pathol. 2004;28(7):921-7.

87. Zhao J, Xiang C, Zhao R, Guo P, Zheng J, Han-Zhang H, et al. Clinicopathologic features and genomic analysis of pulmonary blastomatoid carcinosarcoma. BMC Cancer. 2020;20(1):248.

88. Wu MK, Sabbaghian N, Xu B, Addidou-Kalucki S, Bernard C, Zou D, et al. Biallelic DICER1 mutations occur in Wilms tumours. J Pathol. 2013;230(2):154-64.

89. Gadd S, Huff V, Walz AL, Ooms A, Armstrong AE, Gerhard DS, et al. A Children's Oncology Group and TARGET initiative exploring the genetic landscape of Wilms tumor. Nat Genet. 2017;49(10):1487-94.

90. Vedanayagam J, Chatila WK, Aksoy BA, Majumdar S, Skanderup AJ, Demir E, et al. Cancer-associated mutations in DICER1 RNase IIIa and IIIb domains exert similar effects on miRNA biogenesis. Nat Commun. 2019;10(1):3682.

91. Duma N, Santana-Davila R, Molina JR. Non-Small Cell Lung Cancer: Epidemiology, Screening, Diagnosis, and Treatment. Mayo Clin Proc. 2019;94(8):1623-40.

92. Gan J, Tropea JE, Austin BP, Court DL, Waugh DS, Ji X. Structural insight into the mechanism of double-stranded RNA processing by ribonuclease III. Cell. 2006;124(2):355-66.

93. de Kock L. DICER1 Syndrome – new mutations, novel phenotypes and unexpected mechanisms. eScholarship@McGill. 2019.

94. de Kock L, Sabbaghian N, Plourde F, Srivastava A, Weber E, Bouron-Dal Soglio D, et al. Pituitary blastoma: a pathognomonic feature of germ-line DICER1 mutations. Acta Neuropathol. 2014;128(1):111-22.

95. Wu MK, de Kock L, Conwell LS, Stewart CJ, King BR, Choong CS, et al. Functional characterization of multiple DICER1 mutations in an adolescent. Endocr Relat Cancer. 2016;23(2):L1-5.

96. Wu M. DICER1 syndrome : assays, associations and models. [Montreal]: McGill University Libraries; 2019.

97. Rakheja D, Chen KS, Liu Y, Shukla AA, Schmid V, Chang TC, et al. Somatic mutations in DROSHA and DICER1 impair microRNA biogenesis through distinct mechanisms in Wilms tumours. Nat Commun. 2014;2:4802.

98. Sebire NJ, Malone M. Myogenin and MyoD1 expression in paediatric rhabdomyosarcomas. Journal of Clinical Pathology. 2003;56(6):412-6.

99. Rutter MM, Jha P, Schultz KA, Sheil A, Harris AK, Bauer AJ, et al. DICER1 Mutations and Differentiated Thyroid Carcinoma: Evidence of a Direct Association. J Clin Endocrinol Metab. 2016;101(1):1-5.

100. de Kock L, Wu MK, Foulkes WD. Ten years of DICER1 mutations: Provenance, distribution, and associated phenotypes. Hum Mutat. 2019;40(11):1939-53.

101. Caroleo AM, De Ioris MA, Boccuto L, Alessi I, Del Baldo G, Cacchione A, et al. DICER1 Syndrome and Cancer Predisposition: From a Rare Pediatric Tumor to Lifetime Risk. Frontiers in Oncology. 2021;10(2989).

102. Robinson A, Romao R, Mills J, Davies DA. Decision-Making Criteria for Observational Management of Congenital Pulmonary Airway Malformations (CPAMs). J Pediatr Surg. 2018;53(5):1006-9.

103. Downard CD, Calkins CM, Williams RF, Renaud EJ, Jancelewicz T, Grabowski J, et al. Treatment of congenital pulmonary airway malformations: a systematic review from the APSA outcomes and evidence based practice committee. Pediatr Surg Int. 2017;33(9):939-53.

104. Tam PK. Whole exome sequencing to uncover genetic variants underlying congenital cystic adenomatoid malformations. Hong Kong Med J. 2019;25 Suppl 5(4):36-8.

105. Kalfa N, Ecochard A, Patte C, Duvillard P, Audran F, Pienkowski C, et al. Activating mutations of the stimulatory g protein in juvenile ovarian granulosa cell tumors: a new prognostic factor? J Clin Endocrinol Metab. 2006;91(5):1842-7.

106. Karalok A, Turan T, Ureyen I, Tasci T, Basaran D, Koc S, et al. Prognostic Factors in Adult Granulosa Cell Tumor: A Long Follow-Up at a Single Center. Int J Gynecol Cancer. 2016;26(4):619-25.

107. Foulkes WD, Gore M, McCluggage WG. Rare non-epithelial ovarian neoplasms: Pathology, genetics and treatment. Gynecologic Oncology. 2016;142(1):190-8.

108. Xiao H, Li B, Zuo J, Feng X, Li X, Zhang R, et al. Ovarian Sertoli–Leydig cell tumor: a report of seven cases and a review of the literature. Gynecological Endocrinology. 2013;29(3):192-5.

109. Gui T, Cao D, Shen K, Yang J, Zhang Y, Yu Q, et al. A clinicopathological analysis of 40 cases of ovarian Sertoli-Leydig cell tumors. Gynecol Oncol. 2012;127(2):384-9.

110. Sigismondi C, Gadducci A, Lorusso D, Candiani M, Breda E, Raspagliesi F, et al. Ovarian Sertoli-Leydig cell tumors. a retrospective MITO study. Gynecol Oncol. 2012;125(3):673-6.

111. Bauer AJ, Stewart DR, Kamihara J, Harris AK, Turner J, Shah R, et al. DICER1 and Associated Conditions: Identification of At-risk Individuals and Recommended Surveillance Strategies-Response. Clin Cancer Res. 2019;25(5):1689-90.

112. Schultz KAP, Williams GM, Kamihara J, Stewart DR, Harris AK, Bauer AJ, et al. DICER1 and Associated Conditions: Identification of At-risk Individuals and Recommended Surveillance Strategies. Clin Cancer Res. 2018;24(10):2251-61.

113. Stewart DR, Best AF, Williams GM, Harney LA, Carr AG, Harris AK, et al. Neoplasm Risk Among Individuals With a Pathogenic Germline Variant in DICER1. J Clin Oncol. 2019;37(8):668-76.

114. de Kock L, Druker H, Weber E, Hamel N, Traubici J, Malkin D, et al. Ovarian embryonal rhabdomyosarcoma is a rare manifestation of the DICER1 syndrome. Hum Pathol. 2015;46(6):917-22.

115. Nasioudis D, Alevizakos M, Chapman-Davis E, Witkin SS, Holcomb K. Rhabdomyosarcoma of the lower female genital tract: an analysis of 144 cases. Arch Gynecol Obstet. 2017;296(2):327-34.

116. de Kock L, Yoon J-Y, Apellaniz-Ruiz M, Pelletier D, McCluggage WG, Stewart CJR, et al. Significantly greater prevalence of DICER1 alterations in uterine embryonal rhabdomyosarcoma compared to adenosarcoma. Modern Pathology. 2020;33(6):1207-19.

117. McCluggage WG, Foulkes WD. DICER1-associated sarcomas at different sites exhibit morphological overlap arguing for a unified nomenclature. Virchows Archiv. 2021;479(2):431-3.

118. McClean GE, Kurian S, Walter N, Kekre A, McCluggage WG. Cervical embryonal rhabdomyosarcoma and ovarian Sertoli-Leydig cell tumour: a more than coincidental association of two rare neoplasms? J Clin Pathol. 2007;60(3):326-8.

119. Foulkes WD, Bahubeshi A, Hamel N, Pasini B, Asioli S, Baynam G, et al. Extending the phenotypes associated with DICER1 mutations. Hum Mutat. 2011;32(12):1381-4.

120. Klein S, Lee H, Ghahremani S, Kempert P, Ischander M, Teitell MA, et al. Expanding the phenotype of mutations in DICER1: mosaic missense mutations in the RNase IIIb domain of DICER1 cause GLOW syndrome. J Med Genet. 2014;51(5):294-302.

121. de Kock L, Wang YC, Revil T, Badescu D, Rivera B, Sabbaghian N, et al. High-sensitivity sequencing reveals multi-organ somatic mosaicism causing DICER1 syndrome. J Med Genet. 2016;53(1):43-52.

122. Luke AM, Moroney JW, Snitchler A, Whiteway SL. Ovarian Sertoli-Leydig Cell Tumor with Elevated Inhibin B as a Cause of Secondary Amenorrhea in an Adolescent with Germ Line DICER1 Mutation. J Pediatr Adolesc Gynecol. 2017;30(5):598-600.

123. Trobo S, Ramirez P, Perez- Garrido N, Touzon M, Vaiani E, Costanzo M, et al. SUN-047 Germline and Somatic Mutations in DICER1 Gene Associated with Different Hereditary Tumours in Paediatric Patients. J Endocr Soc. 2019;3(Suppl 1):SUN-047.

124. Weinberg BA, Gowen K, Lee TK, Ou SI, Bristow R, Krill L, et al. Comprehensive Genomic Profiling Aids in Distinguishing Metastatic Recurrence from Second Primary Cancers. Oncologist. 2017;22(2):152-7.

125. Yuan Z, Huo X, Jiang D, Yu M, Cao D, Wu H, et al. Clinical Characteristics and Mutation Analyses of Ovarian Sertoli-Leydig Cell Tumors. Oncologist. 2020;25(9):e1396-e405.

126. Huang KT, Mikeska T, Li J, Takano EA, Millar EK, Graham PH, et al. Assessment of DNA methylation profiling and copy number variation as indications of clonal relationship in ipsilateral and contralateral breast cancers to distinguish recurrent breast cancer from a second primary tumour. BMC Cancer. 2015;15:669.

127. Pugh TJ, Weeraratne SD, Archer TC, Pomeranz Krummel DA, Auclair D, Bochicchio J, et al. Medulloblastoma exome sequencing uncovers subtype-specific somatic mutations. Nature. 2012;488(7409):106-10.

128. Apellániz-Ruiz M, Colón-González G, Perlman E, Bouron-Dal Soglio D, Sabbaghian N, Oehl K, et al. A child with neuroblastoma and metachronous anaplastic sarcoma of the kidney: Underlying DICER1 syndrome? Pediatric Blood & Cancer. 2020;67:e28488.

129. Pugh TJ, Morozova O, Attiyeh EF, Asgharzadeh S, Wei JS, Auclair D, et al. The genetic landscape of high-risk neuroblastoma. Nat Genet. 2013;45(3):279-84.

130. Schumer ST, Cannistra SA. Granulosa cell tumor of the ovary. J Clin Oncol. 2003;21(6):1180-9.

131. Chang YS, Tu SJ, Chen YC, Liu TY, Lee YT, Yen JC, et al. Mutation profile of non-small cell lung cancer revealed by next generation sequencing. Respir Res. 2021;22(1):3.

132. Griffin R, Ramirez RA. Molecular Targets in Non-Small Cell Lung Cancer. Ochsner J. 2017;17(4):388-92.

133. Pao W, Girard N. New driver mutations in non-small-cell lung cancer. Lancet Oncol. 2011;12(2):175-80.

134. Seki M, Yoshida K, Shiraishi Y, Shimamura T, Sato Y, Nishimura R, et al. Biallelic DICER1 mutations in sporadic pleuropulmonary blastoma. Cancer Res. 2014;74(10):2742-9.

135. Chong AS, Nikiforov YE, Condello V, Wald AI, Nikiforova MN, Foulkes WD, et al. Prevalence and Spectrum of DICER1 Mutations in Adult-onset Thyroid Nodules with Indeterminate Cytology. J Clin Endocrinol Metab. 2021;106(4):968-77.

136. Koss MN, Hochholzer L, O'Leary T. Pulmonary blastomas. Cancer. 1991;67(9):2368-81.

137. Sunaga N, Kohno T, Kolligs FT, Fearon ER, Saito R, Yokota J. Constitutive activation of the Wnt signaling pathway by CTNNB1 (beta-catenin) mutations in a subset of human lung adenocarcinoma. Genes Chromosomes Cancer. 2001;30(3):316-21.

138. Arora-Gupta N, Hagedorn CH. Liver, Development. In: Johnson LR, editor. Encyclopedia of Gastroenterology. New York: Elsevier; 2004. p. 530-3.

139. Mucenski ML, Wert SE, Nation JM, Loudy DE, Huelsken J, Birchmeier W, et al. beta-Catenin is required for specification of proximal/distal cell fate during lung morphogenesis. J Biol Chem. 2003;278(41):40231-8.

140. Shu W, Guttentag S, Wang Z, Andl T, Ballard P, Lu MM, et al. Wnt/beta-catenin signaling acts upstream of N-myc, BMP4, and FGF signaling to regulate proximal-distal patterning in the lung. Dev Biol. 2005;283(1):226-39.

141. Guigon CJ, Zhao L, Lu C, Willingham MC, Cheng SY. Regulation of beta-catenin by a novel nongenomic action of thyroid hormone beta receptor. Mol Cell Biol. 2008;28(14):4598-608.

142. Ely KA, Bischoff LA, Weiss VL. Wnt Signaling in Thyroid Homeostasis and Carcinogenesis. Genes (Basel). 2018;9(4).

143. Takeshita D, Zenno S, Lee WC, Nagata K, Saigo K, Tanokura M. Homodimeric structure and double-stranded RNA cleavage activity of the C-terminal RNase III domain of human dicer. J Mol Biol. 2007;374(1):106-20.

144. de Kock L, Sabbaghian N, Plourde F, Srivastava A, Weber E, Bouron-Dal Soglio D, et al. Pituitary blastoma: a pathognomonic feature of germ-line DICER1 mutations. Acta Neuropathologica. 2014;128(1):111-22.

145. Nadaf J, de Kock L, Chong AS, Korbonits M, Thorner P, Benlimame N, et al. Molecular characterization of DICER1-mutated pituitary blastoma. Acta Neuropathol. 2021;141(6):929-44.

146. Pneumologie GfP. Zeitschrift der Gesellschaft für Pädiatrische Pneumologie: Wurms et Partner.; 2006.

147. Farzaneh M, Attari F, Khoshnam SE. Concise Review: LIN28/let-7 Signaling, a Critical Double-Negative Feedback Loop During Pluripotency, Reprogramming, and Tumorigenicity. Cellular Reprogramming. 2017;19.

148. McCluggage WG, Foulkes WD. DICER1-sarcoma: an emerging entity. Modern Pathology. 2021;34(12):2096-7.

149. Torrezan GT, Ferreira EN, Nakahata AM, Barros BD, Castro MT, Correa BR, et al. Recurrent somatic mutation in DROSHA induces microRNA profile changes in Wilms tumour. Nat Commun. 2014;5:4039.

7. APPENDIX I: COMPLETE MUTATIONAL LANDSCAPE OF DICER1-ASSOCIATED NSCLCS FROM CARIS LIFE SCIENCES

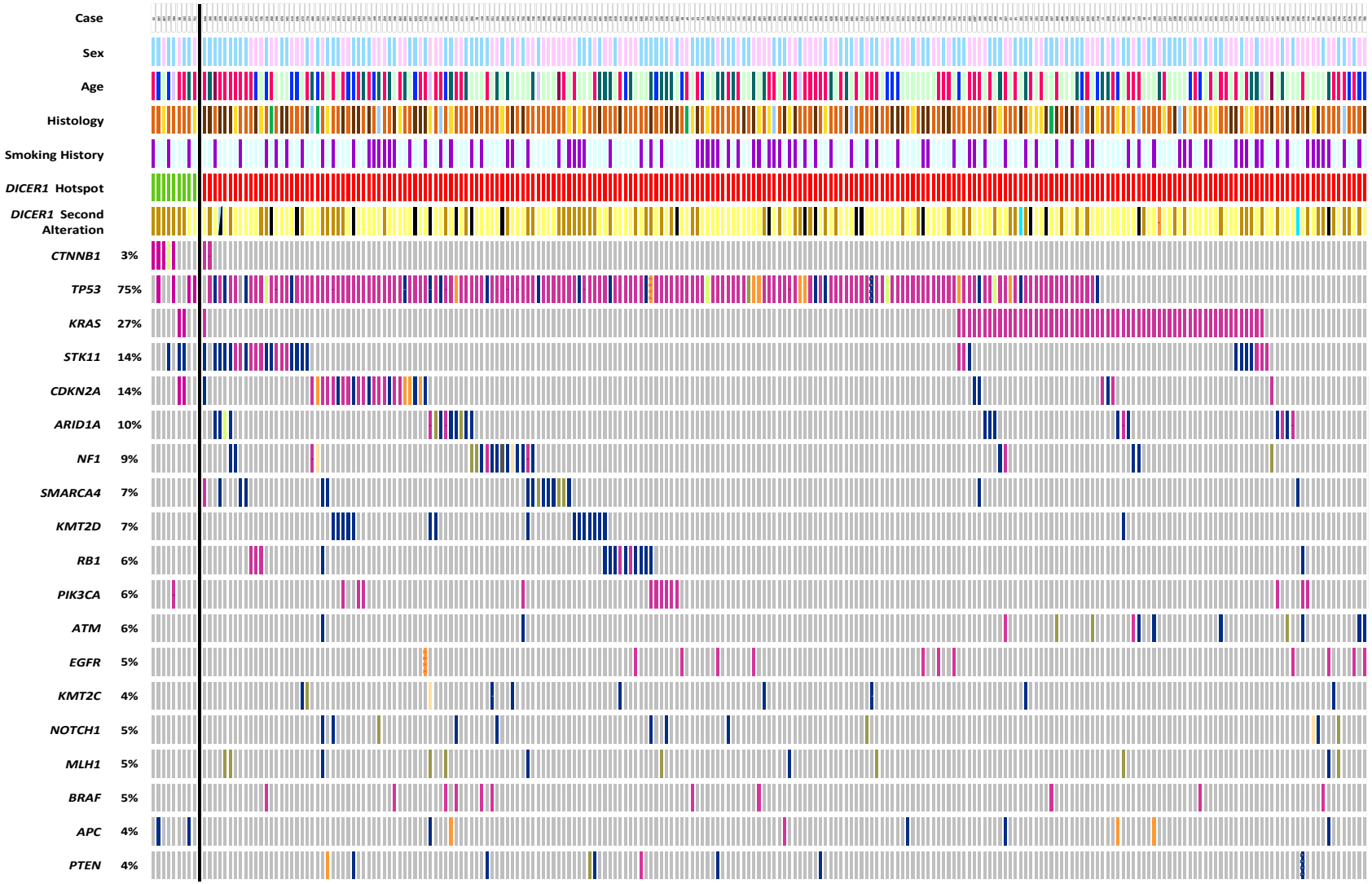

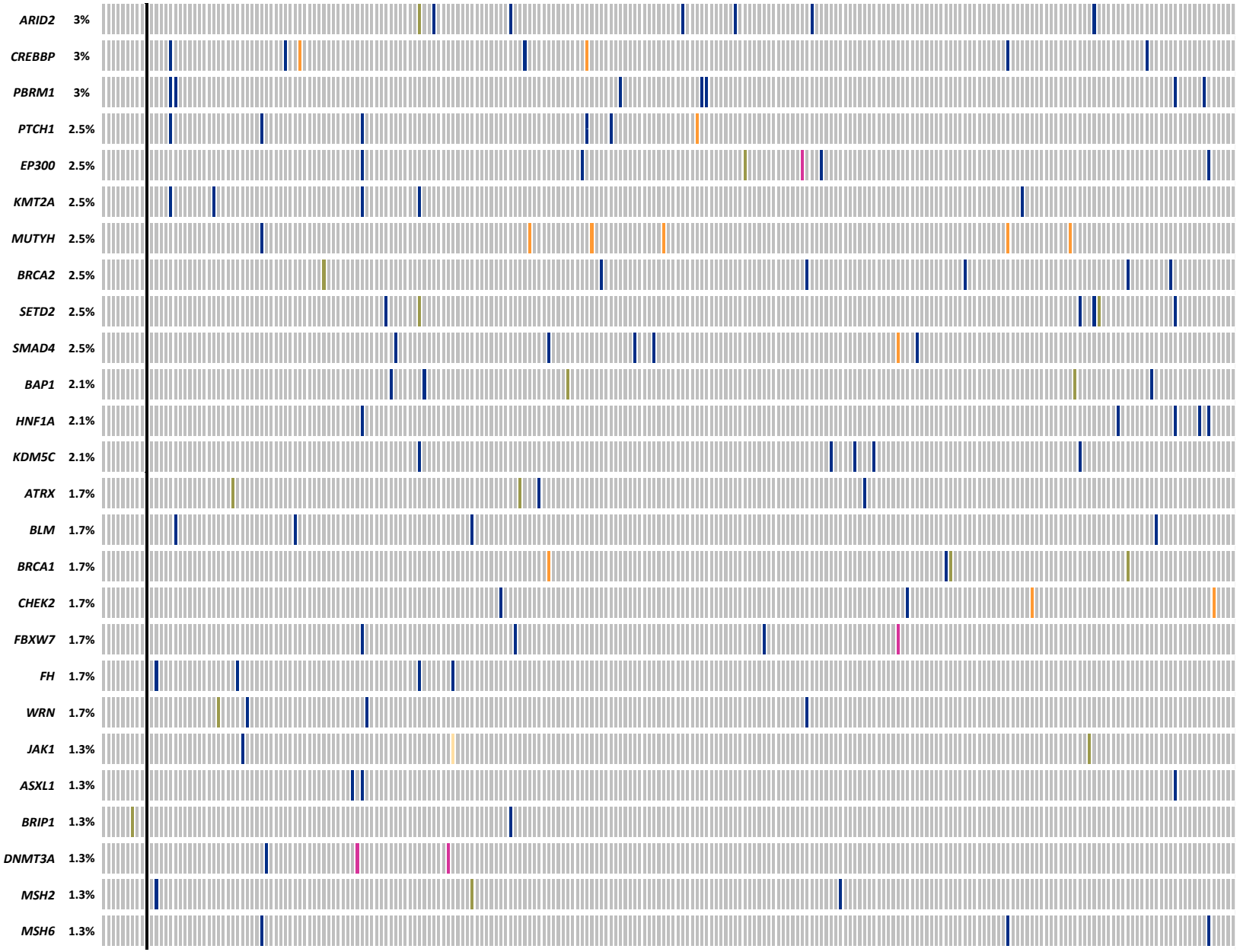
ARID2 3%
CREBBP 3%
PBRM1 3%
PTCH1 2.5%
EP300 2.5%
KMT2A 2.5%
MUTYH 2.5%
BRCA2 2.5%
SETD2 2.5%
SMAD4 2.5%
BAP1 2.1%
HNF1A 2.1%
KDM5C 2.1%
ATRX 1.7%
BLM 1.7%
BRCA1 1.7%
CHEK2 1.7%
FBXW7 1.7%
FH 1.7%
WRN 1.7%
JAK1 1.3%
ASXL1 1.3%
BRIP1 1.3%
DNMT3A 1.3%
MSH2 1.3%
MSH6 1.3%

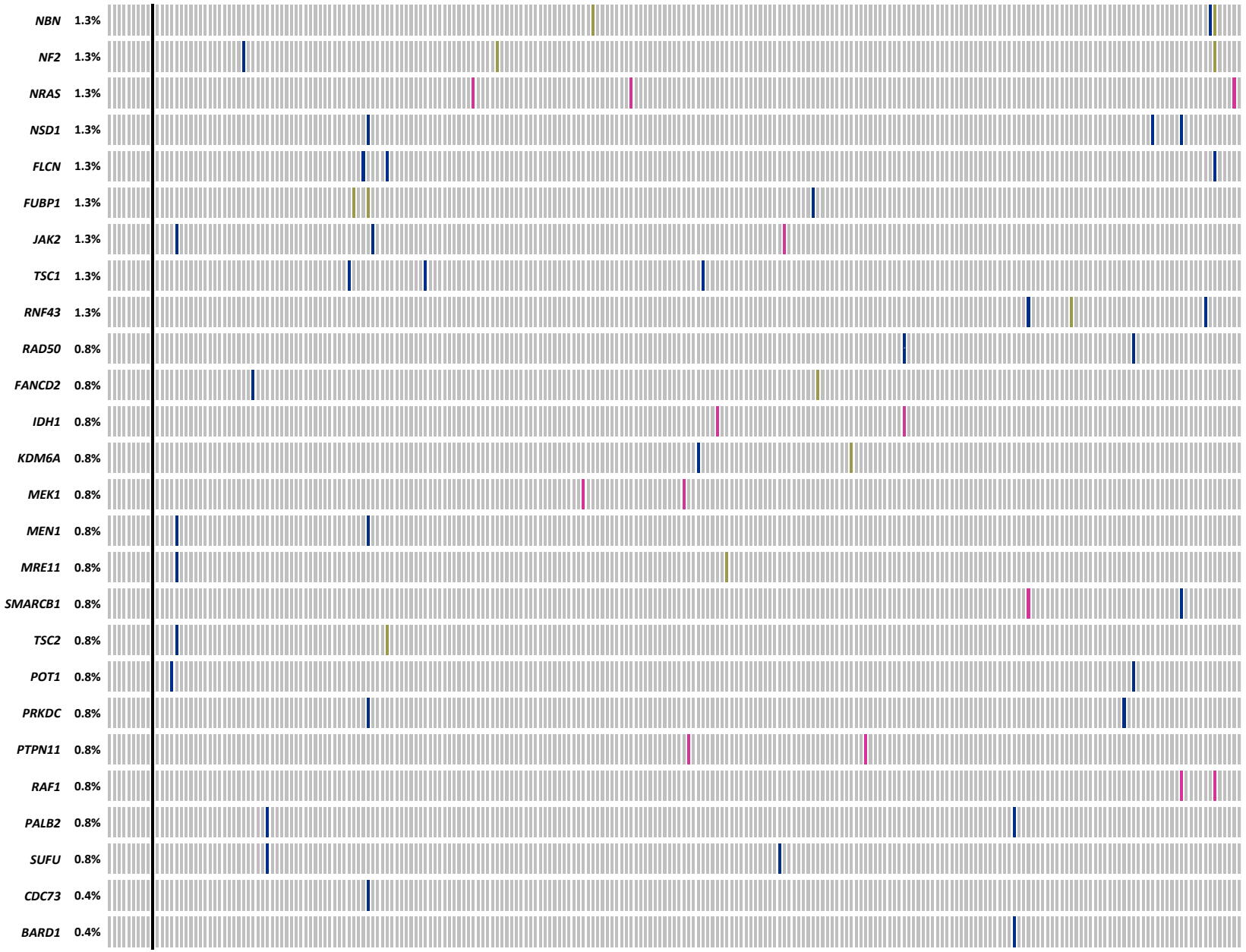
NBN 1.3%
NF2 1.3%
NRAS 1.3%
NSD1 1.3%
FLCN 1.3%
FUBP1 1.3%
JAK2 1.3%
TSC1 1.3%
RNF43 1.3%
RAD50 0.8%
FANCD2 0.8%
IDH1 0.8%
KDM6A 0.8%
MEK1 0.8%
MEN1 0.8%
MRE11 0.8%
SMARCB1 0.8%
TSC2 0.8%
POT1 0.8%
PRKDC 0.8%
PTPN11 0.8%
RAF1 0.8%
PALB2 0.8%
SUFU 0.8%
CDC73 0.4%
BARD1 0.4%

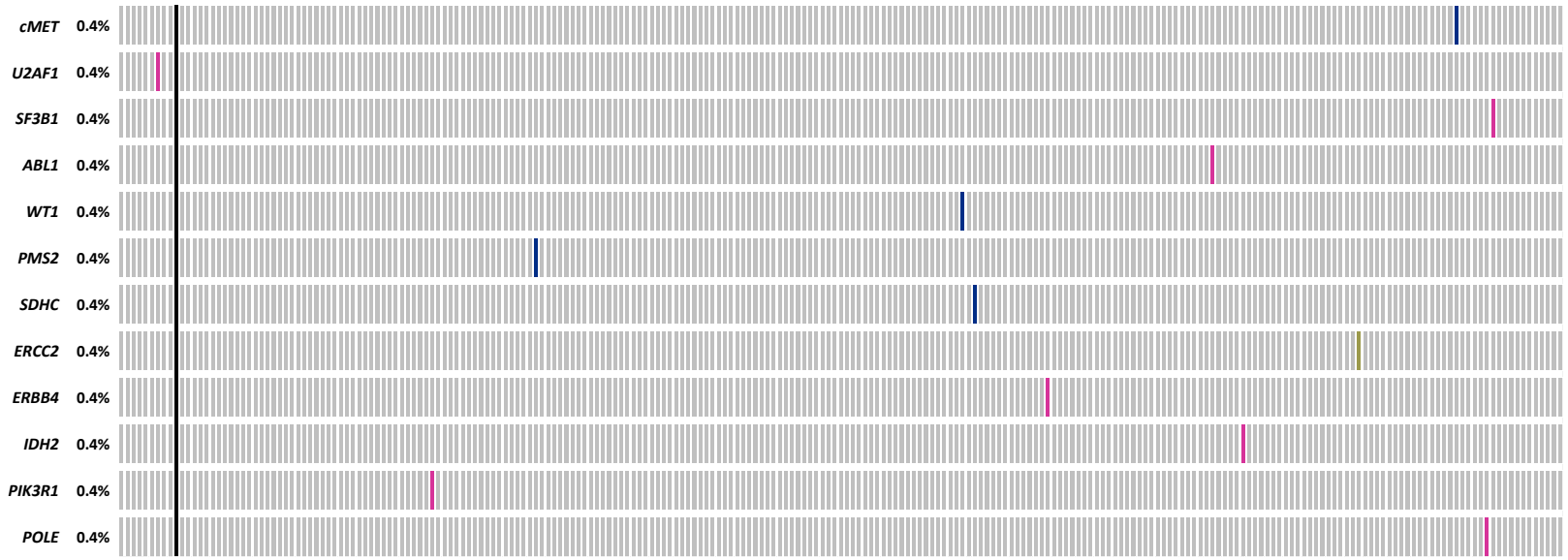

HOTSPOT MUTATION STATUS
- DICER1 hotspot positive
- DICER1 hotspot negative

HISTOLOGY
- Lung Adenocarcinoma
- Lung Squamous Cell Carcinoma
- NSCLC, NOS
- Large Cell Neuroendocrine Carcinoma
- Other

SEX
- Male
- Female

SMOKING HISTORY
- Smoker
- Non-Smoker

TYPE OF SECOND *DICER1* ALTERATION MUTATION
- Truncating variant
- Likely pathogenic missense
- Splice mutation
- Truncating and likely pathogenic missense
- Splice mutation and likely pathogenic missense

AGE
- [40-49]
- [50-59]
- [60-69]
- [70-79]
- [80-89]
- >90

TYPE OF NON-*DICER1* ALTERATION MUTATION
- Other gene hotspot mutation positive
- Other gene truncating mutation positive
- Other gene likely pathogenic missense mutation positive
- Other gene splice mutation positive
- Other gene truncating and hotspot mutation positive
- Other gene truncating and likely pathogenic missense positive
- Other gene hotspot and likely pathogenic miseense positive
- Other gene truncating and splice mutation positive

8. APPENDIX II: List of miRNAs according to Venn diagram class

Class	miRNA name	miRNA type
Class I	mmu-miR-28	5p
	mmu-let-7c	5p
	mmu-miR-100	5p
	mmu-miR-1198	5p
	mmu-miR-149	5p
	mmu-miR-15b	5p
	mmu-miR-16	5p
	mmu-miR-183	5p
	mmu-miR-196a	5p
	mmu-miR-21	5p
	mmu-miR-450a-5p	5p
	mmu-miR-467c	5p
	mmu-miR-532-5p	5p
	mmu-miR-96	5p
Class II	mmu-miR-99b	5p
	mmu-miR-181a	5p
	mmu-miR-205	5p
	mmu-miR-10a	5p
	mmu-miR-423-5p	5p
	mmu-let-7b	5p
	mmu-let-7d	5p
	mmu-let-7i	5p
	mmu-miR-106a	5p
	mmu-miR-17	5p
	mmu-miR-106b	5p
	mmu-miR-146a	5p
	mmu-miR-196b	5p
	mmu-miR-20a	5p
	mmu-miR-20b	5p
	mmu-miR-224	5p
	mmu-miR-484	5p
	mmu-miR-93	5p
	mmu-miR-99a	5p
	mmu-miR-140	5p
	mmu-miR-31	5p

Class	miRNA name	miRNA type
	mmu-miR-322	5p
	mmu-miR-669a	5p
Class III	mmu-miR-574-3p	3p
Class IV	mmu-let-7e	5p
	mmu-let-7f	5p
	mmu-miR-467b	5p
	mmu-miR-674	5p
	mmu-miR-7a	5p
	mmu-miR-98	5p
Class V	mmu-miR-15a	5p
	mmu-miR-374	5p
Class VI	mmu-miR-145	5p
	mmu-miR-30a	5p
	mmu-miR-30c	5p
	mmu-miR-30b	5p
Class VII	mmu-let-7a	5p
	mmu-miR-33	5p
	mmu-miR-340-5p	5p
	mmu-miR-191	5p
	mmu-miR-26b	5p
	mmu-miR-125b-3p	3p
Class VIII	mmu-miR-27b	3p
	mmu-miR-669f	3p
	mmu-miR-103	3p
	mmu-miR-126-3p	3p
	mmu-miR-130a	3p
	mmu-miR-132	3p
	mmu-miR-143	3p
	mmu-miR-148a	3p
	mmu-miR-152	3p
	mmu-miR-199a-3p	3p
	mmu-miR-22	3p
	mmu-miR-221	3p
	mmu-miR-23b	3p
	mmu-miR-25	3p
	mmu-miR-27a	3p
	mmu-miR-301a	3p
	mmu-miR-378	3p

Class	miRNA name	miRNA type
	mmu-miR-423-3p	3p
	mmu-miR-450b-3p	3p
	mmu-miR-652	3p
Class IX	mmu-miR-466a-3p	3p
	mmu-miR-466b-3-3p	3p
	mmu-miR-466d-3p	3p
	mmu-miR-130b	3p
	mmu-miR-148b	3p
	mmu-miR-19b	3p
	mmu-miR-210	3p
	mmu-miR-23a	3p
	mmu-miR-29a	3p
	mmu-miR-29b	3p
	mmu-miR-342-3p	3p
	mmu-miR-350	3p
	mmu-miR-365	3p
Class X	mmu-miR-206	3p
Class XI	mmu-let-7g	5p
	mmu-miR-151-5p	5p
	mmu-miR-30d	5p
	mmu-miR-872	5p
	mmu-miR-125a-5p	5p
	mmu-miR-125b-5p	5p
	mmu-miR-199a-5p	5p
	mmu-miR-125a-3p	3p
	mmu-miR-19a	3p
	mmu-miR-214	3p

9. APPENDIX III: Publication permissions

SPRINGER NATURE LICENSE
TERMS AND CONDITIONS

Dec 12, 2021

This Agreement between Ms. Anne-Laure Chong -- Anne-Laure Chong ("You") and Springer Nature ("Springer Nature") consists of your license details and the terms and conditions provided by Springer Nature and Copyright Clearance Center.

License Number	5206291490754
License date	Dec 12, 2021
Licensed Content Publisher	Springer Nature
Licensed Content Publication	Nature Reviews Cancer
Licensed Content Title	DICER1: mutations, microRNAs and mechanisms
Licensed Content Author	William D. Foulkes et al
Licensed Content Date	Sep 1, 2014
Type of Use	Thesis/Dissertation
Requestor type	academic/university or research institute
Format	electronic
Portion	figures/tables/illustrations
Number of figures/tables/illustrations	1
High-res required	no
Will you be translating?	no
Circulation/distribution	1 - 29
Author of this Springer Nature content	no
Title	DICER1 mutations: clinical applications, novel associations and functional evaluations
Institution name	McGill University
Expected presentation date	Dec 2021
Portions	Figure 1
Total	0.00 CAD

JOHN WILEY AND SONS LICENSE TERMS AND CONDITIONS
Dec 12, 2021

This Agreement between Ms. Anne-Laure Chong -- Anne-Laure Chong ("You") and John Wiley and Sons ("John Wiley and Sons") consists of your license details and the terms and conditions provided by John Wiley and Sons and Copyright Clearance Center.

License Number	5206290645892
License date	Dec 12, 2021
Licensed Content Publisher	John Wiley and Sons
Licensed Content Publication	Human Mutation
Licensed Content Title	Ten years of DICER1 mutations: Provenance, distribution, and associated phenotypes
Licensed Content Author	William D. Foulkes, Mona K. Wu, Leanne Kock
Licensed Content Date	Aug 17, 2019
Licensed Content Volume	40
Licensed Content Issue	11
Licensed Content Pages	15
Type of use	Dissertation/Thesis
Requestor type	University/Academic
Format	Electronic
Portion	
Number of figures/tables	1
Will you be translating?	No
Title	DICER1 mutations: clinical applications, novel associations and functional evaluations
Institution name	McGill University
Expected presentation date	Dec 2021
Portions	Figure 4
Publisher Tax ID	
Total	0.00 CAD

ELSEVIER LICENSE
TERMS AND CONDITIONS

Oct 31, 2021

This Agreement between Ms. Anne-Laure Chong -- Anne-Laure Chong ("You") and Elsevier ("Elsevier") consists of your license details and the terms and conditions provided by Elsevier and Copyright Clearance Center.

License Number	5161950428532
License date	Oct 04, 2021
Licensed Content Publisher	Elsevier
Licensed Content Publication	Journal of Molecular Biology
Licensed Content Title	Homodimeric Structure and Double-stranded RNA Cleavage Activity of the C-terminal RNase III Domain of Human Dicer
Licensed Content Author	Daijiro Takeshita,Shuhei Zenno,Woo Cheol Lee,Koji Nagata,Kaoru Saigo,Masaru Tanokura
Licensed Content Date	Nov 16, 2007
Licensed Content Volume	374
Licensed Content Issue	1
Licensed Content Pages	15
Start Page	106
End Page	120
Type of Use	reuse in a thesis/dissertation
Portion	figures/tables/illustrations
Number of figures/tables/illustrations	5
Format	electronic
Are you the author of this Elsevier article?	No
Will you be translating?	No
Title	MSc Student
Institution name	McGill university
Expected presentation date	Dec 2021
Portions	Figure 1b, Figure 3, Figure 5b, Figure 7a
Publisher Tax ID	GB 494 6272 12
Total	0.00 CAD

ELSEVIER LICENSE TERMS AND CONDITIONS
Oct 31, 2021

This Agreement between Ms. Anne-Laure Chong -- Anne-Laure Chong ("You") and Elsevier ("Elsevier") consists of your license details and the terms and conditions provided by Elsevier and Copyright Clearance Center.

License Number	5179640406579
License date	Oct 31, 2021
Licensed Content Publisher	Elsevier
Licensed Content Publication	Structure
Licensed Content Title	Crystallographic and Modeling Studies of RNase III Suggest a Mechanism for Double-Stranded RNA Cleavage
Licensed Content Author	Jaroslaw Blaszczyk,Joseph E. Tropea,Mikhail Bubunenko,Karen M. Routzahn,David S. Waugh,Donald L. Court,Xinhua Ji
Licensed Content Date	Dec 1, 2001
Licensed Content Volume	9
Licensed Content Issue	12
Licensed Content Pages	12
Start Page	1225
End Page	1236
Type of Use	reuse in a thesis/dissertation
Portion	figures/tables/illustrations
Number of figures/tables/illustrations	2
Format	both print and electronic
Are you the author of this Elsevier article?	No
Will you be translating?	No
Title	DICER1 mutations: clinical applications, novel associations and functional evaluations
Institution name	McGill University
Expected presentation date	Dec 2021
Portions	Figure 3a and 3b
Publisher Tax ID	GB 494 6272 12
Total	0.00 CAD

JOHN WILEY AND SONS LICENSE
TERMS AND CONDITIONS

This Agreement between Ms. Anne-Laure Chong -- Anne-Laure Chong ("You") and John Wiley and Sons ("John Wiley and Sons") consists of your license details and the terms and conditions provided by John Wiley and Sons and Copyright Clearance Center.

License Number	5170610225264
License date	Oct 16, 2021
Licensed Content Publisher	John Wiley and Sons
Licensed Content Publication	Molecular Microbiology
Licensed Content Title	A stepwise model for double-stranded RNA processing by ribonuclease III
Licensed Content Author	Xinhua Ji, Donald L. Court, David S. Waugh, et al
Licensed Content Date	Nov 29, 2007
Licensed Content Volume	67
Licensed Content Issue	1
Licensed Content Pages	12
Type of use	Dissertation/Thesis
Requestor type	University/Academic
Format	Electronic
Portion	Figure/table
Number of figures/tables	1
Will you be translating?	No
Title	DICER1 mutations: clinical applications, novel associations and functional evaluations
Institution name	McGill University
Expected presentation date	Dec 2021
Portions	Figure 4
Publisher Tax ID	EU826007151
Total	0.00 CAD